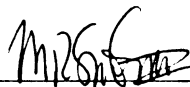This is to certify that the

dissertation entitled

SYNTHESIS, CHARACTERIZATION AND REACTIVITY
OF LATE TRANSITION METAL BORYL COMPLEXES

presented by

Carl N. Iverson

has been accepted towards fulfillment
of the requirements for

_____Ph. D._____ degree in __Chemistry___

_____
Major professor

Date ___8/27/99___

PLACE IN RETURN BOX to remove this checkout from your record.
TO AVOID FINES return on or before date due.
MAY BE RECALLED with earlier due date if requested.

DATE DUE	DATE DUE	DATE DUE

SYNTHESIS, CHARACTERIZATION AND REACTIVITY OF LATE

TRANSITION METAL BORYL COMPLEXES

By

Carl N. Iverson

A DISSERTATION

Submitted to
Michigan State University
in partial fulfillment of the requirements
for the degree of

DOCTOR OF PHILOSOPHY

Department of Chemistry

1999

ABSTRACT

SYNTHESIS, CHARACTERIZATION AND REACTIVITY OF LATE

TRANSITION METAL BORYL COMPLEXES

By

Carl N. Iverson

The hydroboration of unsaturated substrates is a well-known method used for synthesizing organic compounds that contain a wide variety of functional groups. Transition metal catalyzed hydroboration using simple borane analogues was introduced in 1975 using Wilkinson's catalyst and offer the potential control of chemo-, regio- and stereochemical addition to organic substrates. More recently, alternative borane compounds ($E-BX_2$, E = boryl, silyl, and stannyl groups) have been introduced into catalytic addition reactions, allowing for multiple functionalizations of unsaturated substrates.

For instance, catalytic diboration of alkynes using PinB–BPin (Pin = $O_2C_6H_{12}{}^{2-}$) with $(PPh_3)_4Pt$ has been reported. A catalytic cycle that involved alkyne association and insertion into the Pt–B bond of a novel bisphosphinediborylplatinum(II) complex as the key steps was invoked. To better understand the catalytic process, the reactivity of the catalytically active species in simple stoichiometric reactions must be studied. Boryl compounds, and in particular, $(PPh_3)_2Pt(BCat)_2$, were synthesized via oxidative addition of CatB–BCat (Cat = $O_2C_6H_4{}^{2-}$) to the platinum olefin complex, $(PPh_3)_2Pt(\eta^2-C_2H_4)$, with loss of ethylene. The diboryl complex cleanly diborates alkynes to form

(PPh$_3$)$_2$Pt(η^2–alkyne) and the 1,2–diborated–alkene. The clean reactivity allowed the mechanistic details of this addition to be examined. Kinetic studies support phosphine dissociation as the key step prior to association of the alkyne and subsequent insertion between the Pt–B bond.

Kinetic studies of the catalytic reaction bore many similarities to the stoichiometric addition. An analysis of the rate laws allowed us to directly compare rate constants for the two mechanisms. The identical calculated values (within experimental error) are consistent with a catalytic manifold that is indistinguishable to the stoichiometric mechanism. These studies led to the use of base-free Pt complexes as catalysts that would diborate olefins, since the bisphosphine compound accommodates only alkynes.

Activation and functionalization of hydrocarbons has been an area of fundamental interest in organometallic chemistry. Systems where alkane and arene activation have been studied in-depth and are well-understood are Cp*M(PMe$_3$)(R)H (M = Ir, Rh; R = H, alkyl, aryl). Cp*Ir(PMe$_3$)H$_2$ reacts with E–B(OR)$_2$ (E = H, B(OR)$_2$) reagents in hydrocarbon solvents at elevated temperatures to produce thermally stable iridium boryls and H–E. Alternatively, the iridium-borane adduct, Cp*Ir(PMe$_3$)H[HBH(C$_6$F$_5$)$_2$], is formed when the electrophilic borane, [HB(C$_6$F$_5$)$_2$]$_2$, is used. Thermolysis of this compound results in formation of an iridium boryl with loss of H$_2$. Cp*Ir(PMe$_3$)(cy-C$_6$H$_{11}$)H and Cp*Ir(PMe$_3$)(C$_6$H$_5$)H react with HB(OR)$_2$ at elevated temperatures to form both B–Ir and B–C bond containing products. The ratio of products can be controlled through manipulation of temperature and concentration of HB(OR)$_2$. Exclusive B–C bond formation, however, is observed when [HB(C$_6$F$_5$)$_2$]$_2$ is added to Cp*Ir(PMe$_3$)(cy-C$_6$H$_{11}$)H. Although inefficient, a combined thermal and photochemical approach would constitute a catalytic cycle. Arene solutions of Cp*Ir(PMe$_3$)(BPin)H were thermally stable, but when heated in the presence of HBPin catalytic formation of aryl–BPin was observed.

To my family

TABLE OF CONTENTS

LIST OF TABLES

LIST OF FIGURES

xii

LIST OF SYMBOLS AND ABBREVIATIONS

Å	Angstrom
B_2Cat_2	bis(catecholato)diboron, $H_4C_6O_2B-BO_2C_6H_4$
B_2Pin_2	bis(pinacolato)diboron, $Me_4C_2O_2B-BO_2C_2Me_4$
Cat	catechol, $1,2-O_2C_6H_4^{2-}$
cm^{-1}	wave number
COD	1,5-cyclooctadiene
Cp	cyclopentadienyl, $\eta^5-C_5H_5$
Cp*	pentamethylcyclopentadienyl, $\eta^5-C_5(CH_3)_5$
cy	cyclohexyl
°C	degrees Celcius
d	doublet
D	deuterium
d_x	deuterium substitution (x = number of substitutions)
e.u.	entropy units
Et_2O	diethyl ether
h	hour
HBCat	catecholborane, $HBO_2C_6H_4$
HBOp	orthophenylenediamineborane, $HB(NH)_2C_6H_4$
HBPin	pinacolborane, $HBO_2C_2Me_4$
Hz	hertz
IR	infrared
J	coupling constant
k	rate constant
K	temperature in Kelvin, equilibrium constant
kcal	kilocalorie

k_H/k_D	ratio of isotope effect on observed rate constant
k_{obs}	observed rate constant
L	liter, generic ligand
m	multiplet
Me	methyl, $-CH_3$
min	minute
mL	milliliters
mmol	millimole
mM	millimolar
mol	mole
nbe	norbonadiene, bicyclo[2.21]heptadiene
NMR	nuclear magnetic resonance
OTf	trifluoromethanesulfonate, $CF_3SO_3^-$
Ph	phenyl, $-C_6H_5$
PMe_3	trimethylphosphine
PPh_3	triphenylphosphine
Pin	pinacol, $1,2-O_2C_2Me_4^{2-}$
q	quartet
s	singlet, seconds
t	triplet
thf	tetrahydrofuran
δ	delta, ppm for NMR spectroscopy
$\Delta H^\ddagger$	change in enthalpy
$\Delta S^\ddagger$	change in entropy
$\Delta v_{1/2}$	full width at half height
η^n	ligand hapticity of number "n"
μL	microliter

CHAPTER 1

INTRODUCTION

Reasons For Studying Transition Metal Boryl Complexes

The addition of BH_3 to olefins was first described by H. C. Brown in 1950's.[1] In the four decades following that initial report, the hydroboration reaction has been studied in depth and has long been known as an effective synthetic tool for the preparation of organic compounds containing a wide variety of functional groups. The complementary transition metal catalyzed hydroboration was not discovered until 1985 when Männig and Nöth reported the hydroboration of various functionalized alkenes using a simple borane derivative in the presence of Wilkinson's catalyst, $(PPh_3)_3RhCl$.[2] This result opened a new arena in which to study B-C bond formation chemistry, and since that report the use of well–defined systems in boration reactions has yielded an abundance of interesting new results. Several reviews that have appeared in recent years attest to both the practical importance and fundamental interest of metal-boron chemistry.[3-9]

In order to further understand metal boryl chemistry, the study of compounds containing simple metal-boron linkages is needed. The preparation and study of the chemistry of carborane and polyhedral borane transition metal complexes is vast due to boron's unusual electronic properties and penchant for catenation. The chemistry of borohydride complexes is also well established and so, the dearth of compounds containing $-BR_2$ and $-BR_3$ ligands bound to metals is somewhat surprising. For example, homoleptic boryl complexes and terminal borides are unknown, and only recently have terminal borylene (M=B) compounds been described.[10-12] In contrast, many alkylidine complexes are known and a terminal metal carbide was recently reported.[13]

Transition Metal Boryl Complexes

The most obvious and immediate comparisons of metal–boron chemistry should be made to metal–carbon chemistry. The $-BR_2$ fragment has the same formal charge as the $-CR_3$ fragment; however, due to the vacant boron p orbital boryl ligands compare more favorably to carbene fragments. Hence, the strategy of using heteroatom substitution for stabilizing carbene ligands may extend to the synthesis of boryl complexes as well. One major difference between boryl and alkyl ligands is the possibility of π back-bonding to the boron p orbital from appropriate filled frontier orbitals on the metal. Although such back-bonding has not yet been proven conclusively, current arguments are based on numerous structures of metal boryl complexes where the M–B bond distance is shorter than expected based on the sum of covalent radii. Simple representations of both interactions (boryl substituent/boron p orbital and $d\pi$–$p\pi$ back-bonding) are given in Figure 1. Another major difference between the two ligands is in the value of electronegativity; boron is 2.0 and carbon is 2.5 on the Pauling Scale. Therefore, M–B bonds are predicted to be more covalent than M–C bonds and likely to have different bonding properties.

A   **B**
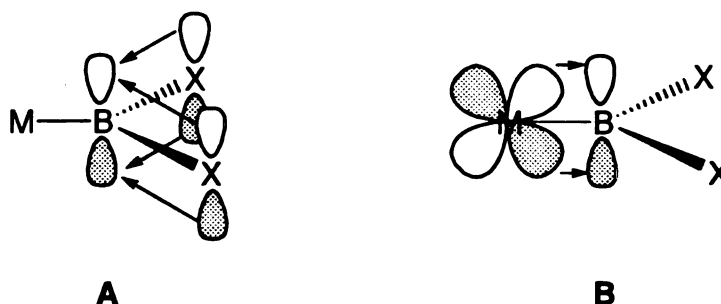
Figure 1. Boryl ligand π interactions involving A) boryl substituent orbitals and B) metal frontier orbitals with the p orbital on boron.

Boryl complexes have been produced through reactions of metal anion salts with haloboranes, oxidative addition of E–B bonds, and metathesis reactions of boranes with metal-ligand bonds (Equations 1-3).[14-19] Although the first of these methods is somewhat limited by the availability of suitable metal anions, the latter two lend a great deal of latitude in terms of useful and interesting starting materials. Complexes containing ligands that readily dissociate leaving an unsaturated metal center are ideal for the oxidative addition of borane reagents. Notably, late metal phosphine systems and η^2-olefins in early and late metal complexes have proven effective in the synthesis of boryl complexes.[19-22] Transition metal hydride, alkyl and olefin complexes also have been used in metathesis reactions with boranes to produce compounds containing metal-boron bonds.[19,23,24]

$$[L_nM^-]A^+ \xrightarrow[- AX]{+ X\text{-}BY_2} L_nM\text{-}BY_2$$

A = alkaline earth metal
X = halide

$$\tag{1}$$

$$L_nML' \xrightarrow{- L'} [L_nM] \xrightarrow{E\text{-}BY_2} L_nM \begin{smallmatrix} \diagup E \\ \diagdown BY_2 \end{smallmatrix}$$

$$\tag{2}$$

$$L_nM\text{-}R \xrightarrow[- E\text{-}R]{+ E\text{-}BY_2} L_nM\text{-}BY_2$$

R = H, alkyl

$$\tag{3}$$
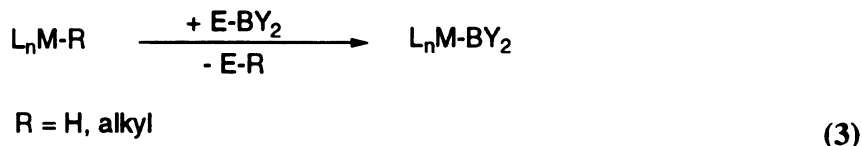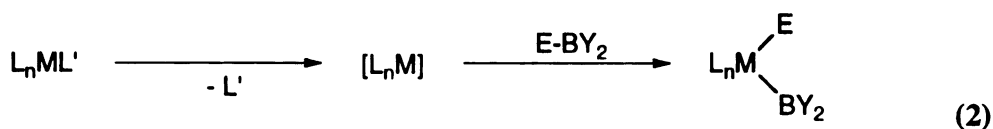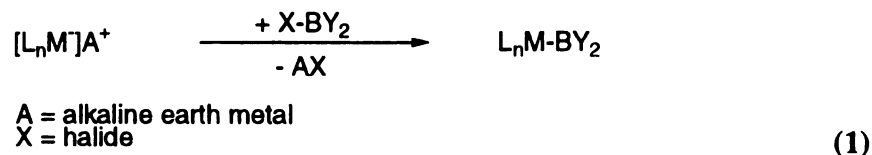
The first compound containing a distinct metal-boron linkage was produced by reacting triphenylborane with lithiumtriphenylgermanate to form a germaniumborate

adduct complex anion as reported by Grim in 1961.[25] The first transition metal–boron compound was reported a few years later by Parshall as rhenium pentacarbonyl anion reacted with borane to form a rhenium–borane adduct.[26] Following that, Nöth and Schmid reported the formation of several metal boryl compounds by reacting boron halides with various transition metal compounds.[27-29] The complexes contained metals in the mid- to late transition block triads.

It should be noted that in some of the earliest reports of these types of compounds, erroneous characterizations were made. For example, the reaction of tungstenocenedihydride with BF_3 was reported to yield "$Cp_2WH_2 \cdot BF_3$" based on IR data and comparisons to related reactivity of protonations of hydride species.[30] The insolubility of the compound precluded NMR spectroscopy and X-Ray crystallography was not a viable option at the time. Reinvestigation of the reactivity of Cp_2WH_2 with BF_3 and other haloborane reagents revealed that zwitterionic and cationic trihydride species are produced, as confirmed by X-Ray crystallography, and not tungstenoceneborane adducts as earlier proposed (Figure 2).[31,32]
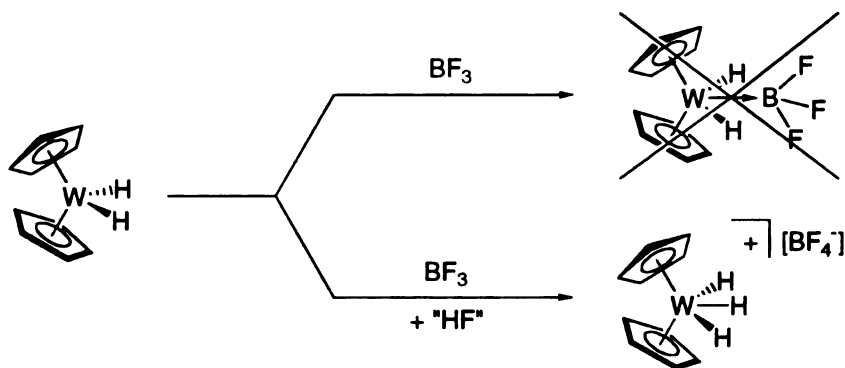
Figure 2. Product characterization of the reaction of BF_3 with Cp_2WH_2 from 1963 (top reaction) and 1996 (bottom reaction).

In 1975, Kono and Ito reported the oxidative addition of 4,4,6-trimethyl-1,3,2-dioxaborinane to Wilkinson's catalyst.[20] In spite of the obvious applications and well-known catalytic ability of rhodium based systems, surprisingly little advancement was made in this field until Männig and Nöth's report. Since then, many accounts centered on reacting common aryloxy and alkyl hydroboration reagents such as HBCat and 9-BBN with late transition metal systems.

More recently, early transition metal systems have been studied as well. In particular, bis-metallocene compounds have been useful for probing fundamental features of borane coordination and activation. Indeed, one of the more interesting facets of these early transition metal complexes is the fascinating array in binding of "simple" metal boryl linkages. A continuum in M–B bonding can be illustrated in a series of bent metallocene compounds. At one extreme, boryl complexes where B–H interactions are absent are observed while borohydride complexes with strong B–H interactions lie at the other extreme. These two extremes are linked by a σ–complex where the borane is bound to the metal through the H–B bond. Representative examples are given in Figure 3.[14,33,34] Compounds along this continuum can be described in terms of these limiting structures.
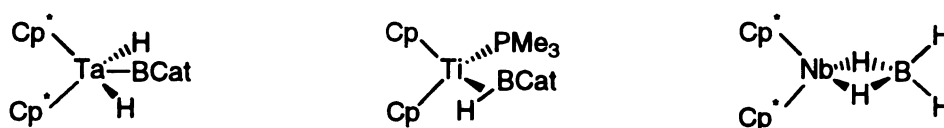
Figure 3. Continuum of metal-boron bonding in simple metal-boron complexes.

Transition metal catalyzed boration

Due in large part to the utility of the hydroboration reaction, the study of transition-metal catalyzed boration chemistry has grown significantly in the past decade. Transition

metal complexes have shown considerable promise in promoting B–C bond formation and although catalysis by late transition metal compounds is most prevalent, lanthanide and early metal systems offer alternative pathways that can alter product distributions.

Besides increasing the efficiency (reduced reaction temperatures and faster rates) of a process, catalysts can also dramatically influence the chemo,[2] regio,[35-38] and stereoselective[38-41] outcome of a reaction. For example, chemoselective addition is observed when catecholborane hydroborates hex-5-en-2-one. In the uncatalyzed reaction the ketone functionality is reduced while the olefin is preferentially attacked in the presence of Wilkinson's catalyst (Figure 4).
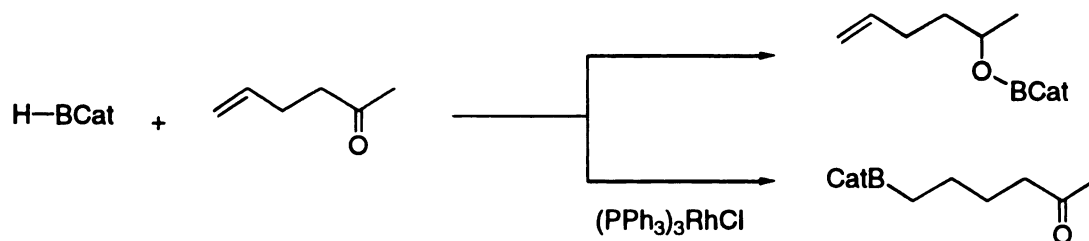
Figure 4. Comparison of chemoselectivity for catalyzed and uncatalyzed hydroborations.

Following Männig and Nöth's report of rhodium catalyzed hydroboration, most of the research in the area of transition metal-boron catalysis was performed using mid- to late transition metal systems, notably Wilkinson's catalyst and other phosphine rhodium and iridium compounds. Late transition metal systems are expected to follow a relatively simple mechanistic pathway (shown in Figure 5 for Wilkinson's catalyst): oxidative addition of the borane, association and subsequent insertion of the unsaturated organic substrate and reductive elimination of the organoborane regenerating the catalytically active species.[42-44] However, strong evidence for a metathetic pathway has been provided in the reaction of $CpRu(PPh_3)_2R$ (R = Me, H) with catechol borane,[24] and

computational investigations predict that oxidative addition and σ-bond metathesis pathways in Rh catalyzed hydroborations have similar energy barriers.[43]
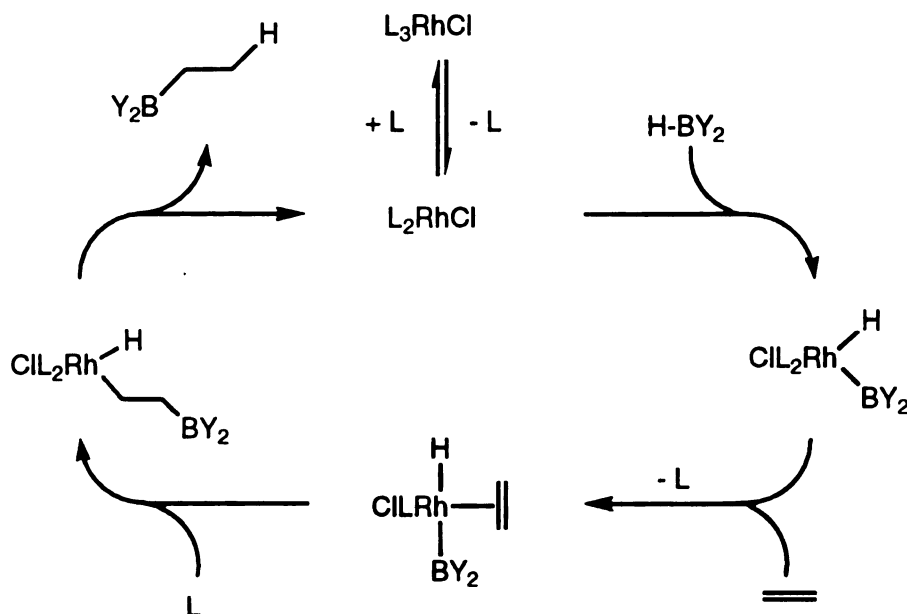
Figure 5. Proposed catalytic cycle for olefin hydroboration by Wilkinson's catalyst.

More recently, several groups have examined early metal systems, primarily utilizing metallocene ligand sets. Also, the use of lanthanide compounds as hydroboration catalysts have been reported, although these have been more sparse.[45] Early transition metal catalysts have been studied both to complement late transition metal systems and in an effort to find less expensive catalyst sources.

Marks has reported the hydroboration of mono-, di-, and trisubstituted alkenes with Cp^*_2LaH. This system features a reaction pathway that involves olefin insertion into the metal hydrogen bond followed by metathesis of the alkyl complex with borane to produce the organoborane and regenerating the lanthanum hydride.

Although a number of complexes have been shown to catalyze hydroboration, care must be taken in labeling any system catalytic in nature. Burgess showed that a variety of

7

complexes thought to be catalytic actually promote the degradation of HBCat to B_2Cat_3 and diborane.[46] Thus, the organoborane products are produced by the reaction of BH_3 and the olefin. Also, phosphine promoted degradation of HBCat in late metal systems has been observed in late metal phosphine systems, leading to lower yields and eventual catalyst poisoning.[47]

Other Boration Reagents

The utility of boration reagents other than diborane, HBCat and 9-BBN (and other alkoxy and alkyl based boranes) has become apparent over the past several years. Amide based boranes, $HB(NR_2)_2$, the very electrophilic borane, $HB(C_6F_5)_2$,[48] reported by Piers and homo/heteroelement boranes, $E-BX_2$ ($E = BX_2$, SiR_3, SnR_3; $X = OR$ or NR_2) have all yielded significant results. Motry and Smith demonstrated aspects of tuning the boryl ligand substituents with their study on $Cp^*_2Ti(C_2H_4)$ catalyzed hydroboration of ethylene.[49] Initial experiments in this system revealed that when stoichiometric amounts of HBCat are added to the organometallic complex the organoborane isolated is the vinylborane, $CH_2=C(H)BCat$. Unfortunately, this dehydrogenative boration did not extend into the catalytic manifold as the major organoborane product is ethylborane, CH_3CH_2BCat. In contrast, when the aminoborane HBOp ($Op = 1,2-(NH)_2C_6H_4{}^{2-}$) is used, dehydrogenative boration is observed under stoichiometric and catalytic conditions.

Like other non-"BH_3" sterically hindered borating agents, Piers' borane is useful for its ability to hydroborate asymmetric and prochiral substrates more selectively. However, it is unique from other reagents in that it reacts with olefins and alkynes facilely at room temperature. This is primarily a result of the borane's high electrophilicity and more rapid dissociation to the monomeric species. As shown in Figure 6 these properties also lead to a stark difference in reactivity with respect to dialkoxy- or dialkylboranes when reacted

in analogous fashion with transition metal compounds. The reaction of three equivalents of HBCat with biscyclopentadieneyldimethyltitanium results in the formation of the bis(borane) adduct of titanocene, $Cp_2Ti(HBCat)_2$.[50] The analogous reaction with $HB(C_6F_5)_2$ is not known, however addition of two equivalents of the electrophilic reagent to the zirconium analog results in methane loss and formation of a borane stabilized carbene complex.[51] A five-coordinate carbon center is featured in this unique compound. The zirconium bound $=CH_2$ bridges two boranes that are, in turn, bound to the metal center through the hydrogen atoms.
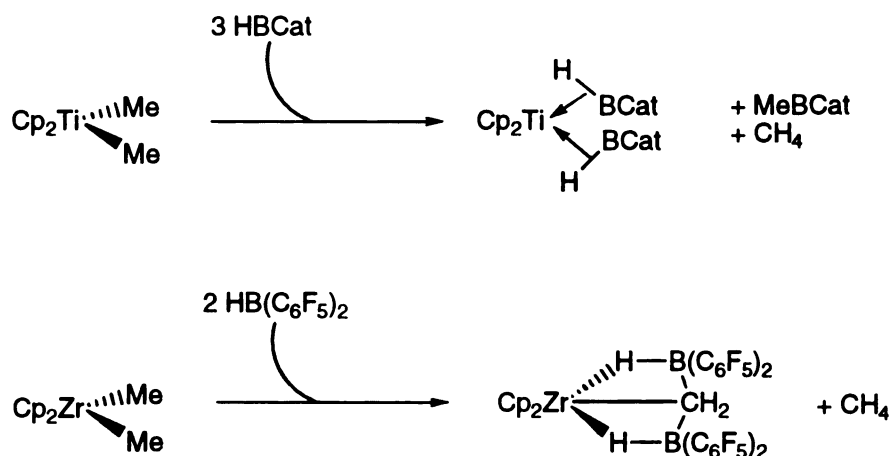
Figure 6. Comparison in reactivity of HBCat versus $HB(C_6F_5)_2$.

Catalytic addition of B–E bonds (E = B, Si and Sn) to unsaturated organic compounds has recently become an intense area of study. In the mid- to late eighties, a small number of reports regarding B–Si and B–Sn reagents appeared.[52,53] These findings utilized trialkylborate silicon and tin compounds for the preparation of vinylsilanes and vinylstannanes from alkynes in good yield. Separately, Ito and Tanaka, using neutral E–B compounds, have further developed this field to include addition products with standard olefins, α, ω-alkenes and mixed alkene/alkyne substrates.[54,55] Given the potential utility of these reactions for sequentially and/or selectively functionalizing unsaturated organic

substrates (Figure 7), a basic understanding of the synthesis, characterization and reactivity of transition metal compounds that simultaneously support M–B and M–E bonds is of obvious interest.
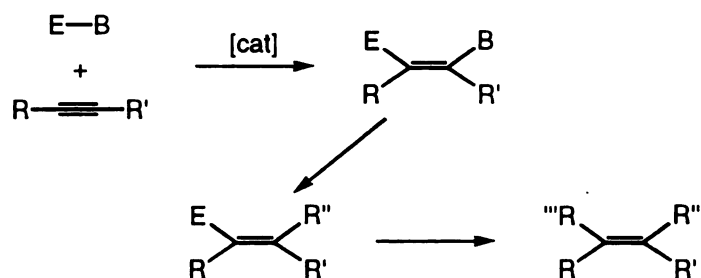
Figure 7. Sequential substitution scheme utilizing heteroborane substrates.

Diboron compounds of the formula X_2B-BX_2 (where X = halide) have been shown to react with unsaturated organic substrates by adding across the multiple bond in a cis fashion. This reaction, first discovered by Schlesinger in 1959, is an appealing method for the synthesis of 1,2-diborated alkenes.[56,57] However, only the halide species react readily with unsaturated compounds. This is unfortunate as these compounds have an arduous synthesis and are relatively unstable. The alkoxide and amide based diboron compounds, on the other hand, have facile syntheses and are more stable than their halide counterparts.[58,59] These compounds, though, are much less reactive.

Simple molecular orbital arguments suggest topological similarities between diboron tetrahalides, and their derivatives, with carbon based fragments and dihydrogen. While comparisons to olefinic fragments are supported by the empirical observation that the B–B bond distance decreases when Ar_2B-BAr_2 derivatives are reduced by two electrons,[60] the comparison to H_2 is not as strong. Nevertheless, early reports indicated that B–B bonds oxidatively add to metal centers with B–B bond cleavage.[17] Therefore, the catalytic diboration of unsaturated organic substrates might be expected to parallel metal

10

mediated reactivity of H_2, and other E–X transfer reactions. In fact, a catalyst is required in order to promote B–B addition across the unsaturated carbon–carbon bond. Miyaura and Suzuki were the first to report such a reaction in 1993 when they reacted bis(pinacolato)diboron (B_2Pin_2) with both internal and terminal alkynes in the presence of catalytic amounts of tetrakis(triphenylphosphino)platinum, $(PPh_3)_4Pt$, to afford *cis*-bis(boryl)alkenes (Equation 4).[61]

$$PinB-BPin + R-\!\!\!\equiv\!\!\!-R' \xrightarrow{(PPh_3)_4Pt} \underset{R}{PinB}\diagdown\!\!\!=\!\!\!\diagup\underset{R'}{BPin} \qquad (4)$$

Alkane Functionalization

Alkanes make up a large fraction of the world's supply of petroleum products and the possibility of using this inexpensive source of C_nH_m compounds to make practical organic molecules is a serious economic driving force. Because of this, alkane functionalization has long been considered a "Holy Grail" by organometallic chemists.[62] Unfortunately, the inert nature of these molecules toward organic substitution chemistry makes this objective a challenging problem. Therefore, great effort has been made toward the study of C–H and C–C bond activation with the ultimate goal of being able to functionalize simple alkanes and alkyl groups. The greatest challenge appears to be in designing systems that generate a catalytically viable intermediate following functionalization of the M–C bond.

One issue concerning alkane functionalization that must be addressed is selectivity of activation in the alkane. For instance, tertiary rather than primary C–H bonds are preferentially activated in both radical and electrophilic reactions. A second issue is also

a matter of selectivity as the functionalized product molecule may be more activated towards C–H cleavage than the parent alkane. For example , in the oxidation of methane, methanol can undergo further reaction to produce CO_2 and H_2.

An indirect route to functionalization, the "synthesis gas" process, uses steam reformation of petroleum products (methane) to produce CO and H_2. Once produced the CO/H_2 mixture can be used in a variety of processes such as hydroformylation of olefins, reduction of aromatic nitro compounds to amines and the production of methanol. The last of these is important as it is a direct source for high-octane gasoline and as a primary chemical feedstock. However, the preparation of methanol from methane in this case is a cumbersome two–step process whose first step is highly endothermic (Eq 5 and 6). A more efficient one–step process is certainly desirable.

$$CH_{4(g)} + H_2O_{(g)} \xrightarrow{[Ni], \Delta} 3 H_{2(g)} + CO_{(g)} \qquad \Delta H^{\circ} = +49.3 \text{ kcal/mol} \tag{5}$$

$$CO(g) + 2 H_2(g) \xrightarrow{[Cu/ZnO]} CH_3OH_{(g)} \qquad \Delta H^{\circ} = -21.7 \text{ kcal/mol} \tag{6}$$
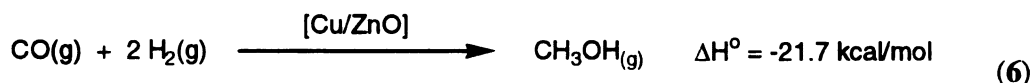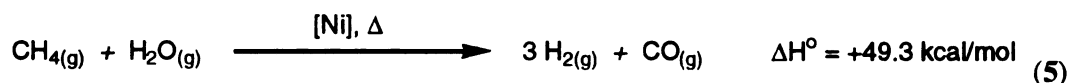
The first step of the functionalization process, C–H activation, has been studied in depth by many groups.[62-82] Mechanisms for C–H activation can be divided into three fundamentally distinct classes: i) oxidative additions where new M–C and M–H bonds are formed[66,67,69,75,77] ii) σ–bond metatheses between metal–ligand and C–H bonds[78,79] and iii) activation by metal radicals.[80-82] Historically, late–metal complexes were believed to operate primarily by class I mechanisms, while C–H activations by d^0 early metal centers can only be explained by class II mechanisms. More recently, cationic Ir and Pt complexes have been found to activate hydrocarbons under mild conditions. It has been suggested that these reactions proceed via σ–bond metathesis (class ii) pathways.

12

Figure 8 illustrates the activation process in four separate systems. Notably, Bergman and Jones have separately investigated the reactivity of the Cp*M(PMe₃) (M = Rh, Ir) moiety.[65,69] This reactive intermediate can be generated via photolysis of Cp*M(PMe₃)H₂ in alkane or arene solutions, via dissociation of H_2. C–H bonds of the solvent molecules then oxidatively add to the metal. Whitesides has investigated C–H activation in chelating bisphosphine complexes of platinum. The thermolysis of Pt(II) hydridoalkyls in this system results in the reductive elimination of the parent alkane and subsequent activation of C–H bonds.[76,77] Wolczanski has used bulky ligand systems to stabilize early transition metal alkyl complexes. Titanium and zirconium complexes that utilize the amide ligand ᵗBu₃SiNH⁻ demonstrate 1,2-R–H elimination upon thermolysis.[71,72] A transient imido complex is produced which forms new alkyl amido complexes via concerted 1,2-R'–H addition. Bergman has also examined C–H activation by the cationic species [Cp*Ir(PMe₃)Me][B(ArF)₄].[63] This system is unique from the other three in that it does not require an elimination reaction prior to activation and the reaction occurs below room temperature.
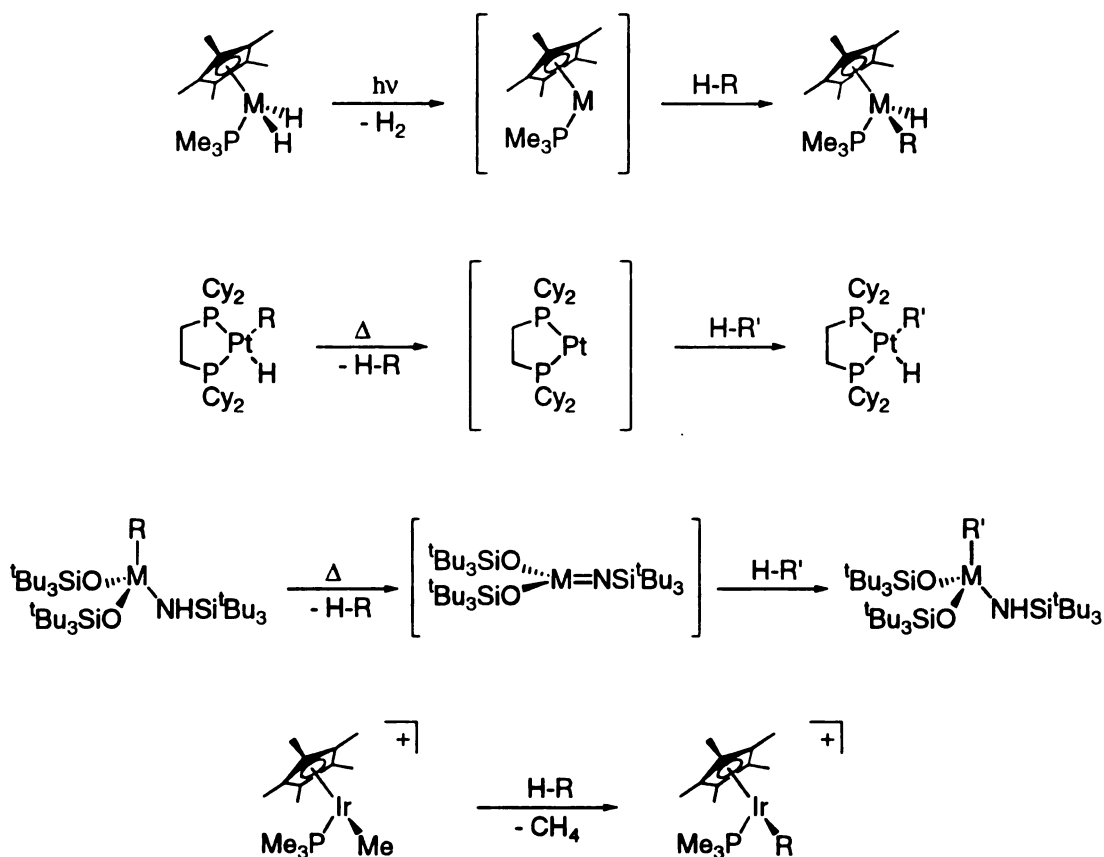
Figure 8. Systems studied for C–H activation.

Common themes to these (and other) systems are the requirement of a coordinatively unsaturated metal center prior to C–H activation, selectivity of activation (generally aryl > primary > secondary), and ligand sensitivity. Ligand substitution can have a dramatic effect on the reactivity. For instance, if trimethylphosphine is replaced by triphenylphosphine in Cp*Ir(PR₃)H₂, then intramolecular C–H activation occurs as orthometallation of a phenyl group of the phosphine is observed as well as C–H activation of the solvent molecules following photolysis. Also, if non-chelating phosphines are used in the Whitesides system, then C–H activation is blocked completely. Lastly, Bergman notes that if the more coordinating anion,

14

trifluoromethanesulfonate (OTf⁻), is used as the counterion to [Cp*Ir(PMe₃)Me⁺] instead of a non-coordinating [B(Ar_F)₄⁻] anion, then higher temperatures are required to effect C–H activation.

To this point, the number of reported examples where alkanes have been converted to functionalized organic compounds has been limited. Shilov first reported the conversion of methane to alcohols and methyl halides utilizing a platinum catalyst.[83] Periana reported the use of a mercury (II) salt to catalyze the oxidation of methane to methanol.[84] More recently, there have been numerous reports appearing in the literature relating to methane oxidation catalyzed by platinum (II) complexes that employ bidentate bisnitrogen ligands.[85,86] In a non-methane functionalization reaction, Jones reported the catalytic cyclization of 2,6–xylyl isocyanide to an indole using a ruthenium compound (Equation 7).[70]

$$H_3C \underset{CN}{\overset{}{\bigcirc}} \quad \xrightarrow[\text{cat. (dmpe)}_2\text{RuH}_2]{140\ ^\circ C} \quad \underset{H}{\overset{}{\bigcirc}}$$

(7)
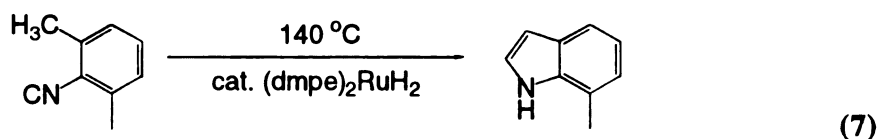
This thesis describes our efforts toward the preparation of late transition metal boryl complexes, the use of non-traditional borating reagents to facilitate boration of unsaturated organic substrates, and the boration of unsaturated organic molecules. In particular, Chapter Two describes the preparation and reactivity of Group 10 boryl complexes as well as the related diboration of alkynes. Chapter Three describes an extension of the catalytic diboration to alkene moieties. Chapter Four describes the metathesis reactivity and the catalytic boration of arenes in the Cp*M(PMe₃) system. Experimental procedures are detailed in Chapter Five.

CHAPTER 2

SYNTHESIS, CHARACTERIZATION AND REACTIVITY OF GROUP 10
BORYL COMPLEXES

We investigated the reactivity of borane reagents with late transition metal olefin compounds for two main reasons. First, the rich reactivity of olefin complexes with various carborane derivatives suggests that olefin complexes are particularly attractive starting materials for preparing compounds with unsupported metal–boron bonds via E–B oxidative addition. Second, reactions of olefin complexes with borane reagents offer the possibility of pathways that are mechanistically distinct from other metal-mediated hydroboration processes. Of particular interest is the synthesis of boryl complexes by reaction of "non-traditional" borane reagents with olefin complexes in hopes of complementing the application of HBCat as the borating reagent. The use of olefin complexes should also avoid complications from side reactions involving dissociated phosphine ligands with borane reagents since the olefin by-product is readily removed (Eq 8).

$$\text{Ph}_3\text{P} \diagdown \text{Pt} \leftarrow \| \quad + \quad \text{E}-\text{BR}_2 \quad \xrightarrow[-\text{ H}_2\text{C}=\text{CH}_2]{} \quad \text{Ph}_3\text{P} \diagup \text{Pt} \diagdown \text{BR}_2 \qquad (8)$$
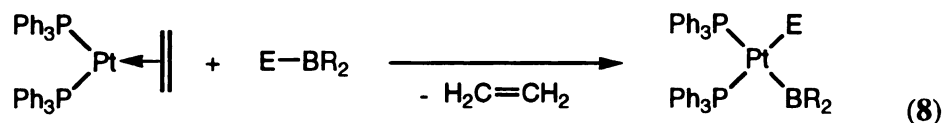
Also, the report by Suzuki that *cis* addition of the B–B bond in pinacol ester derivatives to alkynes can be catalyzed by $(PPh_3)_4Pt$ piqued interest in the reactivity of platinum boryl complexes.[61] It was postulated that *cis*-$(PPh_3)_2Pt(BPin)_2$ is formed in *situ* and serves as the active catalyst in this system. A direct synthesis of this compound,

16

however, was not reported, which hampers attempts for definitively probing the mechanism for B–C bond formation.

Preparation and Reactivity of Diboryl Complexes of Platinum

$(PPh_3)_2Pt(\eta^2\text{-}C_2H_4)$ $(1)^{87}$ reacts with various borane reagents to form platinum boryl complexes (Figure 9). In each case ethylene is readily displaced by the borane, does not react with the boryl complex, and is easily separated from the reaction mixture when the volatile materials are removed in *vacuo*. In most cases (E–B = $B_2(OR)_2$, Me_3Sn–$B(NMe_2)_2$), oxidative addition occurs in a *cis* fashion, although, *trans* addition has been reported in the case of *B*-halocatecholboranes, (XBCat, X = Cl or Br).[88]
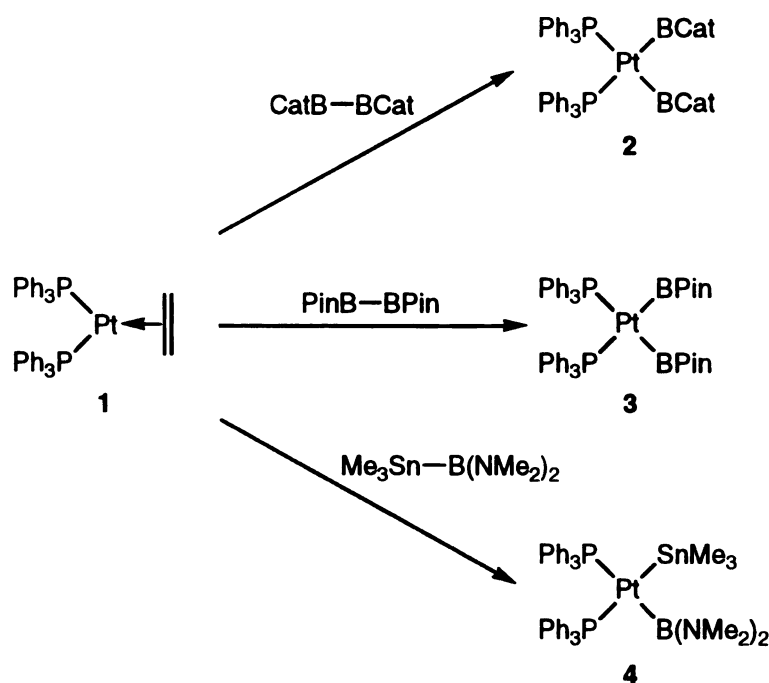
Figure 9. Scheme depicting the preparation of platinum boryl complexes.

17

cis-(PPh$_3$)$_2$Pt(BCat)$_2$ (**2**) is cleanly formed as the sole platinum containing product by reacting (**1**) with B$_2$Cat$_2$ and is isolated in 75% yield. The reaction is accompanied by rapid evolution of ethylene at temperatures as low as −80 °C, precluding quantitative evaluation of the reaction rates. Room temperature ^{1}H NMR in C$_6$D$_6$ exhibited catecholate multiplets at δ 6.54 and 6.77 and the resonances for the triphenylphosphine ligands were typical for a *cis*-bis(triphenylphosphine)platinum (II) complex. A relatively broad singlet with ^{95}Pt satellites (|$^1J_{Pt-P}$| = 1629 Hz, $v_{1/2}$ = 60 Hz) was detected in the ^{31}P{^{1}H} NMR spectrum. Figure 10 demonstrates the effect of cooling a CDCl$_3$ solution of **2** as the peaks sharpen at −50 °C ($v_{1/2}$ = 31 Hz). The ^{11}B NMR spectrum (Figure 11) exhibited a very broad resonances at 47 ppm ($v_{1/2}$ = 1845 Hz). This is an unusually large $v_{1/2}$ value for a metalloboryl resonance. The failure to observe distinct coupling to either ^{31}P or ^{195}Pt nuclei can be explained by potential complications due to the quadrupolar ^{11}B nucleus. Compound **3**, *cis*-(PPh$_3$)$_2$Pt(BPin)$_2$, is formed analogously by employing the pinacolate derivative of the diboron compound. A single environment is observed for the pinacol methyl groups at δ 1.02 and the ^{31}P and ^{11}B NMR spectroscopic data are similar to that of **2**. In contrast, the diboron compounds, C$_6$H$_4$(NH)$_2$B–B(NH)$_2$C$_6$H$_4$ and (Me$_2$N)$_2$B–B(NMe$_2$)$_2$ do not react with (**1**) to produce the amide analogs of **2** and **3**. Evidence for a higher amount of π interaction between the boron atoms has been reported; therefore, it may be more difficult to activate the B–B bond of the amide based diboron compounds.[89]
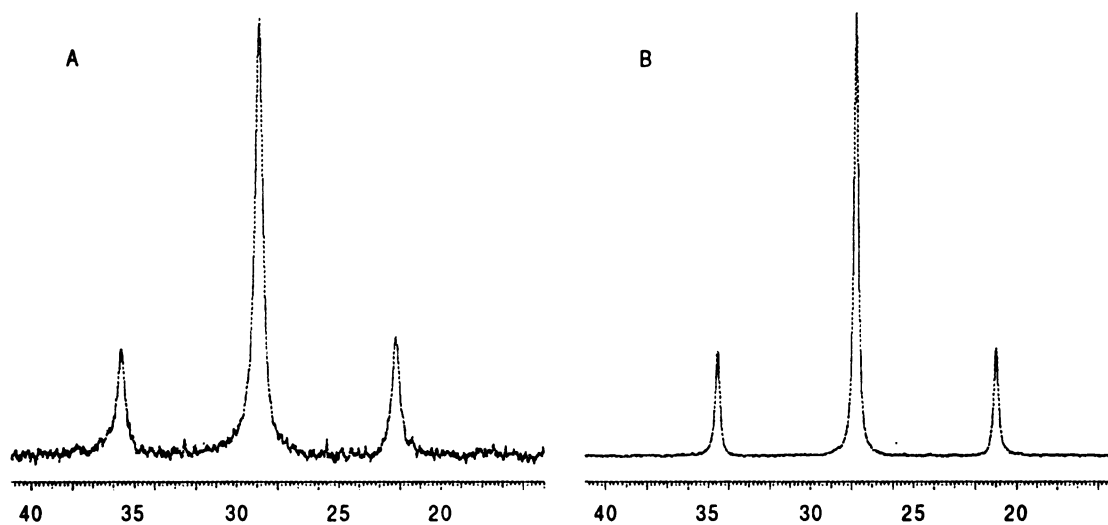
Figure 10. ^{31}P NMR spectra of **2** at A) 20 °C and B) –50 °C. For both spectra, 512 transients were taken of a 32 mM solution in CDCl$_3$.
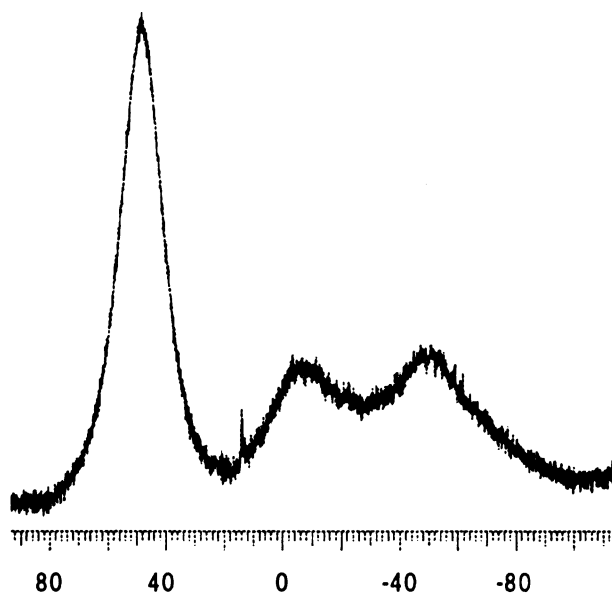
Figure 11. ^{11}B NMR spectrum (quartz NMR tube) of **2** at room temperature. The broad features at –0.6 and –50 ppm are due to borosilicate glass in the probe.

The dicatecholatoboryl complex can also be cleanly formed from bis(phosphine)platinum(η^2-alkyne) compounds. The alkyne complex (PPh$_3$)$_2$Pt(η^2-4-

octyne) (**5**) reacts with B_2Cat_2 to generate **2** (62%) with loss of the alkyne. In the absence of excess quantities of B_2Cat_2, thermolysis of the reaction mixture gives complicated mixtures: however, when an excess of B_2Cat_2 is used, clean conversion to the 4,5-bis(boryl)octene product is observed along with formation of **2**. Presumably, excess B_2Cat_2 prevents decomposition by trapping the transient "$(PPh_3)_2Pt$" fragment.

Diffraction quality crystals of cis-$(PPh_3)_2Pt(BCat)_2$ were grown from a concentrated toluene solution as colorless parallelepipeds. The structure of cis-$(PPh_3)_2Pt(BCat)_2$ (shown in Figure 12) reveals a cis geometry where $\angle P(1)–Pt–P(2)$ (107.4(2)°) and $\angle B(1)–Pt–B(2)$ (77.8(7)°) are among the most obtuse and acute angles reported for a cis-$(PPh_3)_2PtX_2$ complex. This is a common theme among other structurally characterized cis-bis(phosphine)platinumdiboryl compounds.[88,90-94] The platinum–boron distances of 2.07(2) and 2.08(2) Å in cis-$(PPh_3)_2Pt(BCat)_2$ are shorter than would be expected as has been observed for other transition metal boryl complexes as well. An improved refinement of **2** was reported by Marder et al. and confirmed the general characteristics of our structure.[91] Although the Pt–B bonds in Marder's paper were slightly shorter (2.040(6) and 2.058(6) Å) the angles $\angle B(1)–Pt–B(2)$ and $\angle P(1)–Pt–P(2)$ were identical within experimental error. A Pt–B bond distance can be estimated based on comparisons to related aryl complexes. A typical $Pt–C_{aryl}$ bond length is 2.08 Å and sp^2-hybridized $CatB–BCat$ bonds are 0.17 Å longer than sp^2-hybridized $C_{aryl}–C_{aryl}$ bonds.[95-97] These values yield an expected Pt–B bond distance should be approximately 2.16 Å.[7,98] Also, the B–B distance of 2.60 Å precludes significant interactions between the boron centers. For comparison, the B–B distance in B_2Cat_2 is 1.678(3) Å.[17]
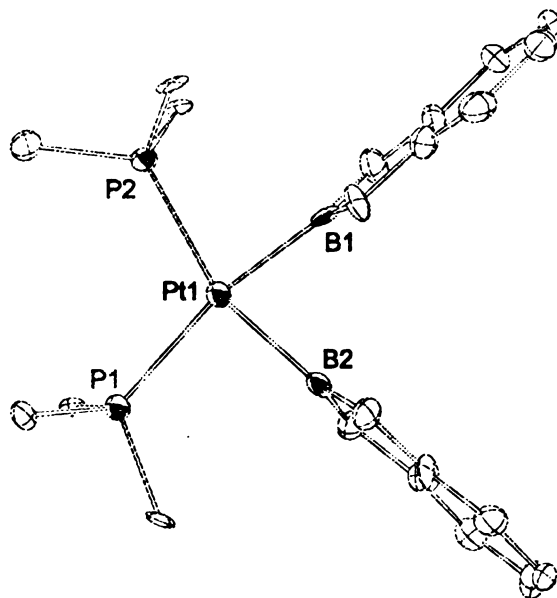
Figure 12. ORTEP diagram of **2**. Thermal ellipsoids are at 25 % probability. Only the *ipso* carbons of the triphenylphosphine ligands are shown for clarity.

Table 1. Selected bond lengths and angles for compound **2**.

bond	distance (Å)	bonds	angle (deg)
Pt(1)–B(1)	2.08(2)	B(1)–Pt(1)–B(2)	77.9(7)
Pt(1)–B(2)	2.07(2)	P(1)–Pt(1)–P(2)	107.3(2)
Pt(1)–P(1)	2.350(5)	P(1)–Pt(1)–B(2)	90.5(5)
Pt(1)–P(2)	2.375(5)	B(1)–Pt(1)–P(2)	84.6(5)
B(1)⋯B(2)	2.60	B(1)–Pt(1)–P(1)	168.1(5)
		B(2)–Pt(1)–P(2)	159.9(5)

Table 2. Selected bond lengths and angles for compound **2** from ref. 91.

bond	distance (Å)	bonds	Angle (deg)
Pt(1)–B(1)	2.058(6)	B(1)–Pt(1)–B(2)	77.1(2)
Pt(1)–B(2)	2.040(6)	P(1)–Pt(1)–P(2)	107.14(4)
Pt(1)–P(1)	2.3465(12)	P(1)–Pt(1)–B(2)	90.7(2)
Pt(1)–P(2)	2.3543(12)	B(1)–Pt(1)–P(2)	85.3(2)
B(1)⋯B(2)	2.552	B(1)–Pt(1)–P(1)	167.6(2)
		B(2)–Pt(1)–P(2)	160.1(2)

Simple Reactivity of Diboryl Complexes

Qualitative observations suggest that cis-$(PPh_3)Pt(BPin)_2$ is intrinsically less stable than cis-$(PPh_3)Pt(BCat)_2$. Figure 13 illustrates the reactions of **3** with various small molecules. For example, when **3** is dissolved in chloroform-d_1 under ambient conditions, cis-$(PPh_3)PtCl_2$ forms readily while **2** exhibits moderate stability under these conditions. For both complexes, reductive elimination can be observed when CO is added, however; **2** is stable with respect to appreciable concentrations of triphenylphosphine, whereas the elimination of B_2Pin_2 from **3** is facile. Again, in contrast to **1**, B_2Pin_2 is displaced when **3** is reacted with Sn_2Me_6 and simple alkynes. In this reaction, some conversion of the alkynes to di(pinacolatoboryl)alkenes was observed. This led us to examine the catalytic prospects of compounds **2** and **3**. The details of this aspect of **2** and **3** are discussed in depth in Chapter 3.
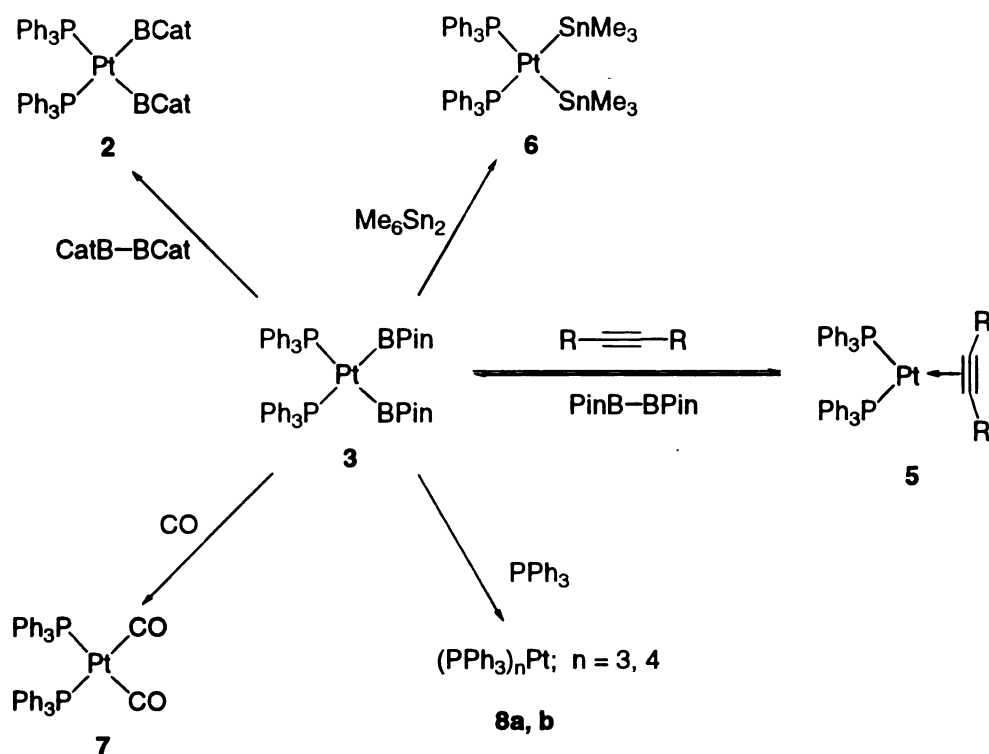
Figure 13. Scheme depicting the reactivity of **3**.

Finally, **3** can be converted to **2** when one equivalent of B_2Cat_2 is added to a solution of **3**. Qualitative disparities between rates for oxidative addition of B_2Cat_2 and B_2Pin_2 to Wilkinson's catalyst have been reported;[17] however, the conversion of **3** to **2** obviously has thermodynamic origins. Although we are not yet certain that Pt-B bond cleavage occurs in the reaction of **3** with B_2Cat_2, this observation clearly indicates that formation of **2** + B_2Pin_2 is thermodynamically favored over **3** + B_2Cat_2. It is tempting to argue that the equilibrium is driven by the formation of stronger Pt–B bonds in **2**; however, a stronger B–B bond in B_2Pin_2 relative to B_2Cat_2 would also be consistent with the experimental observations. The ease with which the elimination reactions proceed is in marked contrast to reductive eliminations of alkanes from cis-dialkylplatinum bisphosphine complexes.

23

Preparation and Characterization of a Stannylboryl Complex of Platinum

The heteroatom borane, $Me_3Sn-B(NMe_2)_2$ reacts with **1** at 45 °C for 3 hr to form the oxidative addition product $(PPh_3)_2Pt(SnMe_3)(B(NMe_2)_2)$ (**4**).[15,99,100] ^1H NMR of the reaction mixture revealed two new resonances for the tin and amino methyl groups at δ – 0.46 and 2.53, respectively. An unsymmetrical *cis* configuration of the phosphine ligands is apparent from the low temperature ^{31}P NMR data. Two resonances are observed at δ 30.6 and 31.3. The phosphine position (*trans*-tin versus *trans*-boron) can be deduced based on coupling constant values and appearance of the peaks. The resonance at δ 30.6 ($|^1J_{P-Pt}| = 2736$ Hz) has a central doublet with $|^2J_{P-P}| = 14.6$ Hz that is typical for asymmetric *cis*-bis(phosphine)platinum complexes. Also, tin satellites are observed with $|^2J_{P-Sn}| = 1487$ Hz, which is typical for a phosphine *trans* to a trimethyltin ligand. The resonance at δ 31.3 ($|^1J_{P-Pt}| = 1404$ Hz) is broad such that neither $|^2J_{P-P}|$ nor $|^2J_{P-Sn}|$ can be distinguished. Expected phosphorous–tin *cis*-couplings are generally small and tin satellites could easily be masked by the broad resonance. Also, phosphines that are *trans* to boryl ligands have been observed to display broad resonances in other platinum boryl complexes and the magnitude of $|^1J_{P-Pt}|$ is consistent with phohsphorous *trans* to boron.

Recrystallization of **4** from a CH_2Cl_2 solution layered with EtOH provided yellow parallelipipeds. X-Ray crystallographic analysis confirmed the *cis* conformation (Figure 14). The compound is pseudo-square planar and distortion from planarity is reduced due to the arrangement of the bis(dimethyl)amino ligand. The Pt–B bond distance is long (2.130(8) Å) relative to other late-metal boron linkages (see above). The amino groups are oriented in a fashion favorable for π-bonding between the lone pair on nitrogen and the p orbital on boron. An indication of this interaction may be found in the B–N distances of 1.430(11) and 1.426(12) Å, which are slightly shorter than the B–N bond

24

lengths obtained for the tris(amino)borane, $B(NMe_2)_3$ (1.441(1), 1.434(1), and 1.441(1) Å).[101]
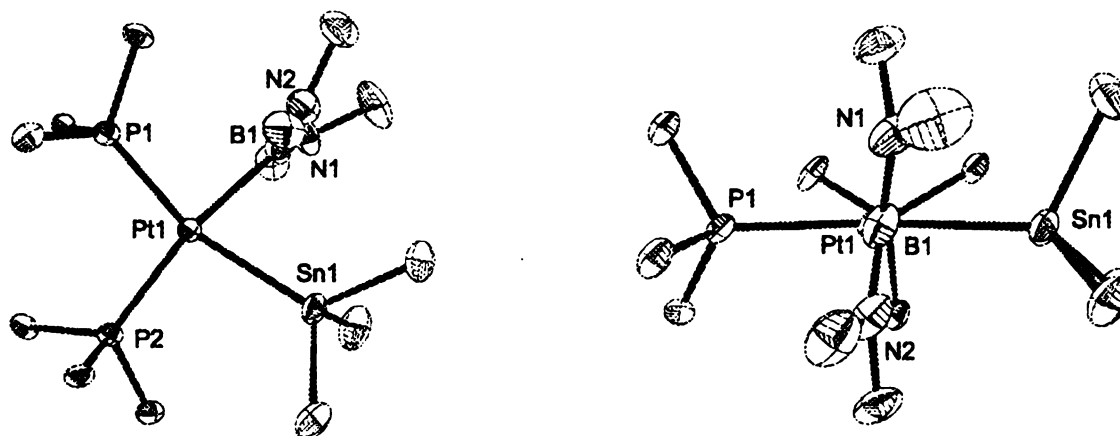
Figure 14. Two different views of compound **4**. Thermal ellipsoids are at 30 %. Only the *ipso* carbons of the triphenylphosphine ligands are shown for clarity.

Table 3. Selected bond lengths and angles for **4**.

bond	distance (Å)	bonds	angle (deg)
Pt(1)–B(1)	2.130(8)	B(1)–Pt(1)–P(1)	88.4(2)
Pt(1)–P(1)	2.297(2)	B(1)–Pt(1)–P(2)	169.7(2)
Pt(1)–P(2)	2.362(2)	P(1)–Pt(1)–P(2)	101.89(6)
Pt(1)–Sn(1)	2.6352(7)	B(1)–Pt(1)–Sn(1)	75.1(2)
N(1)–B(1)	1.430(11)	P(1)–Pt(1)–Sn(1)	163.16(5)
N(2)–B(1)	1.426(12)	P(2)–Pt(1)–Sn(1)	94.67(5)
		N(2)–B(1)–N(1)	120.6(7)
		N(2)–B(1)–Pt(1)	120.2(6)
		N(1)–B(1)–Pt(1)	119.1(6)

Given the static arrangement of the methyl groups of the bis(amino)boryl ligand obtained from the crystal structure, a single resonance in the ^1H NMR indicates dynamic behavior. Decreasing the temperature results in decoalescence of the fast exchange singlet. The slow limit of exchange is reached at –70 °C where two sharp peaks appear (Figure 15). The coalescence temperature is at –20 °C. If the static structure determined

25

by X-Ray analysis holds true at low temperature in solution, then the dynamic behavior is readily explained. The view down the B–Pt–P(2) axis reveals two methyl environments. One pair of methyl groups is internal and the other is external, i.e., pointing towards or pointing away from the axis, respectively. At elevated temperatures, however, rotation about the B–N bonds would lead to coalescence into a single resonance.
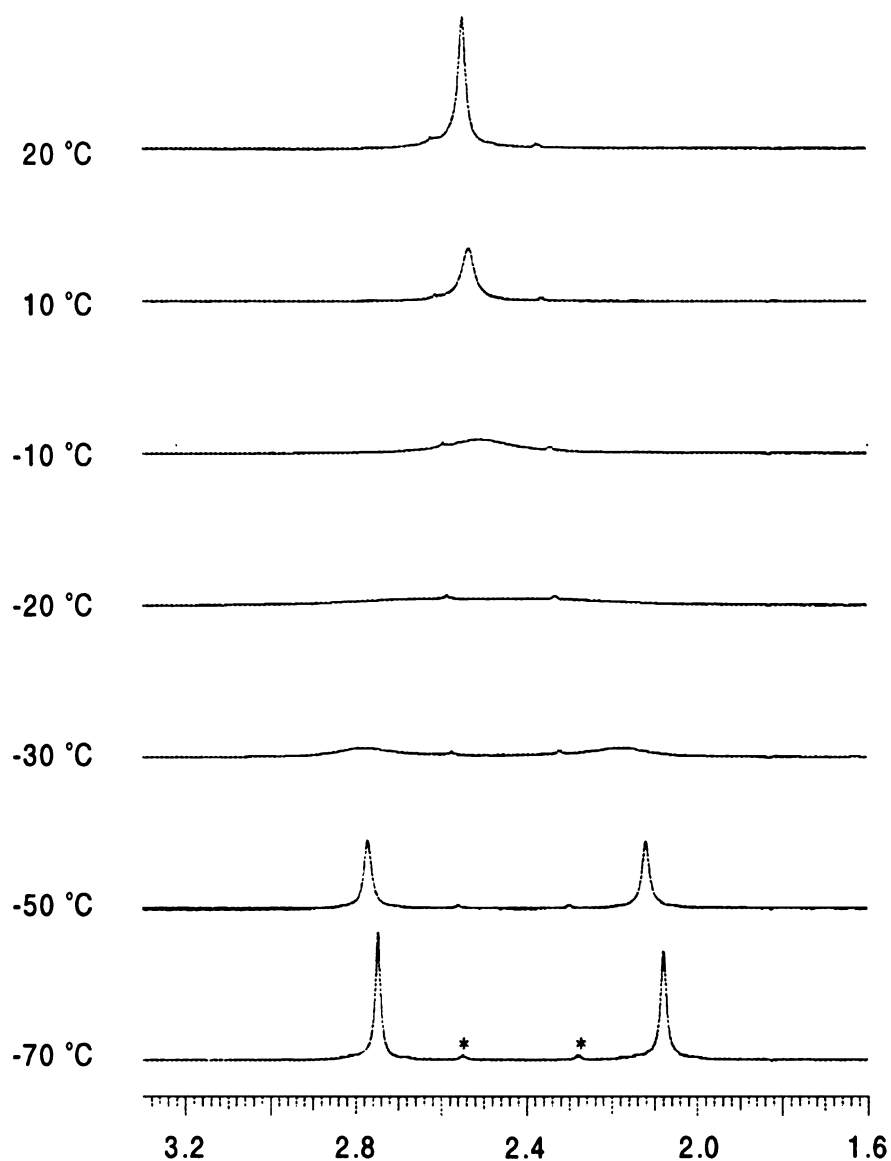
Figure 15. Variable temperature NMR of the amino methyl groups of compound **4** in CD₂Cl₂. Starred resonances at δ 2.3 and 2.55 indicate impurities.

Given the ability of the diboryl compounds, **2** and **3**, to catalytically add diboron compounds to alkynes, and the desire to add heteroborane compounds to alkynes, the catalytic reactivity of **4** was examined. Several alkynes were reacted with Me₃Sn– B(NMe₂)₂ in the presence of **4** (5 mole percent). Catalytic addition does occur but in a far

less efficient fashion than other known systems. For example, **4** requires 36 hours at 80 °C to convert 4-octyne to the 4-boryl-5-stannyl-oct-4-ene product. Related conversions by Pd(0) catalysts occur within an hour at room temperature.[100] Also, with the exception of terminal aliphatic alkynes, selectivity of the addition was poor. Finally, unlike the diboryl compounds **2** and **3**, compound **4** did not survive the reaction conditions. Given these results, this reaction was not pursued further.[102]

Metathesis Reactivity of Group 10 Complexes

Since various related dialkyl complexes are known and a wealth of mechanistic information concerning reactivity of these compounds exist, these systems seemed ideally suited for surveying potential metatheses between metal–carbon and boron–boron bonds. With this in mind, we chose to investigate reactivity of the metallacyclopentane complex, $(PPh_3)_2Pt(CH_2)_4$ (**9**) with B_2Cat_2 since **9** exhibits exceptional stability in comparison to other Pt(II)-dialkyl species, and the decomposition pathways for **9** are well documented. Compound **9** reacts cleanly with two molar equivalents of B_2Cat_2 at 95 °C to form cis-$(PPh_3)_2Pt(BCat)_2$ quantitatively as judged by ^1H NMR. The organic portion of the metallocyclopentane is converted quantitatively to $CatB(CH_2)_4BCat$. When the reaction scaled was increased, **2** and the organodiborane were isolated in 68 and 47 % yields, respectively. It is noteworthy that formation of 1- or 2-butenes, which are known byproducts of the thermal decomposition of **9**, are not observed. Metathesis in this system appears to be general as CatB-BCat also exhibits similar reactivity with other dialkyl and diaryl bisphosphine complexes of platinum (Figure 16). These results marked the first clear demonstration of metathesis reactions of B–B bonds with M–C bonds.

28
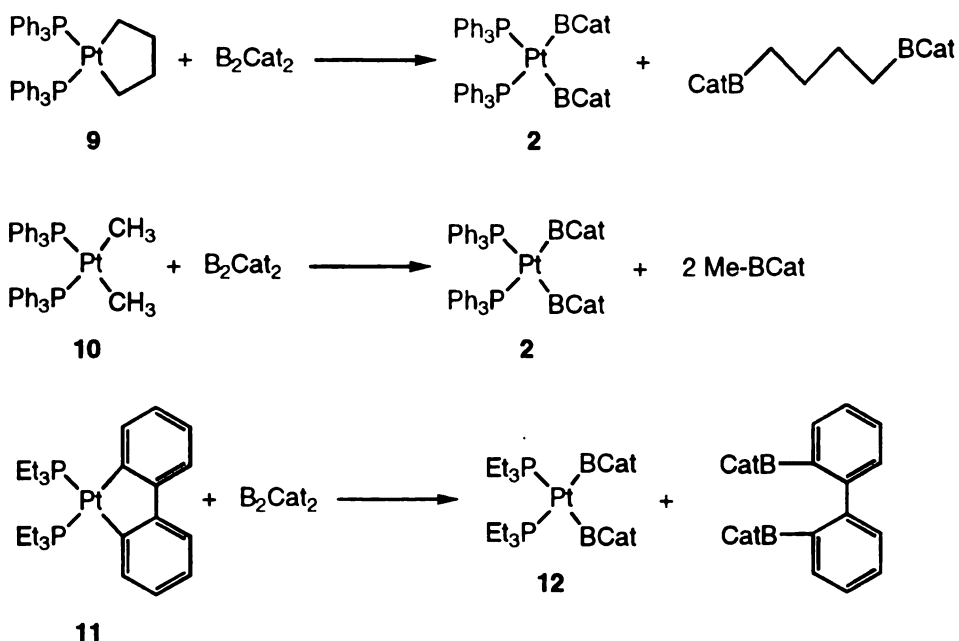
Figure 16. Reactivity of B_2Cat_2 with dialkyl and diaryl bisphosphine platinum complexes.

Kinetic analysis of this reaction revealed a first order dependence in [9] and zero order in [B_2Cat_2]. Since bisphosphine complexes of platinum are well known for dissociative pathways the phosphine dependence was examined. Unfortunately, when triphenylphosphine was added significant amounts of 1-butene were observed in the ^1H NMR. This result was not entirely unexpected as Whitesides has reported accelerated decomposition of the platinacyclopentane with the addition of triphenylphosphine. Even though a dissociative pathway cannot be independently confirmed, examination of the activation parameters extracted from an Eyring plot could argue in favor of or against phosphine dissociation. The sign and magnitude of the entropic term would seem to lend support to a dissociative pathway; $\Delta H^{\ddagger} = 29.7$ kcal/mol and $\Delta S^{\ddagger} = 11$ e.u.

A reasonable mechanism (Figure 17) that can be envisioned for this reaction is similar to related hydrogenations.[103] Initial phosphine dissociation generates a reactive three coordinate Pt (II) intermediate. Subsequent oxidative addition of B_2Cat_2 forms a Pt

(IV) intermediate which rapidly loses organodiborane. Trapping of the platinum fragment by phosphine and B_2Cat_2 would give compound 2.
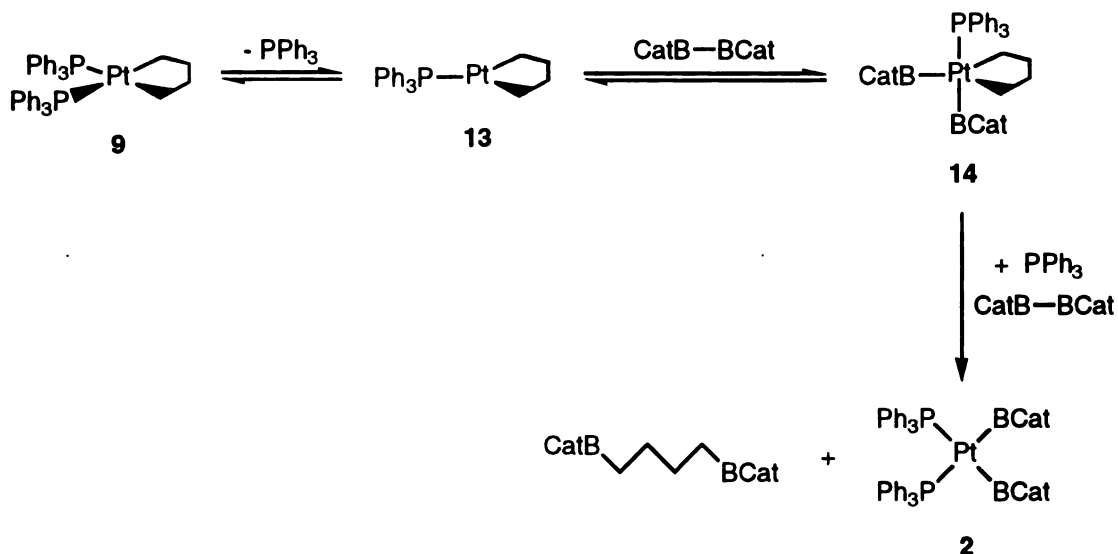
Figure 17. Proposed mechanism for the reaction of B_2Cat_2 with 9.

Substituent Effects on Boryl Ligands

Some discussions regarding the *trans*-influence of boryl ligands and the related issue of π back-bonding to the boryl from a transition metal center have recently appeared.[7,104] The relatively long Pt–P bond distances *trans* to $-BR_2$ moieties indicated that boryl ligands have a strong *trans* influence. The magnitude of the *trans* influence has been estimated by comparing $|^1J_{Pt-P}|$ values within the series of *cis*-$(PPh_3)_2PtX_2$ compounds, which has been shown to decrease with increasing *trans* influence of X for a series of compounds. Thus, the progression of $|^1J_{Pt-P}|$ for X = Cl >> Ph > BR_2 does support the notion that boryl ligands are stronger field ligands than their aryl counterparts.[105] An ordering of *trans* influence strength according to substitution on boron can also be made

using this method. [31]P data for compounds that contain triphenylphosphine ligands *trans* to boryl ligands support the progression of BCat < BPin < B(NMe₂)₂.

Although it is clear that boryl ligands have a strong *trans* influence, the explanations given so far tend to rely simply on the stability of boron to act as a π–acceptor. The real reasons are more likely due to a combination of factors. The arguments put forth so far have not taken into account substituents on the boryl itself. For instance, substituents with atoms that are able to interact electronically with the boron p orbital would be expected to affect the ability of the metal to back-bond with boron (Figure 18). In the case of oxygen based boryl ligands (example A), the lone pairs on oxygen are not aligned for meaningful interaction with the empty p orbital of boron. It is convenient, therefore, to assume that the short bond length is caused by strong π back-bonding with the metal. In contrast, the bis(dimethylamino)boryl ligand is perfectly aligned for an interaction between the empty p orbital of boron and the lone pairs on the nitrogens (example B). Electron donation into boron's p orbital should hinder π back-bonding from the platinum metal center and prevent significant shortening of the Pt–B bond. The longer Pt–B bond in *cis*-(PPh₃)₂Pt(SnMe₃)[B(NMe₂)₂] appears to contrast the expected trend in *trans* influence based solely on $|^1J_{Pt-P}|$. Clearly, there are other factors at work.
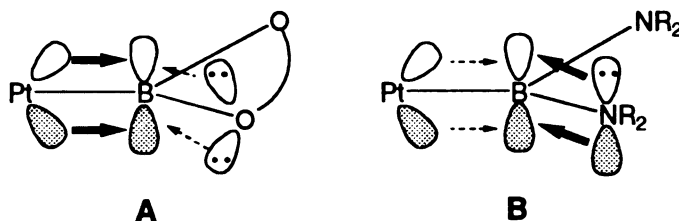
Figure 18. Simple orbital diagrams illustrating π bonding effects in boryl complexes.

The influence of the boryl ligand on $|^1J_{Pt-P}|$ and the apparent absence of a correlation to Pt–B bond distances could be explained by inductive effects. The difference in

electronegativity for boron and oxygen is significantly larger than the difference between boron and nitrogen (Figure 19, examples C and D). Therefore, alkoxide substituents should have a greater capacity to remove electron density from boron. In turn, this would lessen the σ donating ability of the bis(alkoxy)boryl ligand relative to the bis(dimethylamino)boryl ligand.
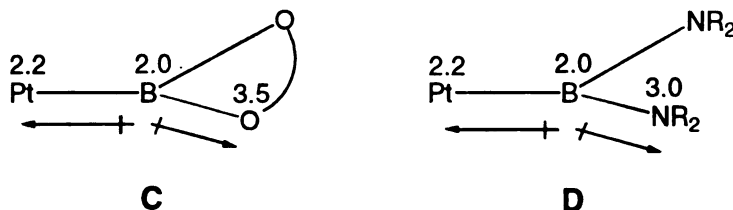
Figure 19. Simple diagrams illustrating inductive effects in boryl complexes.

Certainly, more work is needed to determine the extent of substituent effects and their consequences on the trans influence and bond length in metal boryl systems.

CHAPTER 3

PLATINUM MEDIATED DIBORATION OF OLEFINS AND ALKYNES

Mechanism of Stoichiometric Diboration of Alkynes

Prior to this work, detailed mechanistic information regarding the metal-mediated C–B bond formation was sparse. The earliest work involved H–B activation relating to hydroboration promoted by Wilkinson's catalyst.[18,46,106,107] More recent work has been performed in early to mid transition metal systems, again involving H–B activation.[24,108,109] Despite this, examples where insertions into metal boron bonds proceed cleanly are rare, and factors which determine product selectivities are not well understood.

The previous chapter described the reactivity of simple B–B bonds with olefin, alkyne, and organometallacyclic bis(triphenylphosphine) group 10 complexes. In the case of platinum complexes, $(RO)_2B–B(OR)_2$, $((OR)_2 = Cat^{2-}$ or $Pin^{2-})$ reacted smoothly to generate a common diboryl complex, $(PPh_3)_2Pt(BCat)_2$ (2) or $(PPh_3)_2Pt(BPin)_2$ (3). This species has been postulated by Miyaura and Suzuki to be the active catalyst in the catalytic diboration of alkynes mediated by $(PPh_3)_4Pt$ (8b).[90,110] Preliminary experiments showed that the pure diboryl complex, cis-$(PPh_3)_2Pt(BCat)_2$, catalyzed the addition of CatB–BCat to alkynes, consistent with the supposition put forth by Miyaura and Suzuki. Under catalytic conditions, 2 was the sole platinum containing species in solution as judged by NMR spectroscopy. Since 2 can be prepared and isolated cleanly, this system is ideally suited for addressing fundamental issues of B–C bond formation in this system.[111]

The proposed mechanism for the diboration of alkynes in the presence of 8b is shown in Figure 20. In this mechanism, a species related to 2 was suggested to be the active

catalyst, and the initial B–C bond forming reaction is insertion of the alkyne into the Pt–B bond of 3. Reductive elimination from an alkenylboryl species generates "(PPh₃)₂Pt" and the diborated alkene product. Subsequent oxidative addition of PinB–BPin to "(PPh₃)₂Pt" completes the catalytic cycle.
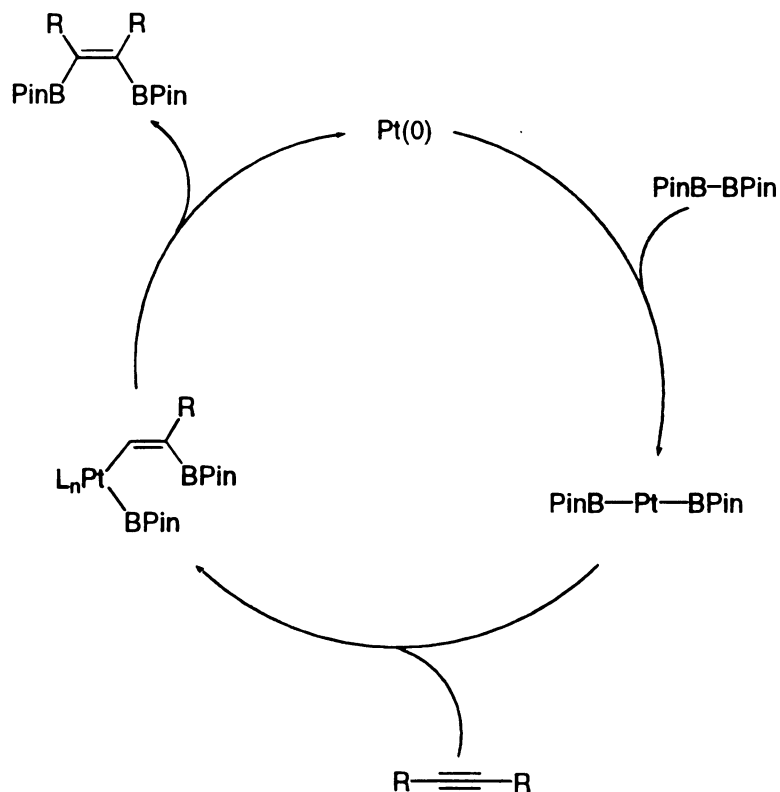
Figure 20. Pathway proposed by Miyaura and Suzuki for the platinum catalyzed diboration of alkynes.

While NMR data indicated that 3 was present under reaction conditions, no experimental evidence was offered to support the postulated mechanism. A better understanding of the steps preceding B–C bond formation could prove useful in designing systems that diborate other unsaturated substrates, however, direct study of the

catalytic reaction would likely be complex. Therefore, in order to gain insights into the mechanism, stoichiometric restraints were applied to diboration mediated by **2** (Eq 9).

$$(PPh_3)_2Pt(BCat)_2 \ + \ Xs\ 4\text{-octyne} \quad \longrightarrow \quad$$

2

$$(PPh_3)_2Pt(\eta^2\text{-}4\text{-octyne})$$

5

$+$

$$\underset{^nC_3H_7}{\overset{CatB}{\diagdown}}C = C \underset{^nC_3H_7}{\overset{BCat}{\diagup}}$$

(9)
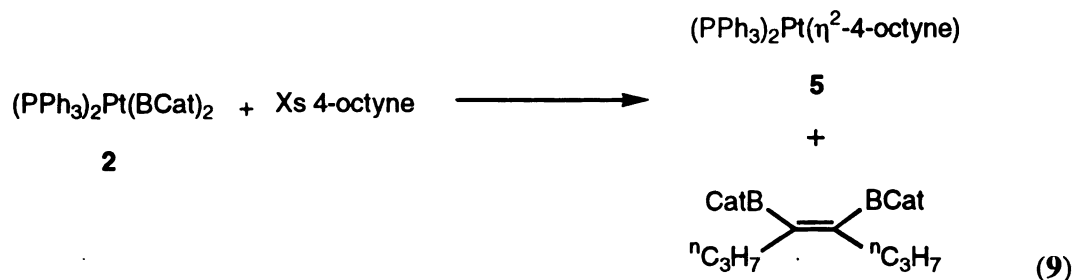
In the absence of added diboron reagent, a clean reaction was observed when excess alkyne was present to trap "$(PPh_3)_2Pt$" as $(PPh_3)_2Pt(\eta^2\text{-alkyne})$ (**5**). Two distinct pathways that involve bimolecular reactions between **2** and alkyne are shown in Figure 21. In both cases, alkyne insertion is presumed to be rate limiting. Both rate laws (Eqs 10 and 11) require a first order dependence in [**2**] and [RC≡CR], and, although these two pathways are mechanistically distinct, they can not be distinguished if intermediate **15** is undetectable.
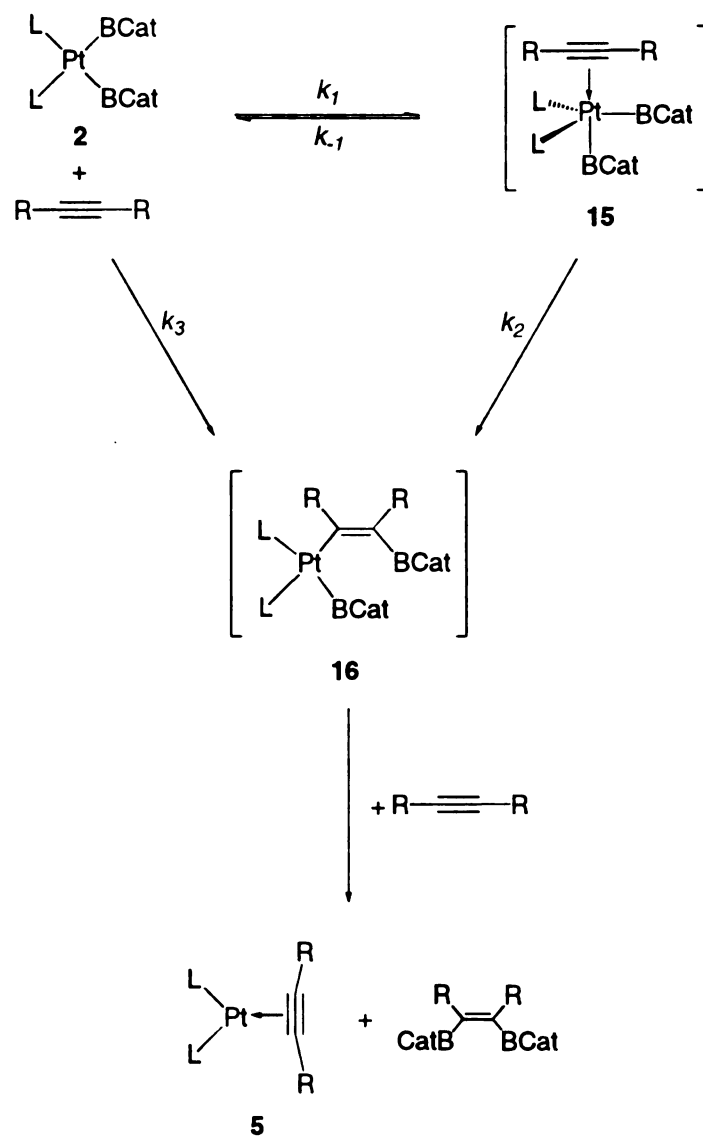
Figure 21. Simple bimolecular pathways for the diboration reaction.

$$\frac{-d[2]}{dt} = \frac{k_1 k_2}{(k_{-1} + k_2)} [2][RC\equiv CR]$$

(10)

$$\frac{-d[2]}{dt} = k_3 [2][RC\equiv CR]$$

(11)

When the reaction in Eq 9 was monitored under pseudo first-order conditions with respect to alkyne concentration, plots of ln[2] vs. time were linear over three half-lives. This suggested that the reaction in Eq 9 is first order in [2]. Although the limited solubility of [2] prevented determination over a broad concentration range, k_{obs} appears to be invariant with respect to [2]. Significantly, varying the alkyne concentration had no effect on k_{obs} (Figure 22). Thus, the mechanisms corresponding to the rate laws in Eqs 10 and 11 can be excluded as the observed kinetics are consistent with the rate law in Eq 12.
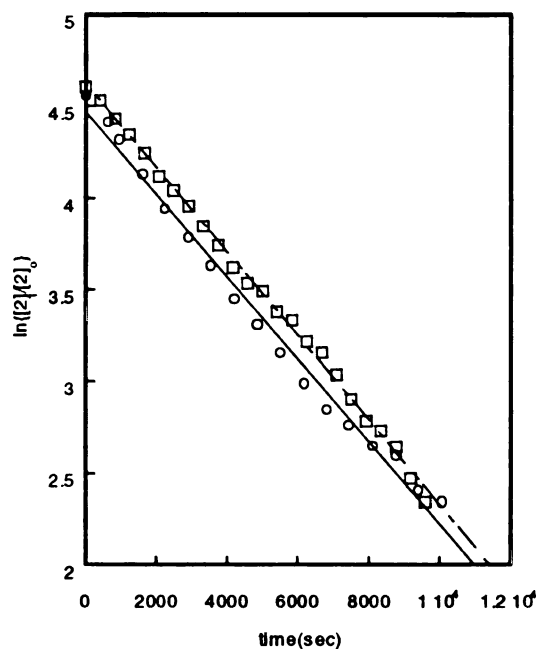
Figure 22. Plots of ln[2] versus time for the reaction of 2 with 4-octyne at 70 °C. ($[2]_o$ = 8.7 mM; O [4-octyne]$_o$ = 27 mM;   [4-octyne]$_o$ = 52 mM).

$$\frac{-d[2]}{dt} = k_{obs}[2] \tag{12}$$

37

Another possible mechanism takes into account a pathway which involves phosphine dissociation. Dissociative pathways leading to three-coordinate intermediates have been invoked for reactions involving reductive elimination in alkyl(bisphosphine)M(II) systems (M = Pd, Pt).[103,112-114] The exclusion of the mechanisms in Figure 21, therefore, suggested this route. The reaction in Eq 9 was monitored at various phosphine concentrations in order to assess this possibility. The addition of phosphine clearly suppressed the reaction rate, and plots of $1/k_{obs}$ vs. [PPh$_3$] were linear (Figure 23).
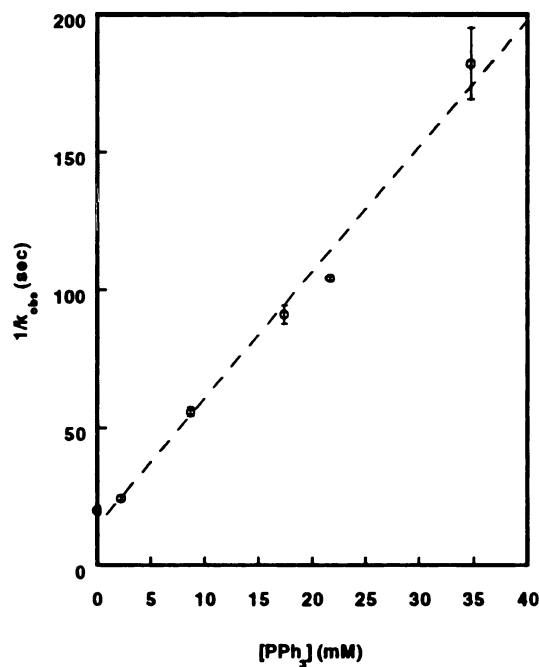
Figure 23. Plot of $1/k_{obs}$ versus [PPh$_3$] for the reaction of 2 with 4-octyne at 90 °C in C$_6$D$_6$. ([2]$_o$ = 8.7 mM, [4-octyne]$_o$ = 52 mM).

Two mechanisms that involve dissociative first steps are shown in Figures 24 and 25. In Figure 24, phosphine dissociation is presumed to be rate limiting, while the subsequent

38

coordination and insertion steps are rapid. In Figure 25, alkyne insertion is presumed to be the rate-limiting step, and **2**, **17**, and **18** are in rapid equilibrium. Unfortunately, the reverse reactions of alkyne coordination or insertion have not been able to be studied in this system, however, crossover experiments showed that elimination of the diborated alkene is irreversible. When a solution of **5** and 4,5-diboryl-4-octene are heated in the presence of 3-hexyne, the formation of 3,4-diboryl-3-hexene is not observed. It should also be noted that the inability to observe intermediates has no bearing on the choice of mechanism, since **2** can be thermodynamically favored to the extent that **17** and **18** are not detectable.
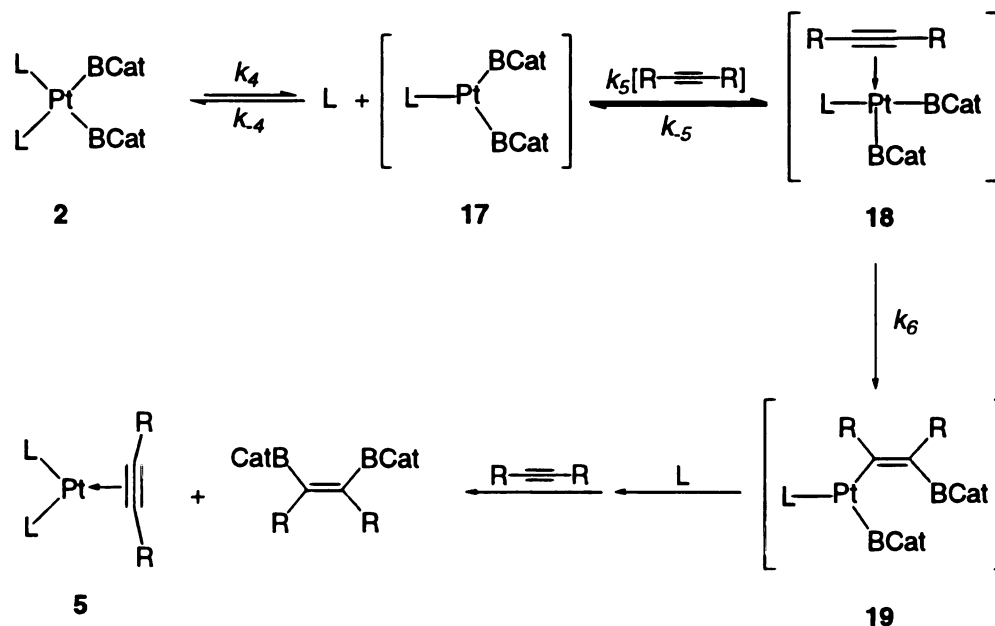
Figure 24. Steady state pathway for the diboration reaction.

39
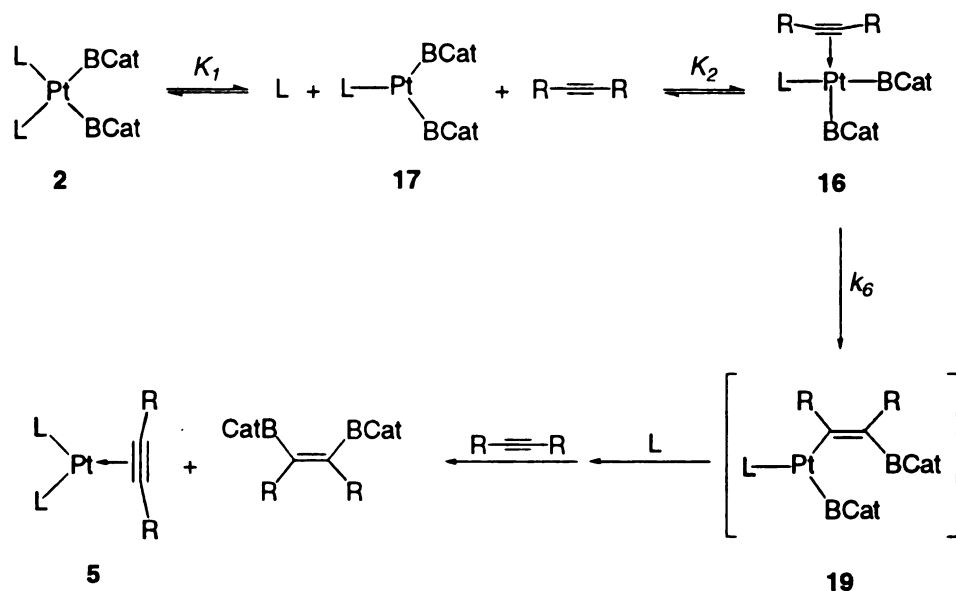
Figure 25. Equilibrium pathway for the diboration reaction.

Simplified rate expressions can be derived by applying steady-state or equilibrium approximations to Figures 24 and 25, respectively.[115] Application of the steady state approximation to Figure 24 gives the rate law and k_{obs} expression shown in Eqs 13 and 14, while the equilibrium treatment for Figure 25 gives the expressions in Eqs 15 and 16.

$$\frac{-d[2]}{dt} = k_{obs}[2] \tag{13}$$

$$k_{obs} = \frac{k_4 k_5 k_6 \,[RC\equiv CR]}{k_{-4}(k_{-5} + k_6)[PPh_3] + k_5 k_6\,[RC\equiv CR]} \tag{14}$$

$$\frac{-d[2 + 17 + 18]}{dt} = k_{obs}\,[2 + 17 + 18] \tag{15}$$

$$k_{obs} = \frac{-K_1 K_2 k_6 [RC\equiv CR]}{K_1 + [PPh_3] + K_1 K_2 [RC\equiv CR]} \quad (16)$$

An inverse dependence on phosphine concentration is consistent with either mechanism, as Eqs 14 and 16 reduce to Eqs 17 and 18 when the phosphine term dominates the denominator. When $[PPh_3] \approx 0$, Eq 6 reduces to $k_{obs} = k_4$, while eq 14 yields Eq 19. In principle, the two mechanisms are distinguishable in the absence of phosphine if $K_1 \gg K_1 K_2 [RC\equiv CR]$. In this regime the mechanism in Figure 25 requires an alkyne dependence. We do not see an alkyne dependence at any concentration of alkyne. Thus, if

$$k_{obs} = \frac{k_4 k_5 k_6 [RC\equiv CR]}{k_{-4}(k_{-5} + k_6)[PPh_3]} \quad (17)$$

$$k_{obs} = \frac{-K_1 K_2 k_6 [RC\equiv CR]}{[PPh_3]} \quad (18)$$

$$k_{obs} = \frac{-K_1 K_2 k_6 [RC\equiv CR]}{K_1 + K_1 K_2 [RC\equiv CR]} \quad (19)$$

the mechanism in Figure 25 operates, $K_1 \ll K_1 K_2 [RC\equiv CR]$, and $k_{obs} \approx k_6$. Both Eqs 17 and 18 predict that an alkyne dependence should be observed for both mechanisms at sufficiently high phosphine concentrations ($k_{-4}[PPh_3] \gg (k_5 k_6/k_{-5} + k_6)[RC\equiv CR]$, or $[PPh_3] \gg K_1 + K_1 K_2 [RC\equiv CR]$). This is indeed the case, as k_{obs} exhibits a first order dependence on $[RC\equiv CR]$ in the presence of added phosphine (Figure 26). Thus, the kinetic data are consistent with either proposal. As the concentration of alkyne is

41

increased at constant [PPh₃], three regimes are possible; k_{-4}[PPh₃] $\gg$ (k_5k_6/k_5 +

k_6)[RC≡CR], k_{-4}[PPh₃] $\approx$ (k_5k_6/k_5 + k_6)[RC≡CR], and k_{-4}[PPh₃] $\ll$ (k_5k_6/k_5 +

k_6)[RC≡CR], or [PPh₃] $\gg$ K_1 + K_1K_2[RC≡CR], [PPh₃] $\approx$ K_1 + K_1K_2[RC≡CR], and

[PPh₃] $\ll$ K_1 + K_1K_2[RC≡CR]. Therefore, at sufficiently high concentrations of alkyne,

the value for k_{obs} could be approached for rates observed in the absence of added

phosphine. Unfortunately, the concentrations of alkyne needed were exceedingly high to

make to make this comparison.
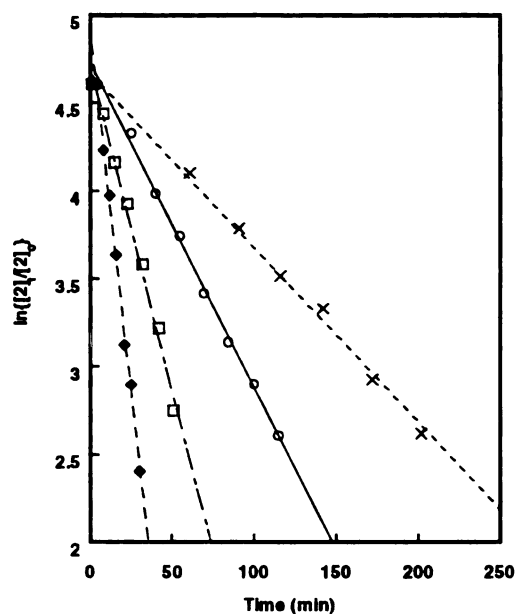
Figure 26. Plot of ln{[2]$_t$/[2]$_o$} versus time for the reaction of **2** with 4-octyne in the

presence of PPh₃-d_{15} at 105 °C in C₆D₆. ([2]$_o$ = 8.7 mM, [PPh₃-d_{15}] = 27 mM; ✕ [4-

octyne]$_o$ = 27 mM; ○ [4-octyne]$_o$ = 52 mM; ☐ [4-octyne]$_o$ = 105 mM; ◆ [4-octyne]$_o$ =

208 mM)

Attempts to determine activation parameters from the temperature dependence of k_{obs} were not successful due to the rapid rate of reaction and poor solubility of **2**. This problem was circumvented by suppression of the reaction rate via addition of phosphine, and k_{obs} was measured from 70 to 110 °C. The Eyring plot in Figure 27 yielded the following activation parameters: $\Delta H^{\ddagger}$ 25.9(7) kcal/mol and $\Delta S^{\ddagger} = 4(2)$ e.u. The magnitude of $\Delta S^{\ddagger}$ would seems to disfavor phosphine dissociation as the rate-limiting step in the mechanism;[116] nonetheless, rate-limiting dissociation is not categorically excluded as contributions from other steps preceding the rate determining step could cause a decrease in the value of $\Delta S^{\ddagger}$.[117] In most cases, a negative value for $\Delta S^{\ddagger}$ might be expected for a pathway that involves rate-limiting alkyne insertion into the Pt–B bond. Investigations of C≡C and C=C insertions into M–X bonds, however, indicate that the magnitude of $\Delta S^{\ddagger}$ can be small, and its sign can be either positive or negative.[118,119]
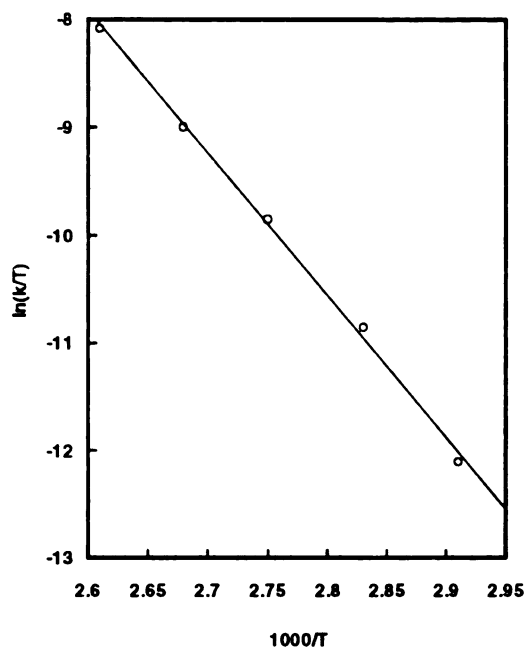
Figure 27. Eyring plot for the diboration of 4-octyne by **2** in the presence of PPh_3-d_{15} in C_6D_6. ($[2]_o$ = 8.7 mM; $[4$-octyne$]_o$ = 52 mM; $[PPh_3$-$d_{15}]$ = 8.7 mM; T = 343 to 383 K, $\Delta H^{\ddagger}$ = 25.9(7) kcal/mol, $\Delta S^{\ddagger}$ = 4(2) e.u.)

In the absence of phosphine, k_{obs} reduces to the rate constant for the rate-determining step in the proposed mechanisms. Thus, boration rates for different alkynes should be identical if phosphine dissociation is rate limiting. On the other hand, if alkyne insertion is rate limiting, then it might be expected that steric and/or electronic variations in the alkyne could affect k_{obs}. In order to assess this question 1-hexyne, phenylacetylene, and diphenylacetylene were reacted with **2**. For 1-hexyne and phenylacetylene, ^{31}P NMR indicated that several metal-containing products form, which unfortunately prevents comparisons between internal and external alkynes. The probable source of the decomposition is the acetylenic proton; therefore, the reaction between **2** and diphenylacetylene was examined. In this case, boration proceeded smoothly, though at a much slower rate in comparison to the dialkyl substituted alkyne, 4-octyne. This result

44

clearly implies that k_{obs} is affected by the nature of the alkyne and that phosphine dissociation is not slower than the alkyne coordination and insertion steps.

The effects of electronic perturbation of the alkyne on the rate of boration was explored by utilizing 4,4'-substituted diarylacetylenes. Boration of 1,2-di-p-anisylacetylene proceeded at a slower rate than the analogous reaction with diphenylacetylene. Unfortunately, boration of 1,2-di-p-(trifluoromethyl)phenylacetylene was too rapid for rigorous kinetic analysis, and other diarylacetylenes did not yield tractable data. The unexpected rapid rate for the trifluoromethyl moiety is somewhat curious as the reaction rate was expected to increase by a factor of only two based on linear free-energy relationships and tabulated σ_{para} values.[120] In this case, rates for substituted diphenylacetylenes appear to offer little information regarding the boration mechanism. Regardless, the results of the data argue that the rate of boration is indeed sensitive to electronic perturbations in substituted diarylacetylenes.

From this stoichiometric investigation emerges an obvious feature concerning reactivity in this system. Specifically, if **2** serves as the active catalyst under stoichiometric conditions, catalysis by **2** liberates PPh_3. This is indeed the case, as alkynes that were diborated sluggishly by catalysis originating from **8b** undergo smooth diboration when pure **2** is used.[90]

Mechanism of Catalytic Diboration of Alkynes

Solutions of the diboryl complexes, **2** and **3**, both exhibit catalytic activity for the diboration of alkynes by B_2Cat_2 and B_2Pin_2, respectively. The rate of catalysis by **2** or **3** is reasonably similar, however, quantitative comparisons of rates were not possible due to deviations from pseudo first-order consumption of alkynes in the absence of added phosphine. The cause of these deviations is not clear; however, boration by other boryl

species generated in the presence of excess diboron reagent could account for the observations.

When phosphine is present during catalytic borations mediated by **2**, well-behaved, pseudo first-order consumption of 4-octyne was observed. Since **2** was the only Pt containing complex detected (as judged by ^{1}H and ^{31}P NMR) when catalytic diborations were run in the presence of added phosphine, and comparisons to the stoichiometric reactivity of **2** could be made, the kinetics of the diboration of 4-octyne, catalyzed by **2**, were investigated.

Two potential mechanisms for this catalysis are illustrated in Figures 28 and 29. Similarities to the mechanisms proposed for the stoichiometric reaction of **2** with alkyne are readily apparent, such as phosphine dissociation from **2**, alkyne insertion into the Pt-B bond of **18**, and reductive elimination of the diborated alkene from **19**. In contrast to the stoichiometric reaction, however, the concentration of **2** remains constant throughout the course of the catalysis. Rates for equilibration between species **2** and **17** and species **17** and **18** are considered to be rapid compared to the rate for alkyne insertion. As in the treatment of the stoichiometric reaction, application of either steady-state or equilibrium approximations gives rate laws for the consumption of alkyne.
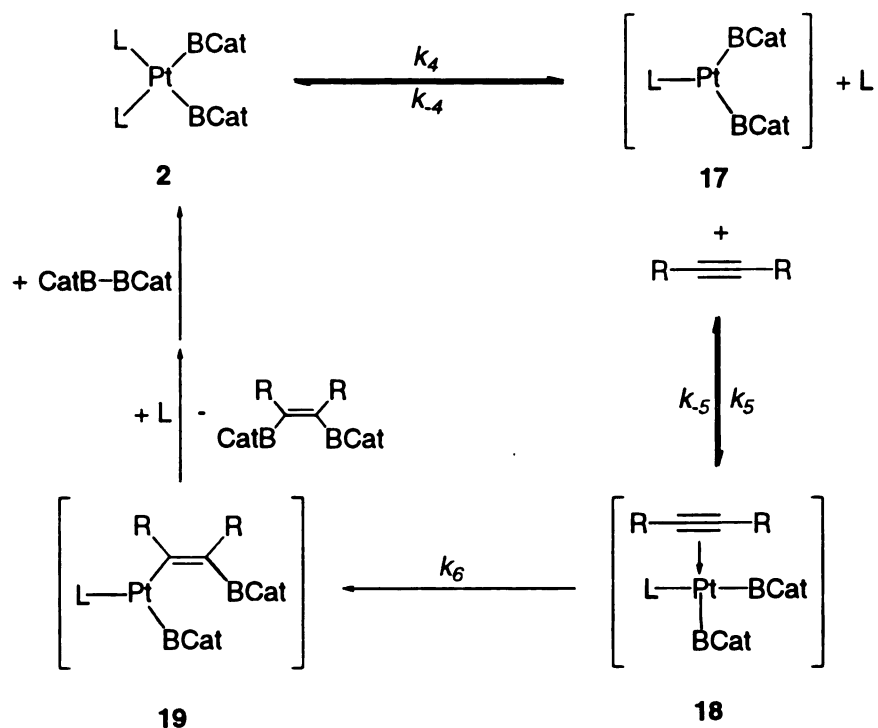
Figure 28. Steady state pathway for the catalytic diboration of alkynes.
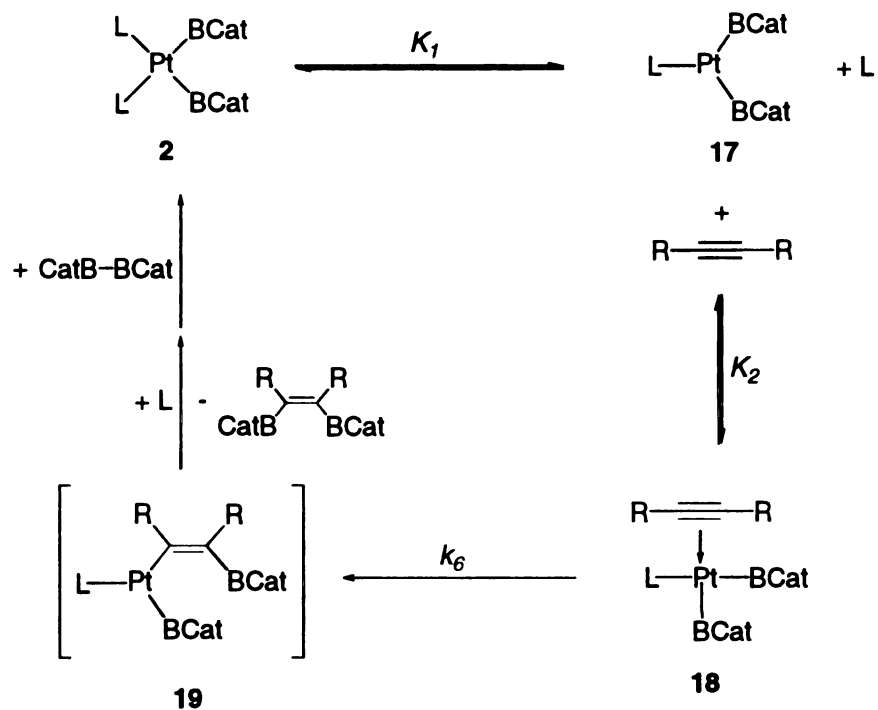
Figure 29. Equilibrium pathway for the catalytic diboration of alkynes.

$$\frac{-d[\mathrm{RC}{\equiv}\mathrm{CR}]}{dt} = \frac{k_4 k_5 k_6[2]}{k_{-4}(k_5 + k_6)[\mathrm{PPh}_3] + k_5 k_6[\mathrm{RC}{\equiv}\mathrm{CR}]}[\mathrm{RC}{\equiv}\mathrm{CR}] \tag{20}$$

$$\frac{-d[\mathrm{RC}{\equiv}\mathrm{CR} + 17 + 18]}{dt} = \frac{-K_1 K_2 k_6[2]}{[\mathrm{PPh}_3] + K_1 K_2[2]}[\mathrm{RC}{\equiv}\mathrm{CR} + 17 + 18] \tag{21}$$

The rate laws in Eqs 20 and 21 simplify to Eqs 22 and 23 and Eqs 24 and 25, respectively when phosphine dominates the denominator of k_{obs}. Under these conditions both mechanisms require that the reaction is first order in [2] and [RC≡CR], and exhibits an inverse dependence on phosphine concentration. Even at modest

$$\frac{-d[\mathrm{RC}{\equiv}\mathrm{CR}]}{dt} = k_{obs}[\mathrm{RC}{\equiv}\mathrm{CR}] \tag{22}$$

$$k_{obs} = \frac{k_4 k_5 k_6[2]}{k_{-4}(k_5 + k_6)[\mathrm{PPh}_3]} \tag{23}$$

$$\frac{-d[\mathrm{RC}{\equiv}\mathrm{CR} + 17 + 18]}{dt} = k_{obs}[\mathrm{RC}{\equiv}\mathrm{CR} + 17 + 18] \tag{24}$$

$$k_{obs} = \frac{-K_1 K_2 k_6[2]}{[\mathrm{PPh}_3]} \tag{25}$$

phosphine concentrations, plots of ln[RC≡CR] vs. time in Figure 30 are linear through three half-lives confirming a first order dependence on alkyne and [2]. Also, plots of $1/k_{obs}$ vs. [PPh₃] are linear as required by Eqs 23 and 25 (Figure 31).

48
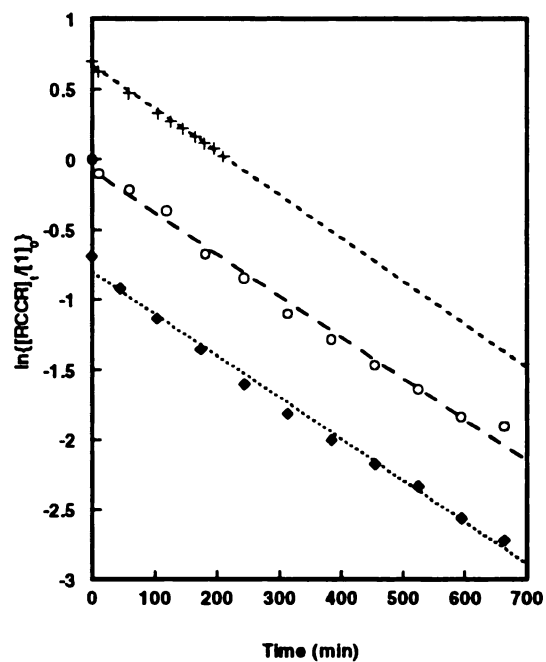
Figure 30. Plot of $\ln\{[4\text{-octyne}]_t/[B_2Cat_2]_o\}$ vs. time for the catalytic diborylation of 4-octyne by B_2Cat_2 in the presence of **2** and PPh_3 at 105 °C in C_7D_8 ($[2]_o = 7.0$ mM, $[PPh_3]$ = 55 mM; ◆ $[4\text{-octyne}]_o = 42$ mM, $[B_2Cat_2]_o = 84$ mM; O $[4\text{-octyne}]_o = 42$ mM, $[B_2Cat_2]_o = 42$ mM; + $[4\text{-octyne}]_o = 84$ mM, $[B_2Cat_2]_o = 42$ mM).

Fig

the

[B-

The

resu

com

follo

phos

mech

T

dibor

theory

stoichi
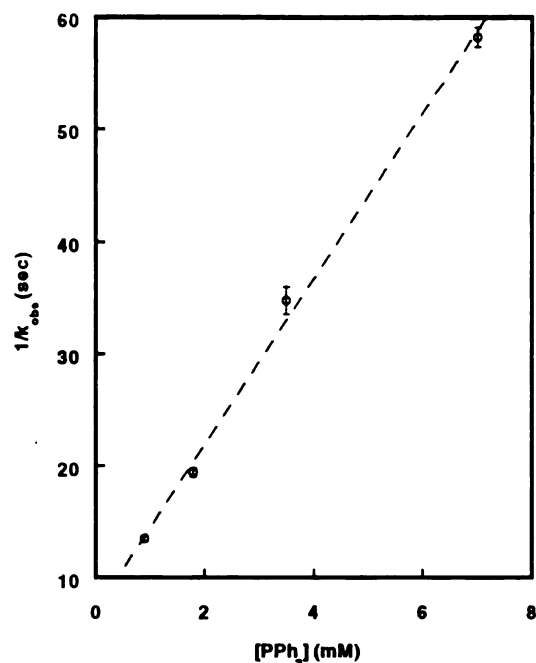
Figure 31. Plot of $1/k_{obs}$ vs. [PPh₃] for the catalytic ciborylation of 4-octyne by B_2Cat_2 in the presence of **2** and PPh_3 at 100 °C in C_6D_6 ($[2]_o = 7.0$ mM, [4-octyne]$_o = 42$ mM, $[B_2Cat_2]_o = 42$ mM).

The concentration of CatB–BCat had no effect on the rate of alkyne consumption. This result is in agreement with the ease with which CatB–BCat oxidative addition to Pt(0) complexes occurs, is consistent with the hypothesis that regeneration of **2** is rapid, and follows the rate determining step. The data from catalytic runs in the presence of phosphine are reliably reproducible, and exhibit dependencies that are required by the mechanisms in Figures 28 and 29.

The dependence of k_{obs} on [alkyne], [PPh₃], and [2] suggest that the mechanisms for diboration within the stoichiometric and catalytic manifolds are essentially identical. This theory could be verified by a direct comparison of rate constants between the stoichiometric and catalytic systems. By rearranging Eqs 18 and 25 we see that a

comparison can be made, as $K_1K_2k_6$ can be expressed in terms of k_{obs}, [PPh$_3$], and [alkyne] for the stoichiometric system and k_{obs}, [PPh$_3$], and [2] for the catalytic system (Eqs 26 and 27). The calculated values for $K_1K_2k_6$ from the stoichiometric and catalytic measurements are 0.019(3) and 0.024(3) sec^{-1}, respectively. Thus, the data, which are identical within experimental error, support the notion that the mechanisms for the diboration in both systems are identical.

$$K_1K_2k_6 \ = \ \frac{k_{obs}[\text{PPh}_3]}{[\text{RC}\equiv\text{CR}]} \tag{26}$$

$$K_1K_2k_6 \ = \ \frac{k_{obs}[\text{PPh}_3]}{[2]} \tag{27}$$

Mechanistic Concerns Regarding *cis*-(PPh$_3$)$_2$Pt(BPin)$_2$

Although the mechanism proposed for the diboration of alkynes is different than the original proposal by Miyaura and Suzuki, the results of this investigation support their assertion that diboryl complex, *cis*-(PPh$_3$)$_2$Pt(BPin)$_2$ (3), acts as the active catalyst.[90] Since 3 is readily prepared, comparison of the stoichiometric boration reaction was expected to be straightforward. In contrast to the catecholatoboryl chemistry, however, spectra recorded under ambient conditions prior to initiation of the diboration reaction indicated that an equilibrium existed between 3, 5, 4-octyne, and PinB–BPin (Eq 28). To test for reversibility of this reaction,

$$(PPh_3)_2Pt(BPin)_2 \qquad\qquad (PPh_3)_2Pt(\eta^2\text{-}RC{\equiv}CR)$$

$$\mathbf{3} \qquad\qquad\qquad\qquad \mathbf{5}$$

$$+ \qquad\qquad\qquad\qquad +$$

$$RC{\equiv}CR \qquad\qquad\qquad\qquad B_2Pin_2 \qquad (28)$$
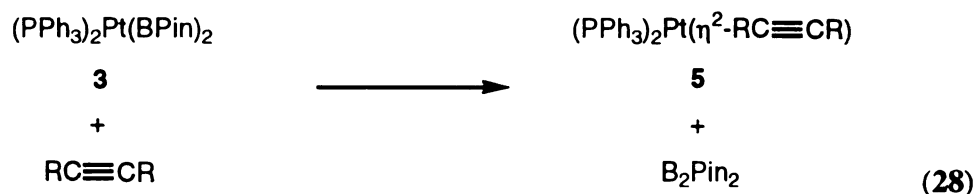
the analogous experiment was performed using a volatile alkyne, 2-butyne. The addition of 2-butyne to a C_6D_6 solution of **3** in an NMR tube showed that the alkyne complex was readily formed with simultaneous elimination of PinB–BPin. Subsequent removal of 2-butyne, in *vacuo*, regenerated **3** and confirmed the reversibility of the elimination.

Another complicating factor is the ease of B_2Pin_2 reductive elimination from *cis*-$(PPh_3)_2Pt(BPin)_2$ by the addition of PPh_3. The observed equilibria between **3**, PPh_3, PinB–BPin, and $(PPh_3)_nPt$ (n = 3, 4; **8a-b**) would obscure comparisons of the relative rates of boration for B_2Cat_2 and B_2Pin_2 under stoichiometric conditions. Since the diboration reaction prevents an accurate evaluation of the equilibrium between **3** and alkynes under usual reaction conditions (50 °C), the equilibrium constant at elevated temperature was determined by extrapolating data from a Van't Hoff plot for the equilibrium in Eq 28. (Figure 32). From these data the equilibrium constant at 50 °C was calculated to be 12.9. Thus, under typical conditions for catalytic diboration of 4-octyne (in the presence of added phosphine), **3** is the principal Pt containing species. As would be expected, the equilibrium is sensitive to the alkyne substrate. For example, when equimolar quantities of **3** and diphenylacetylene are dissolved in C_6D_6 the equilibrium is observed to lie far to the side of the alkyne complex as $(PPh_3)_2Pt(\eta^2\text{-}PhC{\equiv}CPh)$ is the only phosphine-containing species detected by ^{31}P NMR.
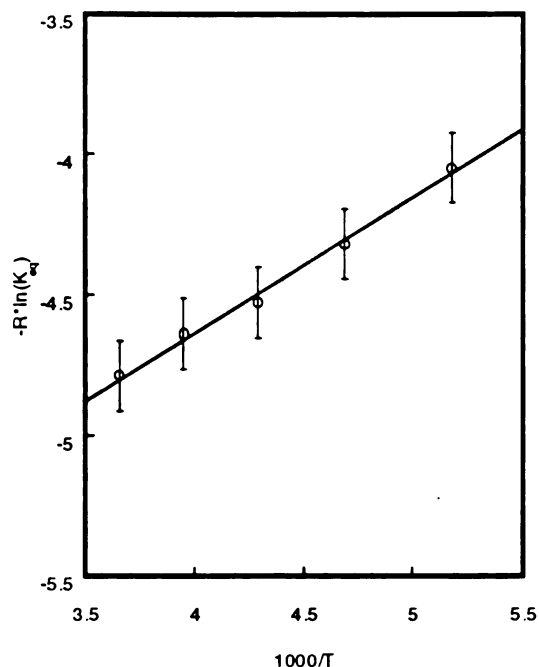
Figure 32. van't Hoff plot for the equilibrium between **3** and 4-octyne. ([3]$_o$ = 8.7 mM; [4-octyne]$_o$ = 52 mM; T = -80 °C to 0 °C; ΔH = 0.49 kcal/mol, ΔS = 6.6 e.u.)

The equilibria in the reactions of **3** with alkynes raise another possibility: that diboration in the catecholate system could be due to a bimolecular reaction between trace quantities of an alkyne complex and CatB–BCat. Despite the fact that in stoichiometric reactions between **2** and 4-octyne neither CatB–BCat nor **5** are detected in solution, alkyne complexes in this system are known to react by both associative and dissociative pathways.[121] This seems unlikely, however, as the boration rates in the stoichiometric reaction between **2** and 4-octyne do not exhibit an alkyne dependence in the absence of added phosphine. If boration proceeded through pathways that are first (or higher) order in **5**, an alkyne dependence would be expected since equilibrium concentrations of **5**, though small, are dependent on alkyne concentration.

Catalytic diboration of olefins
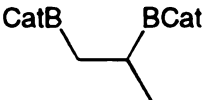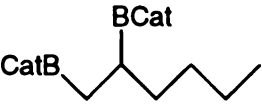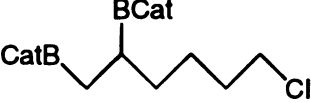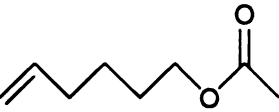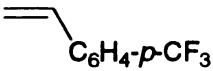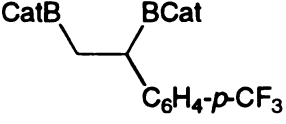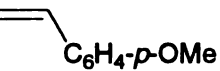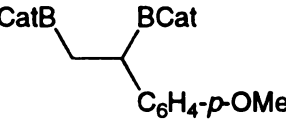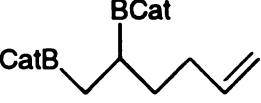
In the previous section details of the Pt-catalyzed addition of B–B bonds to alkynes mediated by cis-(PPh$_3$)$_2$Pt(BCat)$_2$ (**2**) were addressed. Although clean chemistry is observed in this system for alkynes, the analogous addition to olefins does not occur. It became apparent that formation of low-coordinate diboryl complexes, via phosphine dissociation, was necessary to mediate coordination and insertion of the alkyne into the Pt–B bond. Following that line of reasoning it seemed conceivable that catalytic activity could be enhanced, and possibly olefin diboration would be observed, if the requirement for phosphine dissociation could be eliminated. The most obvious candidates for testing this hypothesis are the base-free Pt(0) compounds reported by Stone and co-workers.

In the hopes of forming an olefin platinum diboryl complex to examine this possibility we attempted to react one and two equivalents of CatB-BCat, respectively, with Pt(nbe)$_3$ (**20**, tris(bicyclo[2.2.1]heptene)platinum(0)). In both cases a reaction takes place readily at room temperature as the solution immediately turns red in color. The inability to isolate or identify any platinum containing compounds hampered our efforts toward this goal, however, the chief organic product was a bis(boryl)bicyclo[2.2.1]heptane. From these results we reasoned that if we could not isolate an olefin boryl complex that perhaps catalysis from the olefin complexes themselves would be feasible. With this in mind equimolar amounts of norbornene and CatB-BCat were reacted in the presence of **20** (3 molar percent) in an NMR tube. Catalysis occurs at a rapid rate as diboration was complete within minutes at room temperature.

The facility with which diboration in this reaction occurred might be due to the ring strain associated with the bicyclic organic substrate, norbornene. Thus, in order to ascertain whether this procedure would be a general route to diborated alkanes, a variety

of unactivated olefins (Table 4) were examined with Pt(nbe)$_3$ and bis(cyclooctadiene)platinum(0) (**21**, Pt(COD)$_2$).[110,122]

Table 4. Products and crude yields for the diboration of selected olefins. Yields are based on the crude material following solvent evaporation.

entry	olefin	product	% yield
1	(ethylene)	CatB–CH₂CH₂–BCat	84
2	(propene)	CatB–CH₂–CH(BCat)–CH₃	87
3	(1-hexene)	CatB–CH₂–CH(BCat)–CH₂CH₂CH₂CH₃	95
4	(6-chloro-1-hexene)	CatB–CH₂–CH(BCat)–(CH₂)₃–Cl	85
5	(pent-4-enyl acetate)	CatB–CH₂–CH(BCat)–(CH₂)₃–O–C(=O)–CH₃	88
6	CH₂=CH–C_6H_4-p-CF₃	CatB–CH₂–CH(BCat)–C_6H_4-p-CF₃	90
7	CH₂=CH–C_6H_4-p-OMe	CatB–CH₂–CH(BCat)–C_6H_4-p-OMe	95
8	(1,5-hexadiene)	CatB–CH₂–CH(BCat)–CH₂CH₂–CH=CH₂	82

The reactions were typically complete after stirring for 10 minutes at room temperature. As stated above, the solution turns deep red following addition of the diboron reagent and appears to remain homogenous. Addition of mercury to the reaction mixture had no effect on the catalytic activity; however, we have not been able to identify the catalytically active species. Conversion is clean, as judged by ^{1}H and ^{11}B NMR and product yields are high. Significantly, B_2Cat_3, the decomposition product that is often observed when catecholate-substituted borane reagents are employed, is formed in only minor quantities.

A mechanism similar to the Pt-catalyzed diboration of alkynes can be envisioned for the diboration of alkenes. Following B–B bond addition to the Pt metal center, boration proceeds via insertion of the unsaturated substrate into the Pt–B bond of a Pt-diboryl species and the diborated alkane is released by B–C reductive elimination from a boryl-alkyl intermediate, as depicted in Figure 33. It is reasonable to assume that α-olefin insertion into the Pt–B bond gives a primary alkyl intermediate as related insertions into metal-carbon and metal-hydrogen bonds usually give primary metal-alkyl complexes.

R

CatB   BCat

L$_n$Pt   CatB–BCat

R

L$_n$Pt   BCat
         BCat
24

BCat
L$_n$Pt
         BCat
22

R

L$_n$Pt—BCat
CatB
23

R

R
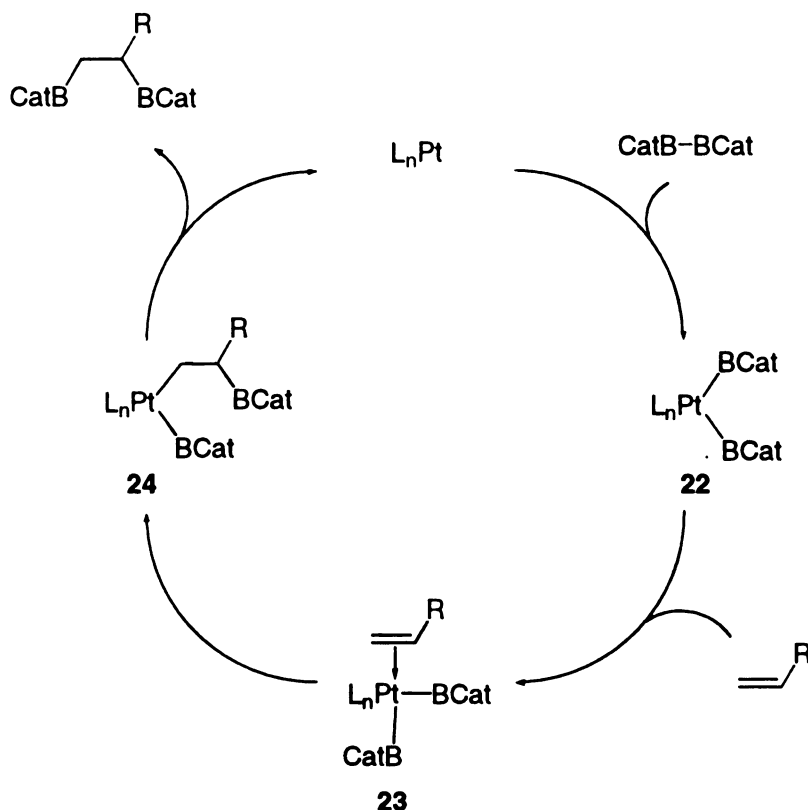
Figure 33. Proposed mechanism for the diboration of olefins by base-free Pt(0) complexes.

1,2-diborated products are observed exclusively for α-olefins and functionality on the olefin substrates is tolerated so long as the functional group resides in a position beyond the allylic carbon. For internal olefins, clean diboration is observed only for the bicyclic compounds norbornene and norbornadiene. Only one stereoisomer is formed for these substrates as the B–B bond adds preferentially to the *exo* olefin face. The stereochemistry was confirmed by deuterolysis of the boryl groups and comparison of the NMR data to the known dideuterionorbornane. Unfortunately, clean reactivity is not observed for other internal olefins. For example, the reaction between CatB–BCat and trans-3-hexene gave a complex mixture of products. ^{11}B NMR spectra indicated significant quantities of HBCat and B$_2$Cat$_3$, in addition to a broad resonance in the region typical for alkylborane

products. Similar complications were observed when diborations of other internal olefins were attempted.

Presumably, β-hydrogen elimination is the source of HBCat in the diboration reactions of internal olefins. Figure 34 shows a likely pathway that can compete with the reductive elimination of the diborated alkane from intermediate **25**. The vinylborane that is formed can then react with additional CatB-BCat to account for the complex mixture of organoborane products. Interestingly, the β-hydrogen elimination pathway does not appear to occur in the diboration of α-olefins. Although the reasons for this discrepancy are not obvious, a possible explanation is that β-hydrogen elimination could be disfavored for hydrogens attached to a boron-substituted β-carbon center.
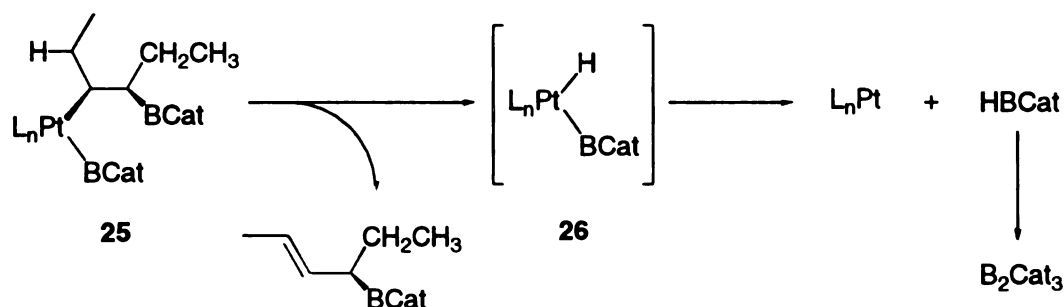
Figure 34. Decomposition pathway for internal olefins via β-hydrogen elimination.

Clean reactivity observed for the boration of norbornene and norbornadiene is not surprising since β-hydrogen elimination from the bridgehead position of intermediate **27** would form a highly strained olefin (Eq 29).

(29)
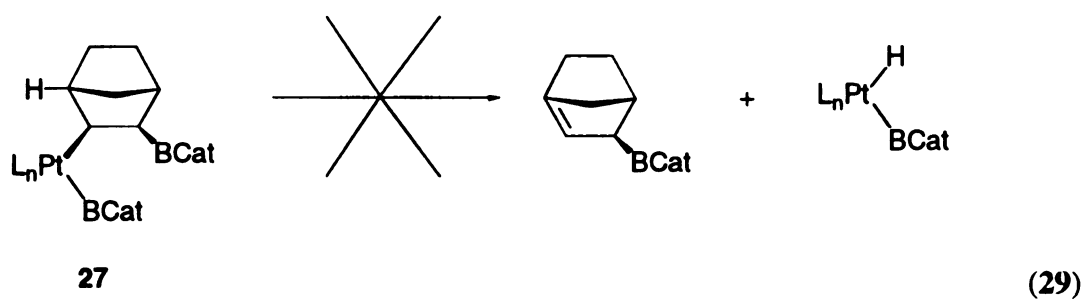
α, ω-dienes are also catalytically diborated by base-free Pt(0) compounds (Figure 35). Significantly, for 1,5-hexadiene, equimolar quantities of diene and CatB–BCat give the 1,2-diborated product exclusively.
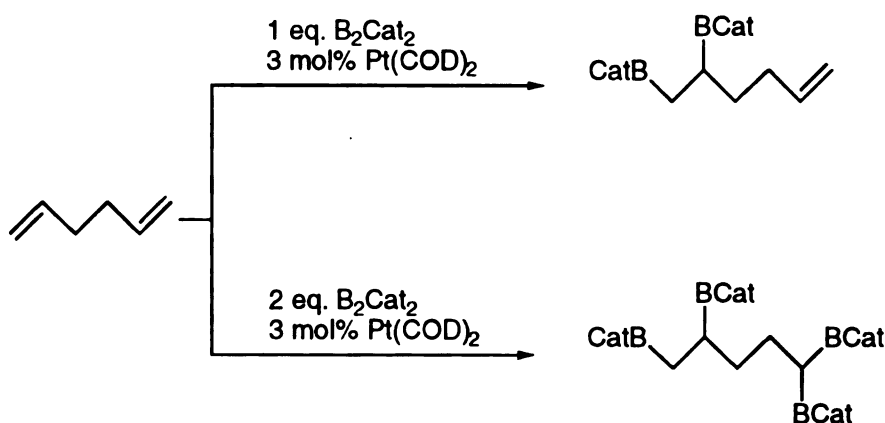
Figure 35. Selective di- and tetraboration of 1,5-hexadiene.

This result is somewhat surprising given that competition between the diborated olefin and 1,5-hexadiene could occur as the reaction proceeds giving rise to tetraborated products. If C=C insertion into the Pt–B bond is slow with respect to olefin exchange at the platinum center, the observed selectivity could be attributed to preferential olefin binding by 1,5-hexadiene, which can form chelate intermediates. Reactivity of conjugated dienes is less clean as 1,3-butadiene gave a mixture of products that included $CatBCH_2CH=CHCH_2BCat$.

CHAPTER 4

SYNTHESIS, CHARACTERIZATION AND REACTIVITY OF IRIDIUM BORYL

COMPLEXES

Metal-mediated B–H activation is notably less difficult than analogous C–H activations, despite the fact that B–H bonds are stronger than the corresponding C–H bonds.[123,124] B–H activation is kinetically more favorable due to the vacant p orbital on boron, thus coordinatively unsaturated boranes are far more reactive than hydrocarbons, lessening the requirements on the metal complex. Conversely, a highly reactive, coordinatively unsaturated complex or intermediate is required for activation of the kinetically inert C–H bonds. The role of Cp*Ir(PMe$_3$)H$_2$ (28) in C–H activation chemistry is well documented and the following mechanism is supported by kinetic data: photoinduced H$_2$ elimination from compound 28 generates the coordinatively unsaturated reactive intermediate, [Cp*Ir(PMe$_3$)].[64,65] Alkyl and aryl hydride complexes are formed *via* C–H activation by this intermediate and can subsequently undergo thermal reactions where hydrocarbon elimination is observed.[66]

Catalytic functionalization of hydrocarbons has been a "Holy Grail" in homogeneous and heterogeneous catalysis.[62] Over the past 20 years a detailed picture of metal–mediated C–H activation has emerged from intensive study by several research groups and was briefly discussed in the introduction. Activation of C–H bonds is necessary for generating species with M–C bonds, however, ensuing reactive chemistry directed toward the M–C bond must be designed with catalytic capabilities in mind. Prior to our work, reported examples of alkane functionalization have been limited primarily to the oxidation of methane to methanol,[83,84,86]. To date, the only example not involving methane conversion was the ruthenium catalyzed conversion of 2,6-xylyl cyanide to an indole.

Combining C–H activation to borane reactivity is potentially useful for more specialized applications, as Suzuki and Miyaura have shown the utility of phenylboronic acids in palladium catalyzed coupling reactions.[4,125,126] It would seem reasonable to utilize Lewis acidic reagents to convert metal alkyl or aryl groups to functionalized organic products due to the fact that the reactive complexes and intermediates responsible for C–H activation can be coordinatively unsaturated or cationic reagents. Lewis basic substrates have the potential to hinder the reactivity of the unsaturated complexes. For borane reagents, thermochemical and computational data establish that the reaction in Eq 30 is essentially thermoneutral.[124] Hence, catalysis is thermodynamically viable. Given the facility with which C–H activation occurs within the "Cp*Ir(PMe₃)" system, our expectations were that the activation of B–H and B–B bonds would also occur relatively easily. For these reasons, we have been examining metathetic reactions of B–B/B–H bonds with M–C/M–H bonds.[127]

$$\text{H-CH}_3 \ + \ \text{H-BCat} \ \longrightarrow \ \text{H}_2 \ + \ \text{CH}_3\text{-BCat} \qquad \Delta H^\circ = +1.1 \text{ kcal/mol}$$

(30)
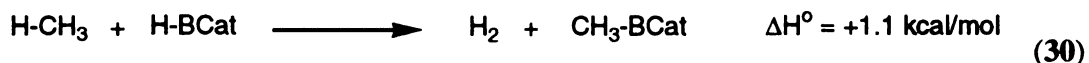
Reactions of Cp*Ir(PMe₃)H₂ with H–B(OR)₂ and (RO)₂B–B(OR)₂ bonds

Thermolysis of Cp*Ir(PMe₃)H₂ (28) in the presence of two molar equivalents of HBCat or B₂Cat₂ gives the diboryl complex, Cp*Ir(PMe₃)(BCat)₂ (29), with generation of H₂ or HBCat respectively (Figure 36). Compound 29 could be isolated in 60% yield as colorless crystals when prepared from compound 28 and two equivalents of B₂Cat₂. ¹H and ³¹P NMR data are typical for Cp*Ir(PMe₃) compounds and ¹¹B NMR revealed resonance at δ 36, which is typical for Ir catecholatoboryl complexes. The formulation was crystallographically confirmed (Figure 37). Ir–B distances of 2.03 and 2.04 Å

compare to those in related Ir complexes.[128] There are no other remarkable features in this piano-stool structural.
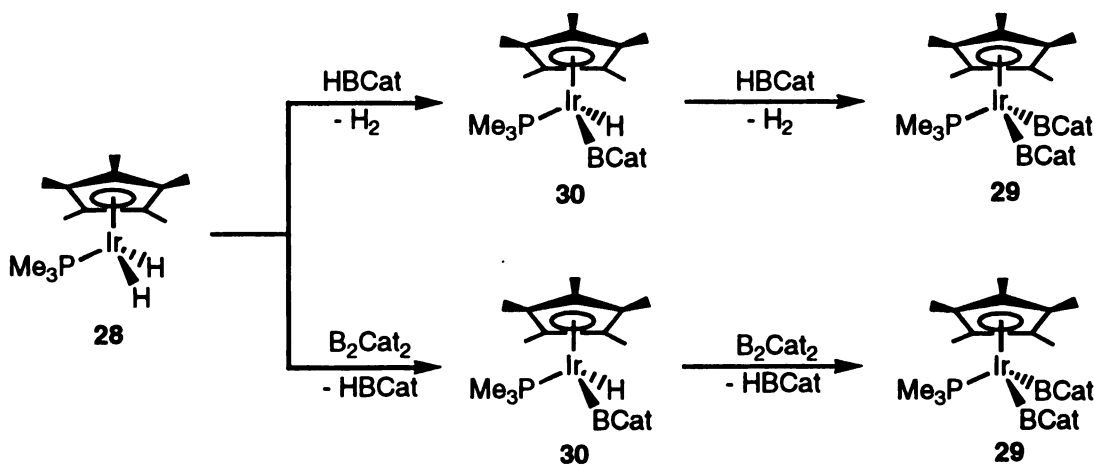
Figure 36. Reaction scheme for the formation of iridium boryls from the reaction of **28** with HBCat and B_2Cat_2.
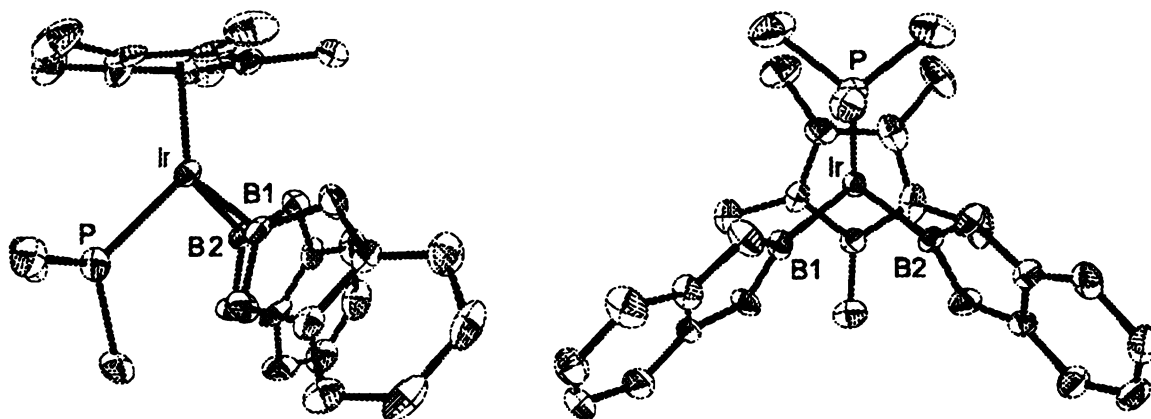
Figure 37. Molecular structure of **29**. Thermal ellipsoids are at 50% probability.

Table 5. Selected bond lengths and angles for **29**.

bond	distance (Å)	bonds	angle (deg)
Ir(1)–B(1)	2.028(11)	B(1)–Ir(1)–B(2)	84.7(4)
Ir(1)–B(2)	2.037(11)	B(1)–Ir(1)–P(1)	90.6(3)
Ir(1)–P(1)	2.248(3)	B(2)–Ir(1)–P(1)	92.1(3)

63

When compound **28** is reacted with one molar equivalent of HBCat or B_2Cat_2 the monoboryl complex, Cp*Ir(PMe$_3$)H(BCat) (**30**), forms with concomitant generation of H_2 or HBCat (Figure 36). Unfortunately, all attempts to isolate analytically pure **30** gave mixtures of compounds **28**, **29**, and **30** and borane decomposition products. Despite this, the identity of compound **30** can be made conclusively from spectroscopic data. ^{1}H NMR spectra indicate new resonances for the catecholate, Cp*, and PMe$_3$ ligands. In addition, a high-field resonance at δ -17.12 is observed for the hydride. This signal appears as a doublet with a typical $|^2J_{H-P}|$ value (29 Hz) for this system. The hydride resonance integrates as one proton, and the presence of a single iridium-bound hydride was confirmed by observation of a doublet in the selectively decoupled ^{31}P NMR spectrum. ^{11}B NMR spectra indicate a new resonance at δ 36 for the boryl compound and a doublet for HBCat for the reaction of **28** with B_2Cat_2 when performed in an NMR tube.

The pinacolate analogue, Cp*Ir(PMe$_3$)(H)(BPin) (**31**), can be generated from the reaction of **28** and HBPin in toluene (Figure 38); however, in contrast to the catecholate analog, higher temperature (120 °C) and increased reaction time (several days) are required for product formation. Interestingly, the concentration of thf also had an effect on product formation as higher concentrations inhibit formation of **31** and lower concentrations lead to the formation of small amounts of Cp*Ir(PMe$_3$)(BPin)$_2$ (**32**).[129] Compound **31** was obtained in 82% yield as an analytically pure orange oil. Decomposition similar to that observed for **30** occurs when this compound is placed under vacuum for an extended period of time. The rate, however, appears to be much slower than that observed for the catecholate analog. The pinacolate analog of **29** can be formed from compound **28** and a large excess of HBPin (24 molar equivalents, 150 °C), but efforts to isolate this compound have been hampered by borane decomposition products. B_2Pin_2 does not react with **28** even at elevated temperatures.
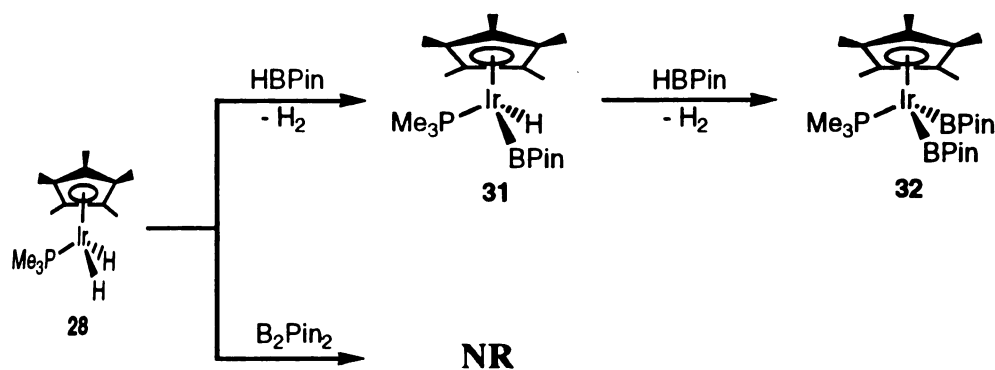
Figure 38. Reaction scheme for the formation of iridium boryls with HBPin and B_2Pin_2.

Kinetics Experiments

Metathesis reactions of M–H bonds with B–H bonds have two potential regiochemical outcomes: i) formation of a metal boryl complex with elimination of H_2 or ii) degenerate H exchange between metal and borane hydrides. While the former is readily identified by the formation of new species in the reaction mixture, the latter process can be inferred from labeling studies. In reactions of transition metal complexes, both processes have been observed in the few cases that have been studied in detail, and general trends in reactivity have not emerged.[15,18,19,23,24,130-132] These reactions are important in stoichiometric and catalytic metal–directed borations of unsaturated organic substrates because metal hydride intermediates can result from B–H/M–C metathesis in *B–C bond forming* steps. Clearly, an area where these metathesis reactions are potentially *relevant is in metal*–mediated functionalization of hydrocarbons.

The reaction between $Cp^*Ir(PMe_3)H_2$ and HBCat to form $Cp^*Ir(PMe_3)(BCat)H$ was *deemed sufficiently* clean for kinetic analysis since the diboryl compound, **29**, could not *be detected until* the third half–life. The loss of compound **28** as a function of [**28**] and **[HBCat] was consistent** with the rate law shown in Eq 31. An Eyring plot (Figure 39) for

k_{obs} between 20 and 70 °C yielded the following activation parameters: $\Delta H^{\ddagger} = 14.9(5)$ kcal/mol and $\Delta S^{\ddagger} = -29(2)$ e.u. In an effort to examine kinetic isotope effects the reaction of **28**–d_2 and HBCat was attempted. Unfortunately, rapid scrambling of the label with respect to the rate of formation of **30** was observed, precluding the extraction of individual isotope effects for the iridium and borane positions. However, the reaction between **28**–d_2 and DBCat gave a $k_H/k_D = 1.7(1)$ (Figure 40), which is a composite of primary and secondary kinetic isotope effects. Rates for the reaction between **28** and B_2Cat_2 were not reproducible, preventing a more detailed examination of this reaction.

$$\frac{-d[1]}{dt} = k_{obs}[1][HBCat]$$

(31)
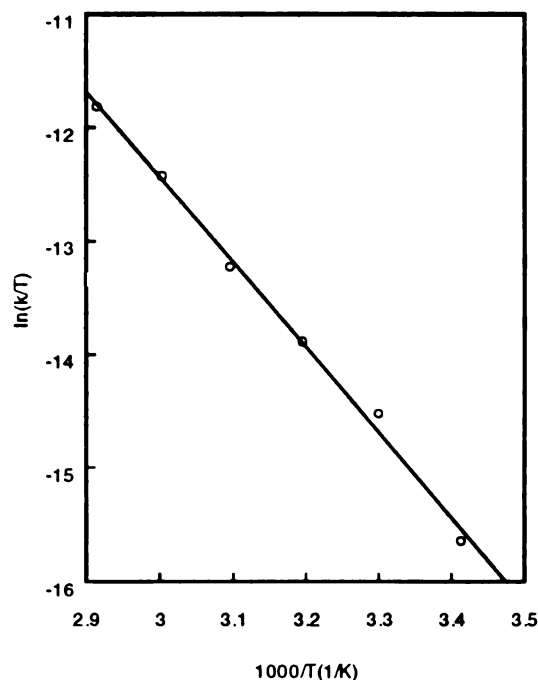
Figure 39. Eyring plot for the reaction of **28** with HBCat in C_6D_6. from 20 °C to 70 °C ($[28]_o = 41$ mM; $[HBCat]_o = 245$ mM).
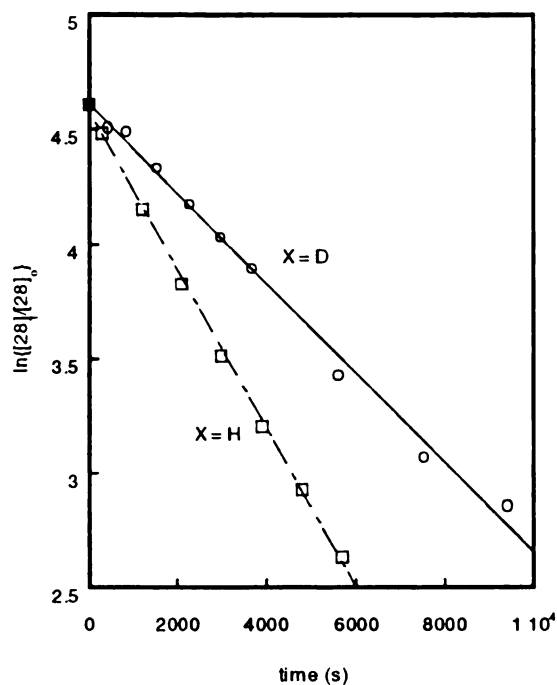
Figure 40. Plots of $\ln\{[Cp^*Ir(PMe_3)X_2]_t/[Cp^*Ir(PMe_3)X_2]_0\}$ versus time for the reaction of $Cp^*Ir(PMe_3)X_2$ with XBCat. ($[Cp^*Ir(PMe_3)X_2]_0 = 41$ mM; $[XBCat]_0 = 245$ mM; O (X = D); $\square$ (X = H)).

The metathesis reactions in Figures 36 and 38 pose interesting mechanistic questions. For reactions between the dihydride, **28**, and substrates with B–H bonds, potential mechanisms are shown in Figures 41 and 42.

A - Oxidative Addition

Cp*Ir(PMe₃)H₂ $\xrightleftharpoons[+ PMe_3]{- PMe_3}$ [Cp*Ir^{III}H₂] $\xrightleftharpoons[- HBCat]{+ HBCat}$ [Cp*Ir^{V}H₃BCat]
28   **33**   **34**

$+ H_2 \Updownarrow - H_2$

Cp*Ir(PMe₃)(BCat)H $\xrightleftharpoons[+ PMe_3]{- PMe_3}$ [Cp*Ir^{III}(H)BCat]
30   **35**

B - Ring Slip

Cp*Ir(PMe₃)H₂ $\rightleftharpoons$ [(η³-Cp*)Ir^{III}(PMe₃)H₂] $\xrightleftharpoons[- HBCat]{+ HBCat}$ [(η³-Cp*)Ir^V(PMe₃)(BCat)H₃]
28   **36**   **37**

$+ H_2 \Updownarrow - H_2$

Cp*Ir(PMe₃)(BCat)H $\rightleftharpoons$ [(η³-Cp*)Ir^{III}(PMe₃)(BCat)H]
30   **38**
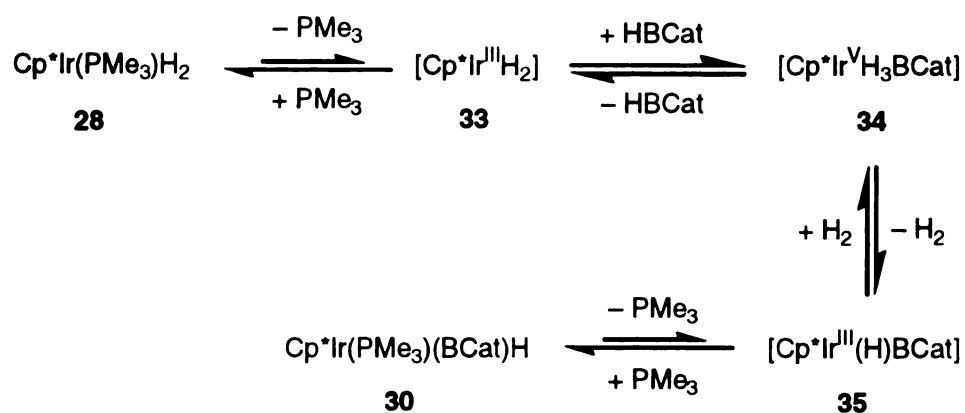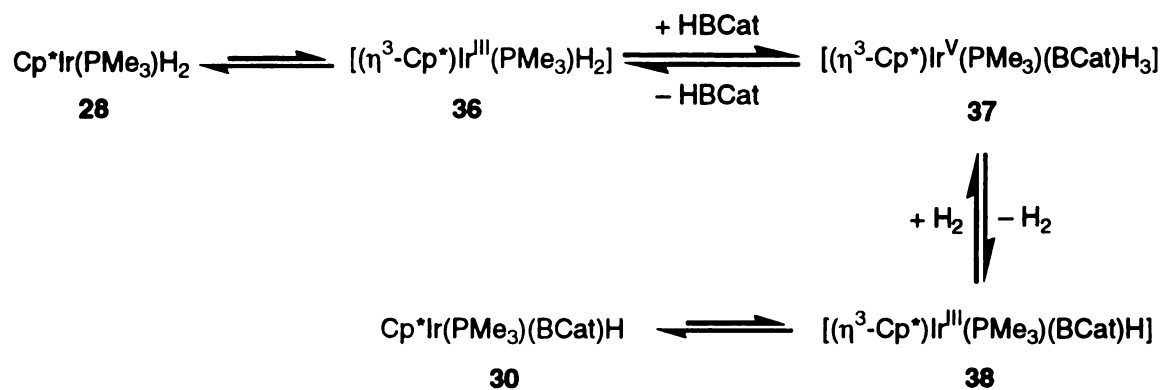
Figure 41. Oxidative addition pathways for the formation of **30**.

C - Ion-pair

Cp*Ir(PMe₃)H₂ ⇌ [Cp*Ir(PMe₃)H⁺][H₂BCat⁻] ⇌ [Cp*Ir(PMe₃)H···HBHCat]‡

$$\text{Cp*Ir(PMe}_3)\text{H}_2 \xrightleftharpoons[-\text{HBCat}]{+\text{HBCat}} [\text{Cp*Ir(PMe}_3)\text{H}^+][\text{H}_2\text{BCat}^-] \rightleftharpoons [\text{Cp*Ir(PMe}_3)\text{H}\cdots\text{HBHCat}]^\ddagger$$

28   **39**   **40**

$+ H_2 \Updownarrow - H_2$

[Cp*Ir(PMe₃)]

Cp*Ir(PMe₃)(BCat)H ⇌ **33**

30   +

HBCat

D - Borane Adduct

Cp*Ir(PMe₃)H₂
28
+
HBCat
⇌ [Cp*Ir(PMe₃)H₂→BHCat] ⇌
41

$$\left[\text{Cp*H(PMe}_3)\text{Ir} \overset{\text{H}}{\underset{\text{B}}{\diamondsuit}} \overset{}{\text{H}} \right]^\ddagger$$

$\begin{array}{c}\text{B}\\\text{Cat}\end{array}$

42

$+ H_2 \Updownarrow - H_2$

Cp*Ir(PMe₃)(BCat)H
30
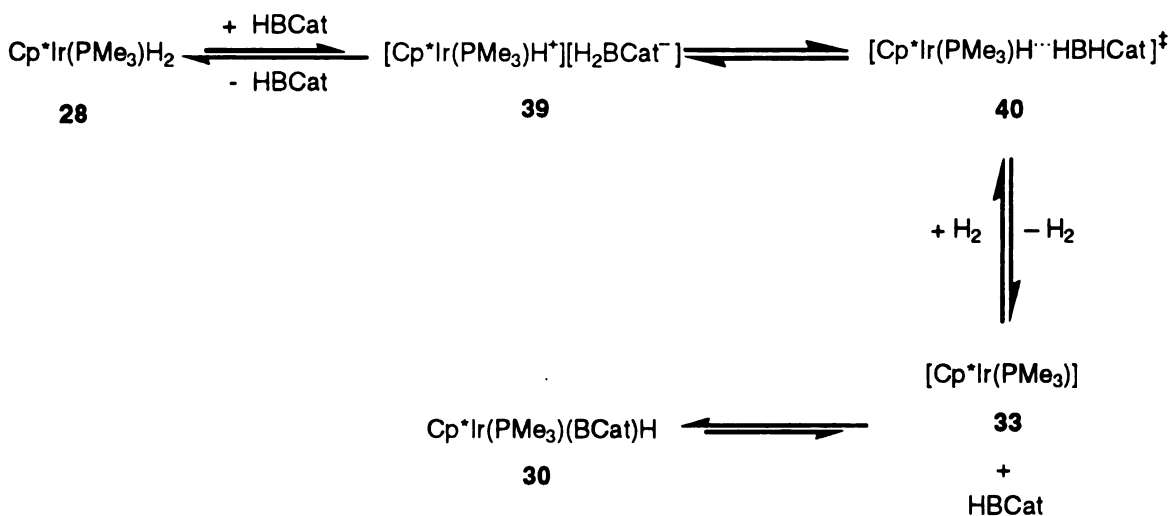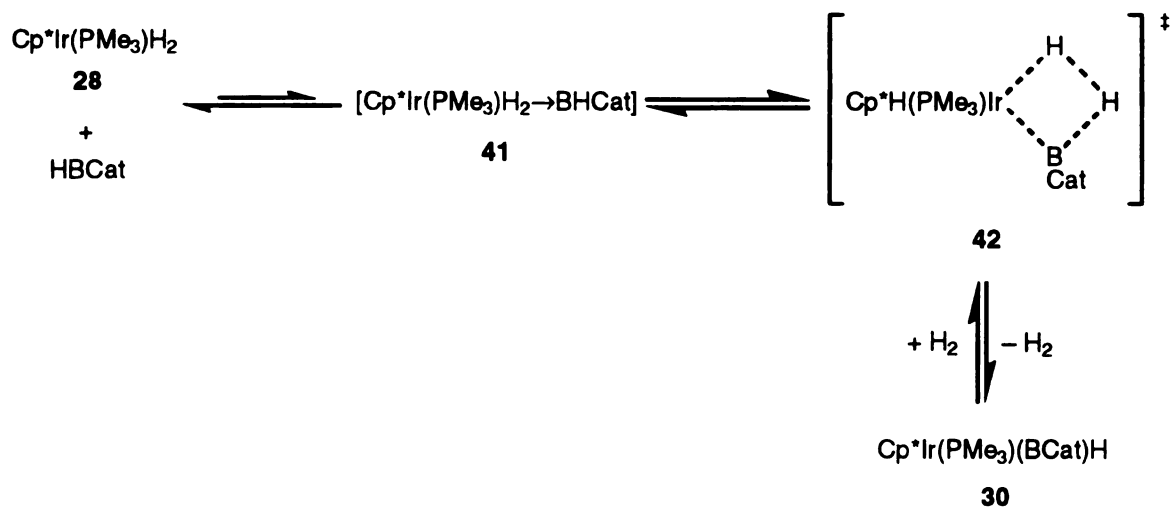
Figure 42. Ion pair and borane adduct pathways for the formation of **30**.

The first two pathways proceed through a series of oxidative addition/reductive elimination steps following an initial ligand dissociation step. Phosphine dissociation could possibly be examined by running the reaction in the presence of PMe₃ or PMe₃-d_9. Unfortunately, phosphines react with catecholborane, leading to eventual boron decomposition products. Ring slip pathways are sometimes invoked in cyclopentadienyl

systems; however, it is difficult to definitively assess this possibility experimentally. The third mechanism requires HBCat to abstract a hydride from compound **28** to form the ion pair, [Cp*Ir(PMe₃)H⁺][H₂BCat⁻] (**39**). Although the cation, [Cp*Ir(PMe₃)H⁺], has not been reported, related cationic alkyl and aryl complexes have been fully characterized.[133,134] In the fourth pathway, formation of a borane adduct precedes Ir–H/B–H metathesis. The iridium adduct, Cp*Ir(PMe₃)(H)₂·AlPh₃, as well as an iridium borane adduct we prepared, which will be described later, provide precedence for the intermediacy of a borane adduct.[135] If a borane adduct lies along the reaction coordinate, the differences in reactivity can be correlated to the Lewis acidity of the borane as competitive binding between these boranes and NEt₃ gave the following ranking: HB(C₆F₅)₂ > HBCat > HBPin. Regardless of the mechanism for boryl formation, a nonproductive pathway that could account for label scrambling proceeds through a four centered transition state analogous to that proposed for exchange between hydride positions of CpRu(PPh₃)₂H and HBCat (Figure 43).[24]

$$Cp^*Ir(PMe_3)H_2 \;\rightleftharpoons\; \left[Cp^*Ir(PMe_3)H \underset{D}{\overset{H}{\diamond}} BCat \right]^{\ddagger} \;\rightleftharpoons\; Cp^*Ir(PMe_3)H(DB(H)Cat)$$

28

+
DBCat

43

44

Cp*Ir(PMe₃)(H)D

28-d₁

+
HBCat
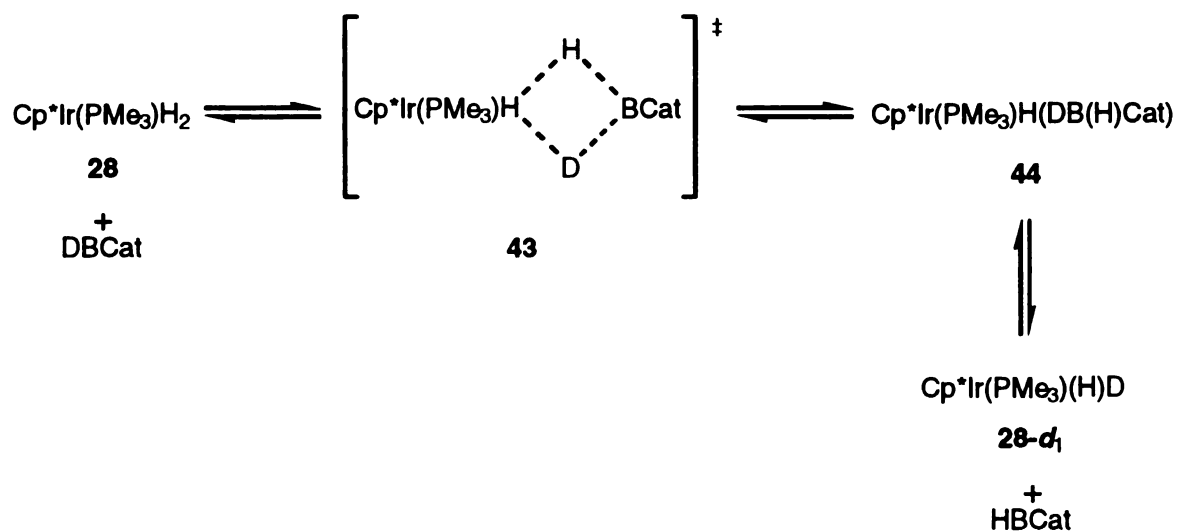
Figure 43. Degenerate hydride exchange in the reaction of Cp*Ir(PMe₃)H₂ with DBCat.

We also attempted to examine the kinetics of the reaction of $Cp*Ir(PMe_3)H_2$ with HBPin to form $Cp*Ir(PMe_3)(BPin)H$, but non-linear plots for the loss of [28] were seen (Figure 44). Despite the lack of quantitative kinetic data, the temperature and reaction time needed to form 31 from 28 and HBPin clearly suggested that the rate for boration by HBCat is faster than by HBPin.[136] Also, HBPin is far more stable to decomposition in the presence of phosphines, therefore a kinetic run was prepared where approximately a one-to-one ratio of HBPin to PMe_3-d_9 was used. The reaction proceeded very slowly, and after 38 hrs of heating at 120 °C, the reaction had proceeded to 10 % completion according to ^1H NMR. Integration of the $P(CH_3)_3$ resonances in the ^1H NMR of $Cp*Ir(PMe_3)H_2$ and free PMe_3 indicated that exchange between PMe_3-d_9 and Ir-bound PMe_3 had occurred to only 4%.
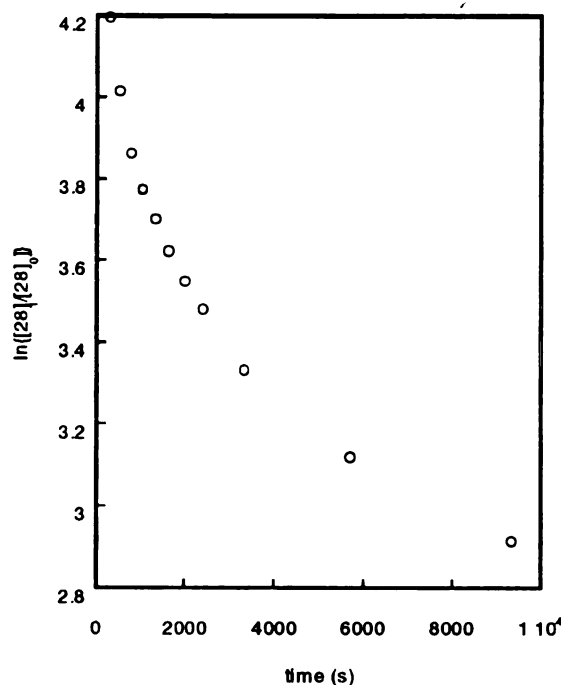
Figure 44. Plot of $\ln\{[28]_t/[28]_o\}$ versus time for the reaction of $Cp*Ir(PMe_3)H_2$ with HBPin. ($[Cp*Ir(PMe_3)H_2]_o = 41$ mM; $[HBPin]_o = 254$ mM).

71

Reaction of Cp*Ir(PMe₃)H₂ with the electrophilic borane, HB(C₆F₅)₂

When Cp*Ir(PMe₃)H₂ was reacted with the electron deficient borane, $[(C_6F_5)_2BH]_2$,[48] the borane complex, Cp*Ir(PMe₃)(H)[HBH(C₆F₅)₂] (**45**) was isolated in 84% yield. Signals due to the Cp* and PMe₃ ligands were visible in the room temperature ^{1}H NMR spectrum, but resonances in the hydride region could not be detected. At –70 °C, a single high-field doublet (2 H, $|^2J_{PH}| = 27$ Hz), corresponding to the Ir–H nuclei, was observed at –15.9 ppm. A broad resonance at 4.4 ppm was assigned to a boron hydride that is not coordinated to Ir. The high frequency v_{BH} (2508 cm^{-1}) in the IR spectrum of compound **45** is typical for a terminal boron hydride and corroborates the NMR data.[48,137,138]

The molecular structure of **45** was determined and is shown in Figure 45. In the solid–state, the two Ir–H positions are chemically inequivalent, and terminal B–H group is clearly present. The hydrides were refined isotropically, and their positions did not deviate substantially from electron density maxima found in difference Fourier maps generated from low angle data. Although these peaks were located in chemically reasonable positions, the Ir–H1 distance of 1.38(3) Å is short for a terminal Ir hydride. The value is considerably shorter than a typical terminal Ir–H bond distance determined from X–ray (1.47–1.70 Å)[16,66,139,140] or neutron (1.587–1.617 Å)[141-145] data, however, shorter lengths for iridium hydrides have been reported.[146-148] This is not unusual as X–ray data commonly underestimate M–H distances for hydrides attached to third period transition elements. The Ir–H2 and Ir–B distances are 1.68(2) and 2.614(2) Å, respectively, and significant elongation of the B–H2 bond (1.34(2) Å) is observed. The Ir–H(2)–B angle of 119.6(8)° is outside of the range reported for η^1-metal borohydrides (121–173.9°). The short angle may be a consequence of Ir–B bonding interactions; however, an η^2-borohydride complex with a substantially shorter M–H–B angle of

112(5°) has been reported by Girolami. In valence bond terms, Cp*Ir(PMe₃)(H)[HBH(C₆F₅)₂] can be described as a borohydride complex, a borane adduct related to the recently reported Lewis acid-base adduct, Cp*IrPMe₃(H)₂·AlPh₃, or a combination of these two extremes.[135]

A   B
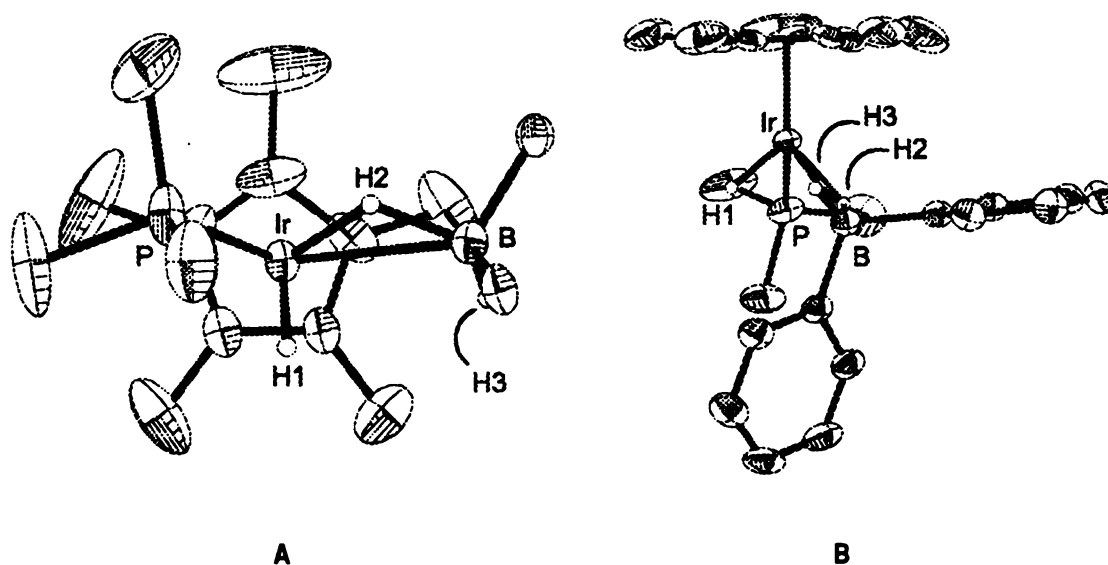
Figure 45. Two different views of **45**. Thermal ellipsoids are at 30% probability. In (A) all hydrogen atoms except H1 are omitted and only the ipso carbons of the pentafluorophenyl groups are shown and in (B) all hydrogen atoms except H1 and all fluorine atoms are omitted for clarity.

Table 6. Selected bond lengths and angles for **45**.

bond	distance (Å)	bonds	angle (deg)
Ir(1)–B(1)	2.613(2)	B(1)–Ir(1)–H(1)	77.8(12)
Ir(1)–H(1)	1.38(3)	B(1)–Ir(1)–H(2)	26.5(8)
Ir(1)–H(2)	1.68(2)	H(1)–Ir(1)–H(2)	87.1(14)
B(1)–H(2)	1.34(2)	P(1)–Ir(1)–H(1)	77.8(11)
Ir(1)–P(1)	2.258(1)	P(1)–Ir(1)–H(2)	82.9(8)
B(1)–H(3)	1.05(2)	B(1)–Ir(1)–P(1)	104.88(6)

In light of the solid state structure, in which H1, H2, and H3 are chemically inequivalent, the inability to observe resonances for these hydrogen atoms suggested

dynamic behavior. When a toluene-d_8 solution of **45** was cooled to –50 °C a doublet was observed at δ –15.9 and a broad resonance was observed at δ 4.3. Upon cooling to –80 °C, the doublet appeared to broaden somewhat but further decoalescence was not observed in this solvent. Therefore, the low melting (–135 °C) solvent, $CDCl_2F$, was used to access a lower temperature regime.[149] As in toluene-d_8, a doublet in the hydride region (δ –15.6) and a broad resonance for the borane hydrogen were observed upon cooling; however, at –105 °C, the doublet decoalesced to a broad singlet at δ –14.6 and a doublet at δ –16.7 ($|^2J_{PH}|$ = 38 Hz). The broad singlet is assigned to the hydride corresponding to the bridging position (H_a) and the doublet is assigned to the terminal Ir hydride (H_b) of the static structure (Figure 46). The broad nature of H_a can be attributed to coupling to the quadrupolar boron nucleus and has been observed in other metalloboryl complexes.[14,50,51]

45
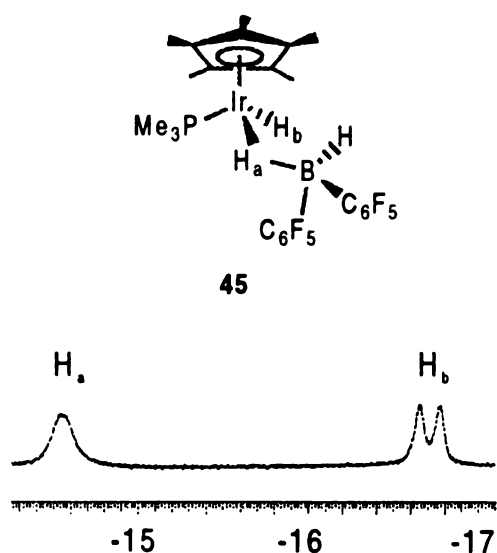
Figure 46. ^1H NMR of the hydride region of **45** in $CDCl_2F$ at –105 °C.

Line shape analysis was performed for spectra from –105 °C to –55 °C and an Eyring plot (Figure 47) yielded activation parameters for the exchange, $\Delta H^\ddagger$ = 12.4(6) kcal/mol and $\Delta S^\ddagger$ = 25(3) e.u..[150] The magnitude of the entropy term is consistent with a

dissociative process (Figure 48). Intermolecular hydride transfer at room temperature between all hydride positions was independently confirmed by reacting 28-d_2 with Cp*Ir(PMe$_3$)(H)[HBH(C$_6$F$_5$)$_2$], which gave statistical scrambling of the deuterium label as determined by ^{2}H NMR.
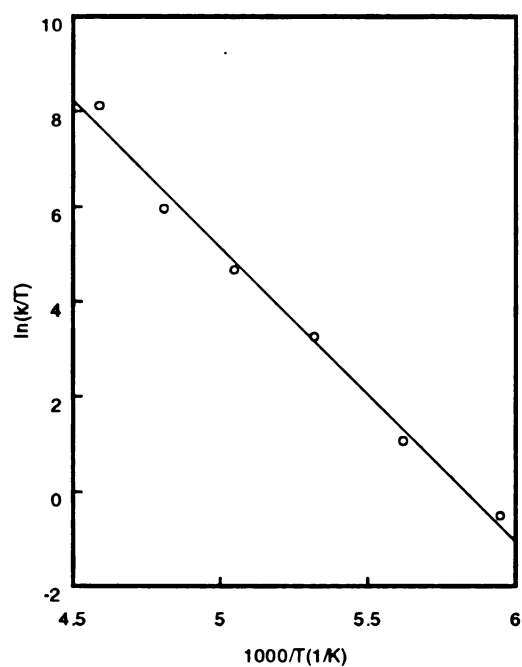
Figure 47. Eyring plot for the exchange between H$_a$ and H$_b$ of **45** in CDCl$_2$F from −105 °C to −55 °C.
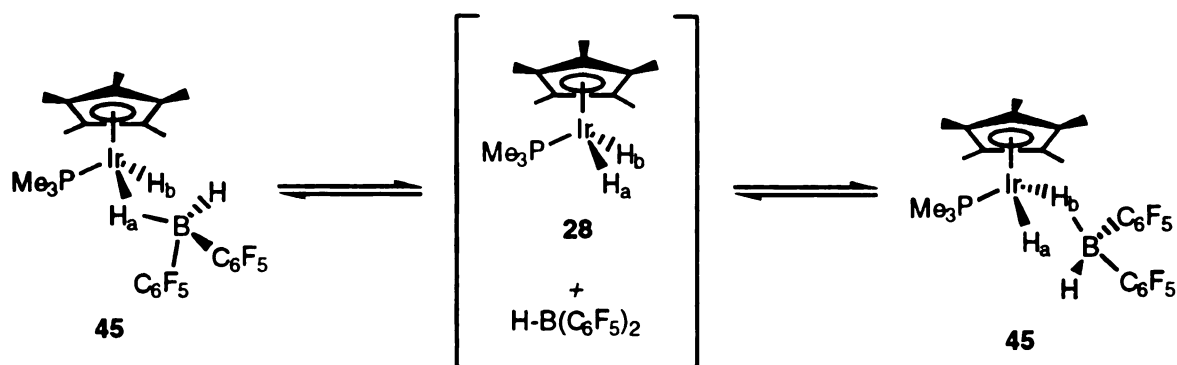
Figure 48. Exchange between H_a and H_b in **45**.

In $CDCl_2F$ or CD_2Cl_2 solutions of **45**, a two major new sets of Cp*, PMe₃, and hydride resonances gradually form irreversibly at low temperature in approximately a one-to-one ratio. One set was identified as the dihydride compound, **28**. For the other set of resonances in particular, the two hydride resonances at δ –12.5 and δ –13.9 integrate in a 1:2 ratio, and the triplet of doublets at –12.5 is coupled to the doublet of doublets at – 13.9. All of the ^1H and ^{31}P NMR data for this iridium species correspond to the previously reported cation, Cp*Ir(PMe₃)H₃⁺.[139] In the ^{11}B spectrum, a triplet at δ –31.4 is assigned to the borohydride anion, $H_2B(C_6F_5)_2^-$. Resonances for **28** and the cation are not observed in C_7D_8 spectra taken at the same temperatures. The formation of the ionic compound might be a result of differences in solvent polarity. Polar solvents such as CD_2Cl_2 and $CDCl_2F$ would be better able than a non-polar solvent like C_7D_8, to support ionic species.

The appearance of a single high–field resonance upon heating a toluene solution of Cp*Ir(PMe₃)(H)[HBH(C₆F₅)₂] to 80 °C indicated rapid exchange between the borane hydrogen and both iridium hydride positions. This resonance was approximately the weighted average of limiting Ir–H and B–H chemical shifts. The cause of this deviation from the exact weighted average is unknown. Perhaps an equilibrium between **45** and transient Cp*Ir(PMe₃)H₂ results if the borane fully dissociates to a small extent.

Compound **45** reacts with Lewis bases such as PMe_3, pyridine, and thf to give

$Cp*Ir(PMe_3)H_2$ and the corresponding Lewis base adducts of $HB(C_6F_5)_2$ (Eq 32), but it is

stable towards the weaker Lewis base diethyl ether. This is interesting in light of the fact

that diethyl ether is known to form an adduct with $HB(C_6F_5)_2$.[48] The fact that **28** is a

stronger base than Et_2O was corroborated by examination of this reaction from the

reverse direction. In situ generation of $(Et_2O)·HB(C_6F_5)_2$ (confirmed by ^1H NMR)

followed by the addition of an equimolar amount of compound **28** revealed only **45** and

Et_2O in solution. A qualitative ordering of the Lewis basicity of $Cp*Ir(PMe_3)H_2$ with

respect to other bases can be determined based on these observations: pyridine > PMe_3 >

thf > **28** > Et_2O.

$$(32)$$
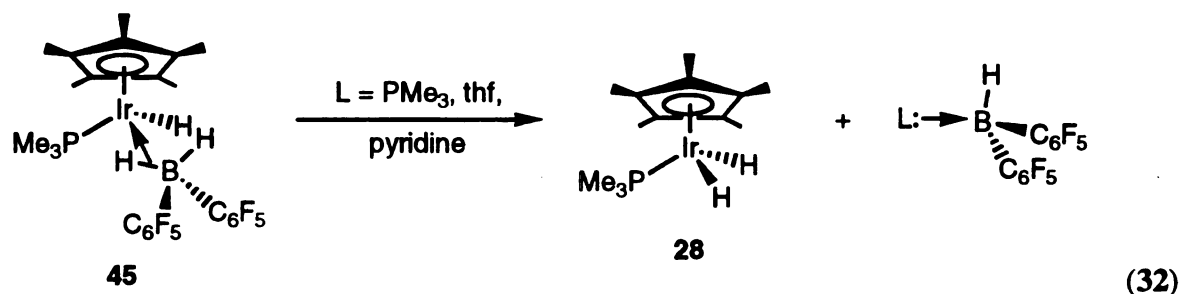
At elevated temperatures, $Cp*Ir(PMe_3)(H)[HBH(C_6F_5)_2]$ eliminates H_2 and is

gradually converted to a new species, **46**, which was isolated in 39 % yield. A new high

field doublet at δ –16.6 in the ^1H NMR was accompanied by a doublet at δ –44.7 in the

^{31}P NMR spectrum, and a low field resonance at δ 81 in the ^{11}B NMR spectrum. Based

on these data, compound **46** was identified as the boryl complex,

$Cp*Ir(PMe_3)(H)[B(C_6F_5)_2]$.[151,152]

Single crystals of **46** were grown from pentane at –78 °C and the structure was

confirmed by X–Ray crystallographic analysis. The molecular structure of compound **46**

is shown in Figure 49. The Ir–H distance (1.51(4) Å) is well within the typical range of iridium hydride bonds and the compound adapts a piano-stool geometry.
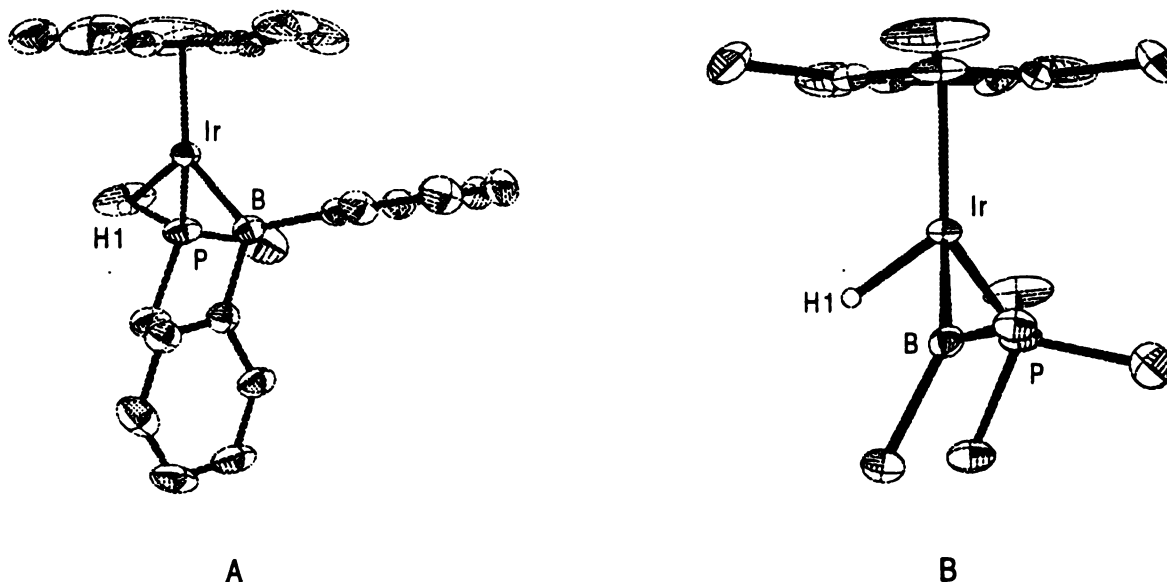
Figure 49. Two different views of 46. Thermal ellipsoids are at 30% probability. In (A) all hydrogen atoms except H1 and all fluorine atoms are omitted and in (B) all hydrogen atoms except H1 are omitted and only the *ipso* carbons of the pentafluorophenyl groups are shown for clarity.

Table 7. Selected bond lengths and angles for 46.

bond	distance (Å)	bonds	angle (deg)
Ir(1)–B(1)	2.014(4)	B(1)–Ir(1)–H(1)	78.1(16)
Ir(1)–P(1)	2.255(1)	P(1)–Ir(1)–H(1)	82.8(16)
Ir(1)–H(1)	1.51(4)	B(1)–Ir(1)–P(1)	92.33(8)

The thermolysis of 45, although not very clean, also resulted in the appearance of new Cp*, PMe$_3$, and hydride resonances. In particular, two hydride resonances, a doublet of doublets at δ −19.2 and a triplet of triplets at δ −23.0, integrate in a 2:1 ratio, and are coupled to each other. ^{1}H and ^{31}P NMR data for this Ir species correspond to the previously reported cation, (Cp*Ir(PMe$_3$)H)$_2$(μ-H)$^+$.[139] In the ^{11}B spectrum, a doublet at

δ –23.9 is assigned to the borohydride anion, $HB(C_6F_5)_3^-$. The NMR spectroscopic data for this species is identical to that observed when one equivalent of $B(C_6F_5)_3$ is reacted with two equivalents of $Cp*Ir(PMe_3)H_2$. ^1H and ^{19}F NMR also supported the formation of HC_6F_5 as a minor product.

Stoichiometric C–B Bond Forming Reactions

The reaction of borane reagents with $Cp*Ir(PMe_3)(R)H$ (R = cy-C_6H_{11} (**47**), C_6H_5 (**48**)) has four possible outcomes (Figure 50); i) M–C/B–H bond metathesis leading to metal boryl and R–H, ii) M–C/H–B bond metathesis leading to metal hydride and organoborane, iii) degenerate M–H/B–H bond metathesis, and iv) M–H/H–B metathesis leading to a complex containing both M–C and M–B bonds. Outcome iii is non-productive and outcome iv, although possible, seems unlikely due to the scarcity of compounds that simultaneously support both M–C and M–B linkages.[104]
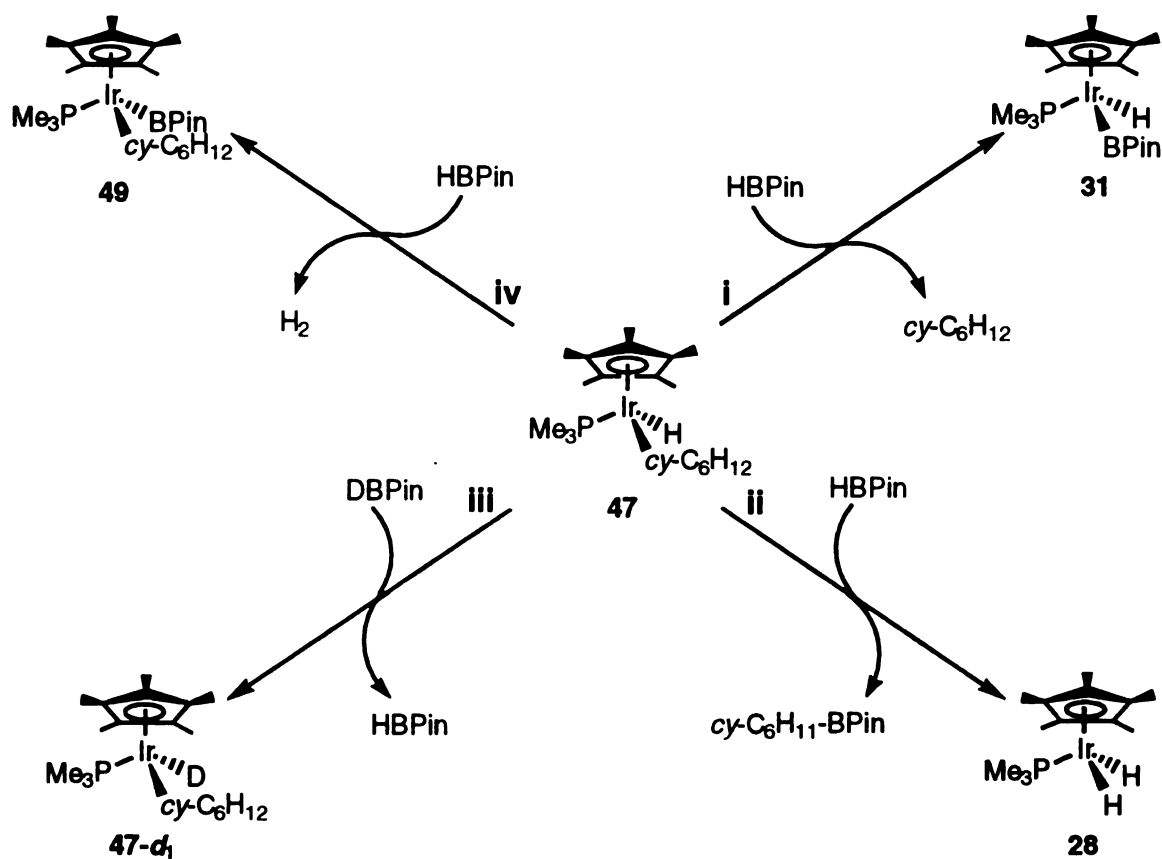
Figure 50. Metathetic outcomes for the reaction of HBPin with Cp*Ir(PMe₃)(cy-C₆H₁₁)H.

Cp*Ir(PMe₃)(H)(Cy) and Cp*Ir(PMe₃)(H)(Ph) reacted with HBX₂ reagents in C_6D_6 to yield the alkylborane derivatives, CyBX₂ and PhBX₂ (X₂ = $(C_6F_5)_2$, Pin, Cat). The rates for B–C bond formation and Ir product distributions were borane dependent. The reaction between $[HB(C_6F_5)_2]_2$ and compound **47** gave **28** and cy-C_6H_{11}–$B(C_6F_5)_2$ (Eq 33). Conversions were quantitative and complete within 5 min at ambient temperature as judged by ^1H NMR. Elimination of cyclohexane from compound **47** was not observed, and Ir products from solvent activation were not detected. Characterization of the organic product, cy-C_6H_{11}–$B(C_6F_5)_2$, was established by comparing ^1H and ^{11}B NMR data to an authentic sample, prepared from $[HB(C_6F_5)_2]_2$ and cyclohexene.[153] The reaction between

[HB(C$_6$F$_5$)$_2$]$_2$ and compound **48** resulted in a mixture of products, indicating a more complicated reaction.

$$ + \; cy\text{-}C_6H_{11}\text{-}B(C_6F_5)_2 \qquad (33)$$
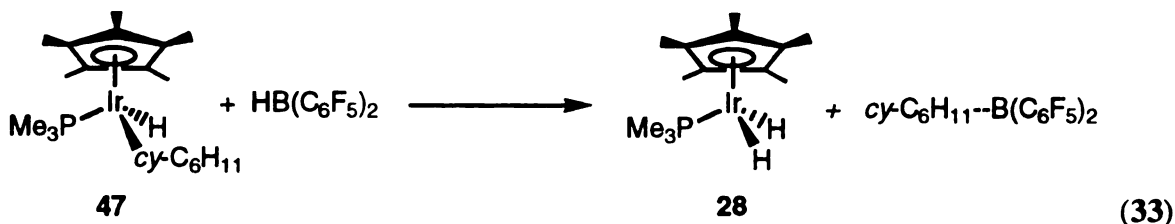
For oxygen-substituted boranes, B–C bond formation required more forcing conditions as illustrated by the reactivity of pinacolborane (HBPin) with compound **47**. When a cyclohexane solution of Cp*Ir(PMe$_3$)(H)(cy–C$_6$H$_{11}$) and HBPin was heated at 100 °C for 65 hr, Cp*Ir(PMe$_3$)H$_2$ was not formed. Instead, Cp*Ir(PMe$_3$)(H)(BPin) formed as the major Ir containing product. In order to determine the fate of the cyclohexyl and hydride ligands, thermolysis of Cp*Ir(PMe$_3$)(H)(cy–C$_6$H$_{11}$) in the presence of HBPin was monitored by ^{1}H NMR. In benzene–d_6 solutions, this reaction yielded cy-C$_6$H$_{11}$–BPin and cyclohexane and the major Ir containing products were **31** and **48**–d_6.[154] The amounts of products formed, both organic and metal based, depend on the reaction conditions. Typical product distributions obtained for the reaction of **47** with HBPin at various reaction conditions are shown in Table 8. Some general trends are noteworthy. Higher concentrations of HBPin relative to **47** (comparison of entries 1 and 2, 3 and 4, and 5 and 6) results in increased percentages of the monoboryl complex **31** and the organoborane product. Higher reaction temperatures lead to an increased percentage of phenyl hydride complex **48** (entries 3 and 5, and 4 and 6) but not necessarily an increased yield of cyclohexane. Increased amount of thf contaminant in the borane (entries 1 and 5) appears to lead to a decreased amount of **31**. Although rigorous kinetic analysis was precluded by irreproducible rate data, the qualitative rates for cyclohexane formation were, in general, higher than expected for thermal elimination of

cyclohexane from compound **47**. The amounts of $Cp*Ir(PMe_3)(Ph)H$ and cy-C_6H_{12} expected can be calculated given the k_{obs} value for the thermal decomposition of $Cp*Ir(PMe_3)(Cy)H$ in C_6D_6. Buchanon and Bergman measured the rate for the clean, first order conversion of **47** to **48** in C_6H_6 over a range of temperatures and displayed the data in an Arrhenius plot.[66] The rates were identical in C_6H_6 and C_6D_6 and so the appropriate k_{obs} values for the reaction performed at 95 and 135 °C were calculated from their data and allowed for the estimation of the amounts of **20** and cy-C_6H_{12}.

Table 8. Reaction conditions and yields for the addition of HBPin to **47**.[173]

entry	eq HBPin	thf (% of HBPin)	temp (°C)	time (min)	% conv.	% **31**	% **48** (actual/theor.)	% Cy–BPin	% CyH (actual/theor.)
1	6	17.7	135	215	88	24	64/78	15	73/78
2	12	17.7	135	50	90	45	45/30	22	68/30
3	6	11.5	95	1986	90	77	13/10	31	59/10
4	24	11.5	95	245	95	89	5.6/1.3	35	60/1.3
5	6	11.5	135	252	92	45.5	46/83	19	73/83
6	24	11.5	135	32	92	76	16/21	40	52/21

The reaction manifold for this conversion is likely quite complex, with multiple pathways leading to the eventual product distributions. Pathway A (Figure 51) starts with the thermal elimination of cyclohexane, to yield the coordinatively unsaturated intermediate [Cp*Ir(PMe₃)] (33), which can then activate the C-D bonds (Ai) or B–H bonds (Aii) to yield complexes 31 and 48-d_6, respectively. Pathways B and C (Figure 52) are complementary in that both are assumed to involve simple metathetic exchange involving Ir–C/B–H bonds. Pathway B generates 31 and cy-C_6H_{12}, whereas pathway C yields compound 28 and cy-C_6H_{11}–BPin instead. Cp*Ir(PMe₃)H₂ can then be converted to 31 as discussed earlier. Other mechanisms involve oxidative addition/reductive elimination steps following ligand dissociation. Phosphine dissociation seems unlikely, however, given the small amount of PMe₃-d_9 incorporation into Cp*Ir(PMe₃)H₂ and Cp*Ir(PMe₃)(BPin)H when 28 is reacted with HBPin in the presence of labeled PMe₃ (see above). A ring slip mechanism (Pathway D, Figure 53) would also account for an increased amount of cy-C_6H_{12}. Formation of an η^3-pentamethylcyclopentadienyl complex followed by oxidative addition of HBPin to the Ir metal center would yield intermediate 51. Reductive elimination of cy-C_6H_{11}–BPin (Di) or cy-C_6H_{12} from 51 and rearrangement of the Cp* ring to η^5-coordination gives 28 and 31, respectively.
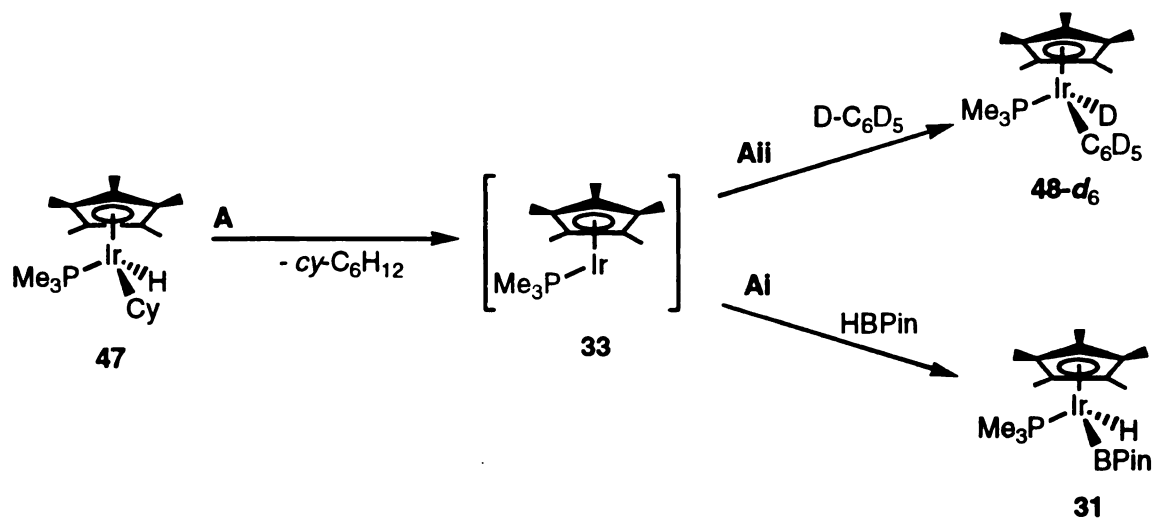
Figure 51. Thermal decomposition pathway for the reaction of HBPin with **47**.
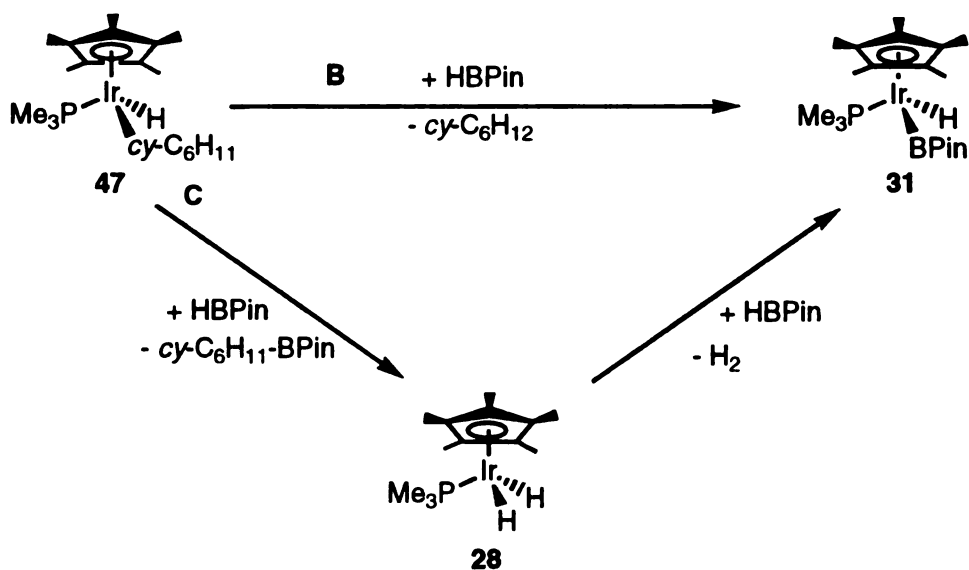
Figure 52. Simple metathesis pathways for the reaction of HBPin with **47**.
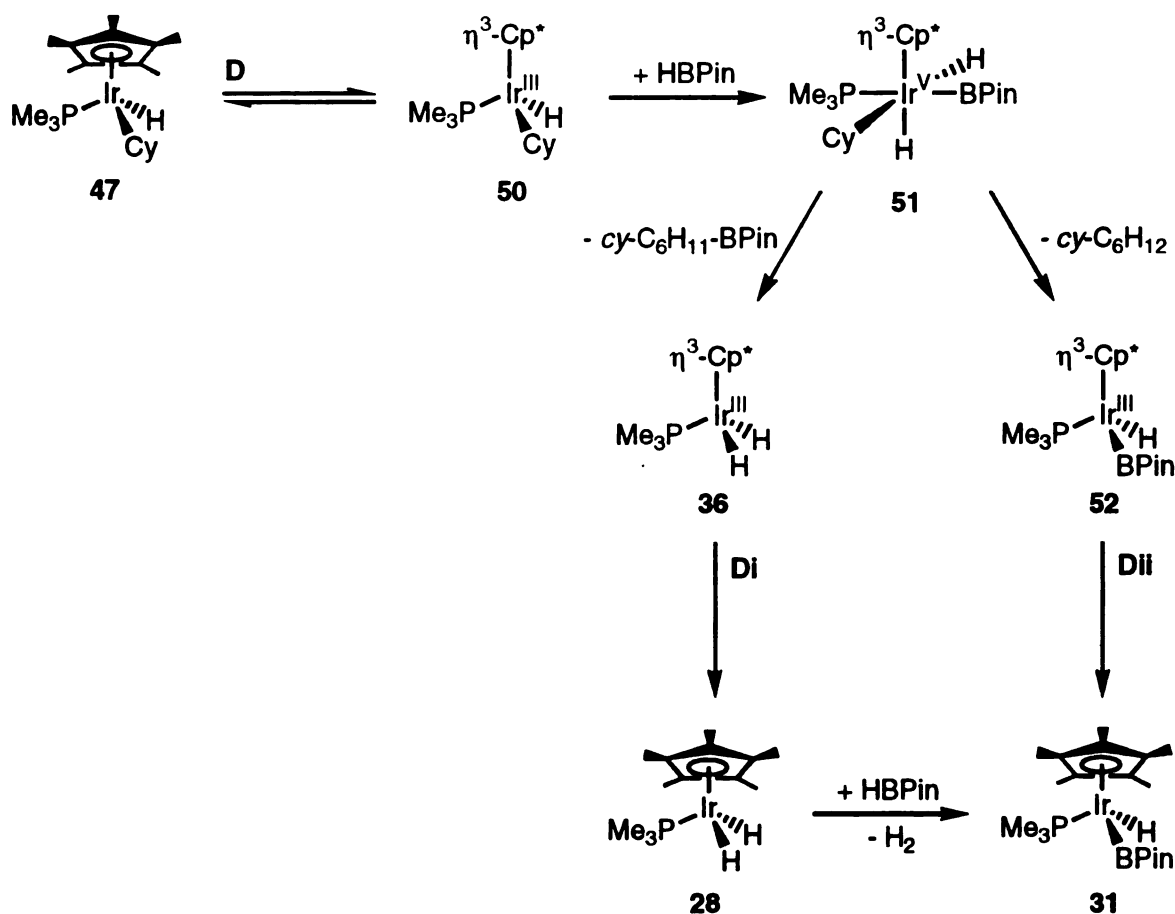
Figure 53. Ring slip pathways for the reaction of HBPin with **47**.

Two potential mechanisms besides pathway **B** could account for enhanced cyclohexane formation. These include the reaction of cy-C_6H_{11}–BPin with compound **28** to generate Cp*Ir(PMe$_3$)(BPin)H and cyclohexane (Eq 34) or pathways that involve metathesis between compound Cp*Ir(PMe$_3$)(Cy)H and C_6D_6.[155] Neither of these occur as control experiments indicated that (i) cy-C_6H_{11}–BPin and Cp*Ir(PMe$_3$)H$_2$ do not react and (ii) deuterium incorporation in compound **31** was insignificant as judged by GC-mass spectrometry of an NMR tube reaction sample. The metathesis of C_6D_6 with **47** would provide $C_6H_{11}D$ and the mass envelopes for both cyclohexane and cyclohexane-d_1 can be calculated. The envelope of the parent peak for cyclohexane produced in this reaction matched that calculated for C_6H_{12}.

$$\text{28} \ + \ cy\text{-}C_6H_{11}\text{--}B(C_6F_5)_2 \ \xrightarrow{\ \ \ \times \ \ \ } \ \text{31} \ + \ cy\text{-}C_6H_{12} \tag{34}$$
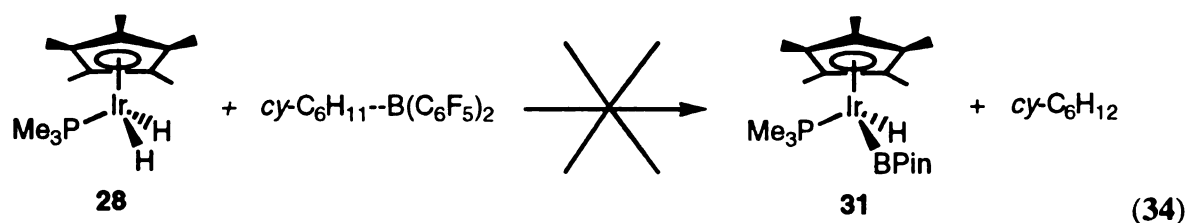
The reaction between compound **47** and HBCat also gave a mixture of C_6H_{12} and cy-C_6H_{11}–BCat. In addition to Cp*Ir(PMe$_3$)(BCat)H and phenyl hydride (**48**), the diboryl compound (**29**), was also formed in this reaction.

Reactions of **48** with HBPin and HBCat required elevated temperatures (Figure 54. 150 °C or higher). In both cases Ph–BX$_2$ was the major organoboron product although a sharp C_6H_6 resonance appears downfield from residual C_6D_5H in the deuterated solvent. This observation supports the notion that metathesis of B–H bonds with M–C bonds can result in formation of M–B and C–H bonds in this system. For HBCat, the diboryl compound, **29**, was the predominant Ir containing product. The reaction with HBPin yielded the monoboryl compound, **31**, as the major Ir containing compound. This last reaction was performed at 150 °C with 12 and 24-fold excesses of HBPin and was monitored intermittently by ^{1}H NMR. Neither reaction was taken to completion as plots of $\ln\{[48]_t/[48]_0\}$ versus time were not linear (Figure 55) and indicated that excessive reaction times were necessary to complete conversion to **31**.
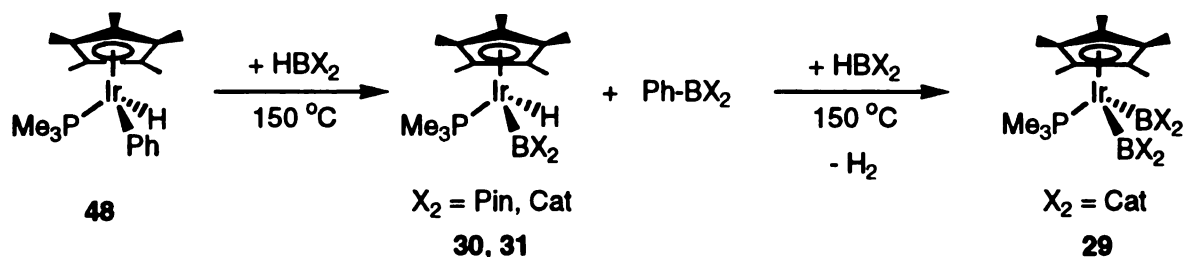
Figure 54. Reactivity of **48** with HBPin and HBCat.
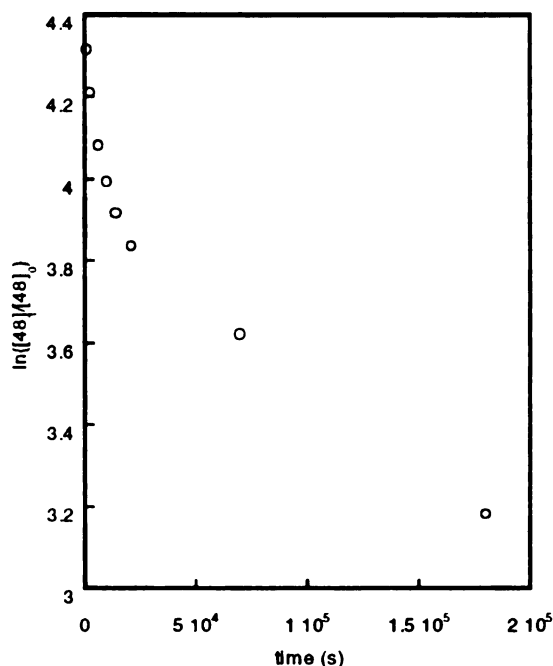
Figure 55. Plot of $\ln\{[48]_t/[48]_0\}$ versus time for the reaction of **48** with 12 equivalents of HBPin at 150 °C. The last data point indicates two half-lives completion.($[Cp^*Ir(PMe_3)H_2]_o = 35$ mM; $[HBPin]_o = 407$ mM).

Catalytic Boration of Arenes

The stoichiometric chemistry of compounds $Cp^*Ir(PMe_3)(Cy)H$ and $Cp^*Ir(PMe_3)(Ph)H$ suggested a potential catalytic conversion of unactivated hydrocarbons to organoboranes in this system as shown in Figure 56. Since B–C bond formation was most facile for reactions of compounds **47** and **48** with $[HB(C_6F_5)_2]_2$, the catalytic viability of this borane reagent was assessed first. The dihydride product from Eq 31 reacts with $[HB(C_6F_5)_2]_2$, to generate the borohydride complex, $Cp^*Ir(PMe_3)(H)[HBH(C_6F_5)_2]$.

88

H-B(C$_6$F$_5$)$_2$ cy-C$_6$H$_{11}$-B(C$_6$F$_5$)$_2$

Cp*Ir(PMe$_3$) complexes:

Me$_3$P—Ir—H / cy-C$_6$H$_{11}$ **47**

Me$_3$P—Ir—H / H   **28**

H$_2$

$h\nu$

cy-C$_6$H$_{12}$

Me$_3$P—Ir—H / H   **28**

+

HB(C$_6$F$_5$)$_2$

H-B(C$_6$F$_5$)$_2$

Me$_3$P—Ir···H—B···H / C$_6$F$_5$ C$_6$F$_5$ **45**
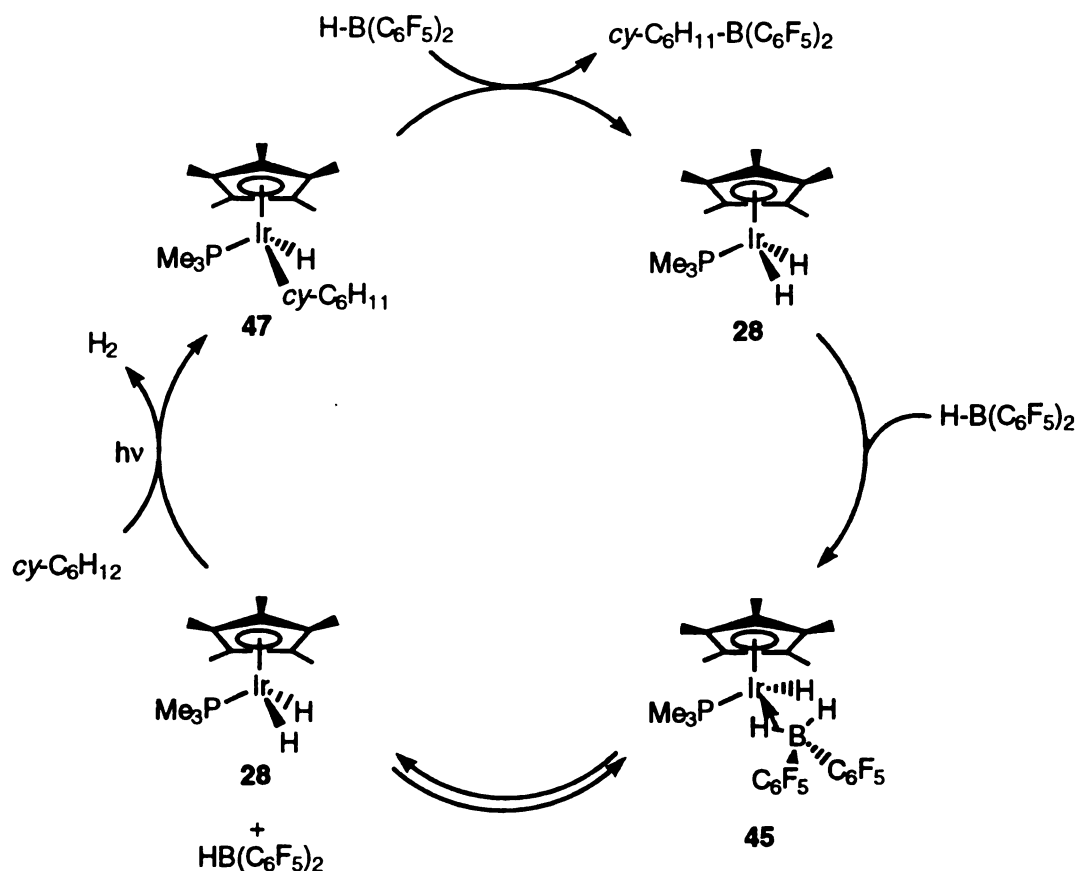
Figure 56. Proposed catalytic cycle for the conversion of alkanes to organoboranes.

Following the C–B activation process, the dihydride product reacted with excess [HB(C$_6$F$_5$)$_2$]$_2$ in solution to generate compound **45**. At elevated temperatures, a complex mixture formed when benzene or cyclohexane solutions of **45** were heated with excess [HB(C$_6$F$_5$)$_2$]$_2$, eliminating the possibility of a clean thermal catalytic process. Since photolyses of compound Cp*Ir(PMe$_3$)H$_2$ in the appropriate solvent generates compounds **47** and **48**, similar photochemical generation of compounds **47** and **48** from Cp*Ir(PMe$_3$)H[HBH(C$_6$F$_5$)$_2$] would complete a photocatalytic cycle. Unfortunately, compound **45** was photochemically inert.

In the course of investigating the general reactivity of iridium boryl compounds, thermal B–H or B–B elimination from compounds Cp*Ir(PMe$_3$)(BCat)$_2$ and

89

Cp*Ir(PMe₃)(BPin)H was assessed by heating C_6D_6 solutions of the pure compounds. No evidence for elimination or C–B bond formation was observed even after several days at 200 °C. Thus, photochemical reactivity of mono or diboryl derivatives seemed necessary for catalytic activity. Although the diboryl compound, **29**, was photochemically inert, the phenylhydride compound, **48**, was regenerated when a benzene solution of the monoboryl compound, **31**, was photolyzed (Eq 35). Although less efficient, the regeneration of **47** also occurred when a cyclohexane solution of **31** was photolyzed. These two reactions, thermal B–C and photochemical Ir–C bond formation, constitute a catalytic cycle for HBPin when performed consecutively.

$$\text{Me}_3\text{P}^{-}\underset{\substack{|\\\text{BPin}}}{\overset{\text{Ir}}{\,\,}}\!\!\text{H} \quad \xrightarrow{\text{hv, H-C}_6\text{H}_5} \quad \text{Me}_3\text{P}^{-}\underset{\substack{|\\\text{C}_6\text{H}_5}}{\overset{\text{Ir}}{\,\,}}\!\!\text{H} \quad + \quad \text{HBPin}$$

$$\mathbf{31} \qquad\qquad\qquad\qquad\qquad\qquad \mathbf{48} \qquad\qquad\qquad (35)$$
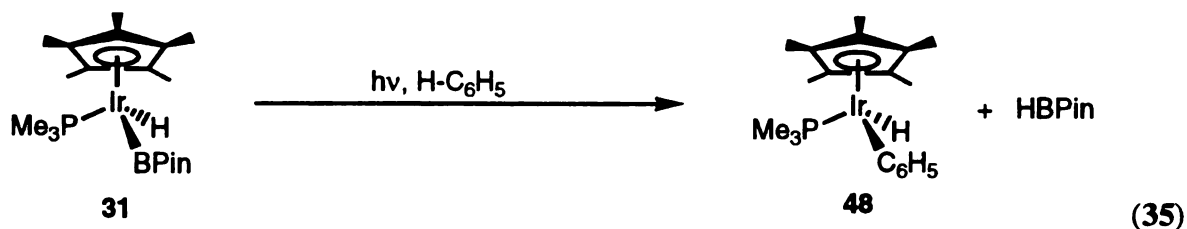
To evaluate the potential of photocatalytic cyclohexane and benzene activation, two thick-walled flasks were charged with Cp*Ir(PMe₃)H₂ (0.15 mol) and HBPin (0.89 mmol) and the contents were dissolved in C_6H_{12} and C_6H_6, respectively. After the solutions were photolyzed to generate compounds **47** and **48** (confirmed by ^{31}P NMR), the flasks were heated in an oil bath to convert the phenyl and cyclohexyl compounds to to Cp*Ir(PMe₃)(BPin)H and R–BPin. After the thermal conversion was complete, the solutions were photolyzed to regenerate compounds **47** and **48**. From the initial Ir and borane concentrations, full conversion should have required five thermal/photolytic cycles; however, ^{11}B NMR indicated full conversion of the borane after the third thermolysis in the C_6H_6 solution. On the other hand, no significant conversion to organoborane was apparent in the ^{11}B NMR. In fact, ^{31}P NMR indicated that probable

formation of the diboryl was occurring. As mentioned earlier, the diboryl complex, **29**, was photolytically inactive and it stands to reason that the pinacolate analog also is unreactive. Indeed this appears to be the case as continued thermolysis/photolysis cycling yielded no further reaction.

A thermal catalytic process, however, was clearly implicated in the case of the benzene solution. Although we had determined that solutions of $Cp^*Ir(PMe_3)(BPin)H$ do not react with C_6H_6, reexamination of the NMR spectra for the "stoichiometric" reaction between **48** and 6 equivalents of HBPin in C_6D_6 indicated that the intensity of the pinacolate resonance for Ph–BPin was greater than anticipated. When a solution of **31** and five molar equivalents of HBPin was heated in C_6D_6, ^{11}B NMR indicated exchange between the boron hydride and solvent deuterons after 18 h at 150 °C. Most importantly, conversion to C_6D_5BPin was quantitative after 60 h at 150 °C (Eq 36), as judged by ^1H (Figure 57) and ^{11}B NMR.

$$\text{HBPin} \; + \quad \overset{d_6}{\text{(benzene)}} \quad \xrightarrow[\text{20\% 31}]{\text{60 h, 150 °C}} \quad \text{PinB}-\overset{d_5}{\text{(benzene)}} \; + \; \text{HD} \tag{36}$$
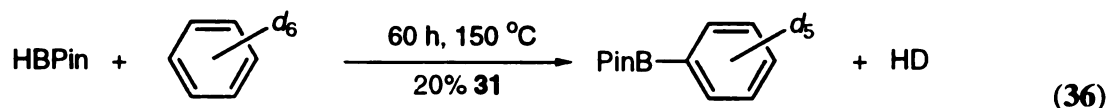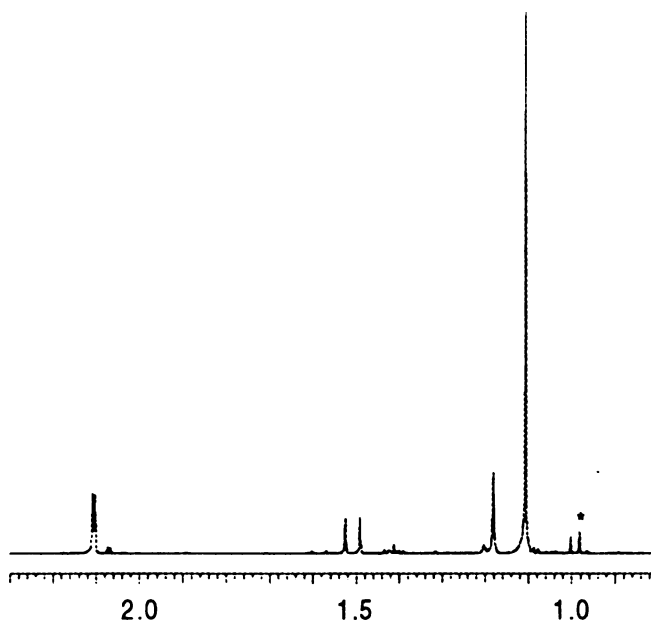
Figure 57. ^1H NMR of the aliphatic region from the catalytic borylation of C_6D_6 with **31** after 60 hours at 150 °C. The tall resonance at δ 1.1 is due to C_6D_5–BPin and the peak at δ 0.98 (denoted with an asterisk) is due to residual HBPin.

The reaction was repeated on a larger scale (**31**, 0.15 mmol; HBPin, 0.75 mmol) in C_6H_6, and C_6H_5BPin was isolated in 53% yield although ^{11}B NMR again indicated quantitative conversion. The catalytic process is very clean as judged by ^1H, ^{11}B and ^{31}P NMR spectra taken of the crude reaction material at the end of the large scale reaction following removal of the solvent (^1H and ^{11}B NMR are shown in Figures 58 and 59, respectively).
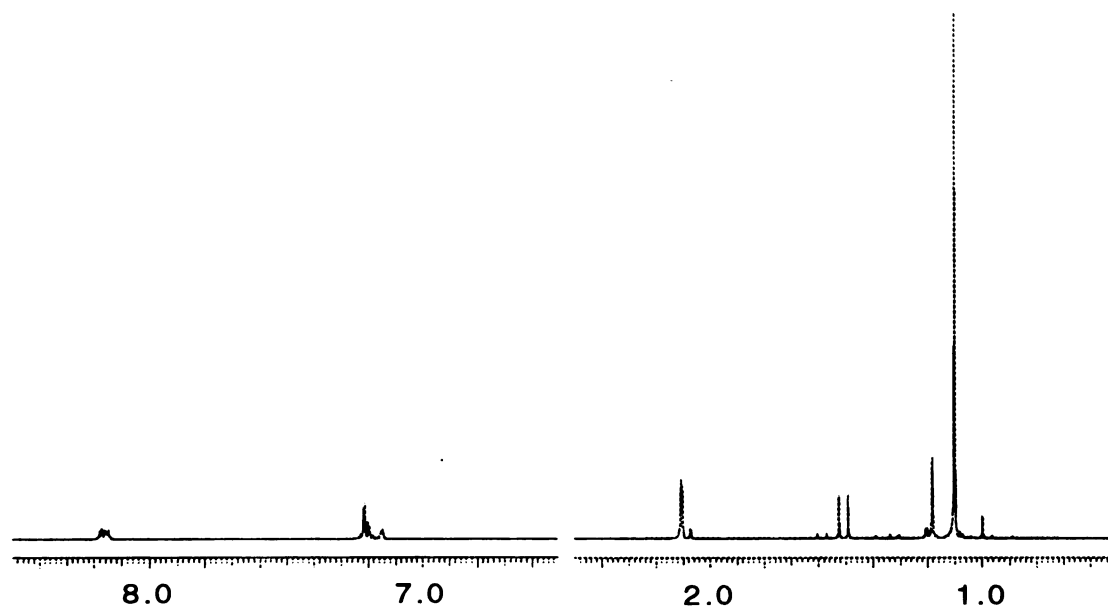
Figure 58. ^{1}H NMR of selected regions of the crude material for the catalytic formation of Ph–BPin.
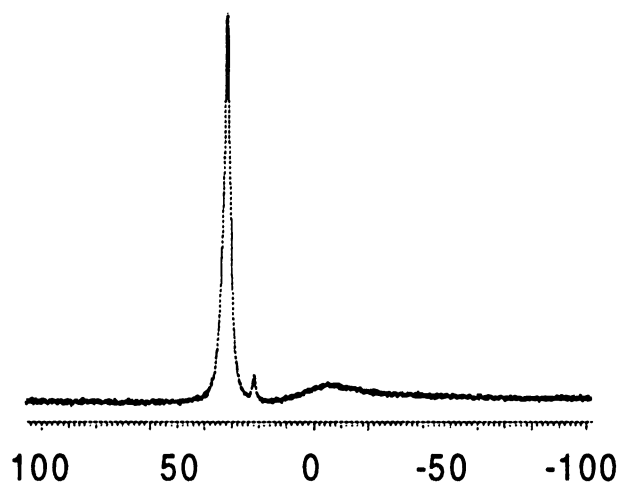
Figure 59. ^{11}B NMR of the crude material for the catalytic formation of Ph–BPin.

In order to assess the selectivity of the reaction towards aromatic versus alkyl C–H bonds an NMR tube reaction utilizing toluene as the reaction solvent was performed. When the reaction was complete (as judged by ^{11}B NMR), the contents of the tube were placed in a Schlenk tube and the solvent was removed. ^{1}H NMR analysis of the residue

did indicate that more than one isomer was formed. Evaluation of the aromatic region, however, indicated that boration had occurred at only the *para* and *meta* positions of the arene. The *para* and *meta* isomers were identified by comparison to literature values or to an authentic sample prepared according to the method of Ishiyama et al.[125] Other functionalized arenes were used as reaction solvents in order to probe the generality of this reaction. In each case boration was observed to occur at only the *para* and *meta* positions. Steric interactions have been used to explain the lack of substitution at the *ortho* position in similar systems. Consistent with this line of reasoning is the fact that when boration of *p*-xylene was attempted the reaction was much slower and mesitylene did not react. For comparison, after two and a half weeks at 150 °C ^{11}B NMR indicated that the reaction in *p*-xylene had not even reached two turnovers. Again, ^{1}H NMR analysis of the residue was consistent with attack at the arene C–H bond as only one isomer could be detected in the aromatic region (Eq 37).

$$\text{H-BPin} \ + \quad \xrightarrow[\substack{\text{2.5 weeks} \\ 20\% \ 31}]{150 \ ^\circ\text{C}} \quad \text{PinB-} \tag{37}$$
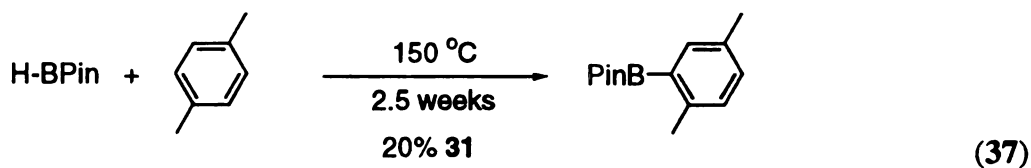
In the case of monofunctionalized arenes the ratio of *para* and *meta* substituted products was essentially statistical; i.e. approximately two-thirds of the product was *meta* substituted and one-third was *para* substituted (Figure 60). Another interesting feature of these reactions was the relative rate of boration. The qualitative order, based on the disappearance of the doublet due to HBPin in the ^{11}B NMR, was R = CF$_3$ >> H > CH$_3$ > NMe$_2$.

R	% para	% meta	selectivity para : meta
CH$_3$	34	66	1 : 0.97
CF$_3$	30	70	1 : 1.17
NMe$_2$	35	65	1 : 0.93

Figure 60. Product distributions for the catalytic conversion of monosubstituted arenes.

This observation is consistent with the progression for nucleophilic aromatic substitution where electron withdrawing groups promote increased rates of reaction. The usual substitution patterns for *ortho* and *para* directors (R = CF$_3$) and *meta* directors (CH$_3$, NMe$_2$) in nucleophilic aromatic substitutions, however, are not observed. Metal mediated nucleophilic aromatic substitutions have previously been reported for η^6-arene compounds.[156,157] Coordination of the arene to a transition metal center produces a highly electrophilic aromatic substrate that is more readily attacked by nucleophiles. In general, this system has the same directing effects that are observed in the strictly organic reactions; however, the similarities are seen primarily with the strongest donors, such as amides and alkoxides (*meta*) and trifluoromethyl (*para*).

Similar qualitative observations regarding the rates and product distributions in the thermolysis of Cp*Ir(PR$_3$)Me$_2$ in arenes have been reported by Diversi et al.[158] Exclusive *meta* and *para* activation of toluene has also been observed by the cationic Ir(III) species Cp*Ir(PMe$_3$)(Me)OTf at 25 °C and by the hydrido rhodium complex, Cp*Rh(PMe$_3$)(Ph)H, at 60 °C.[133,159] On the other hand, an η^3-benzylic complex is formed when *p*-xylene is reacted with Cp*Ir(PMe$_3$)(Me)OTf at 40 °C, benzylic and *ortho* activation were observed to occur during photolysis of a *p*-xylene solution of 31 at room temperature.[65,133] Low temperature photolysis of a toluene solution of Cp*Rh(PMe$_3$)H$_2$ produces a small amount (7 %) of the *ortho* activated product and a trace amount (< 1 %)

of the benzylic product along with the major *para* and *meta* products (36 % and 56 %, respectively).[69]

Competitive borylation experiments between benzene and substituted arenes were performed in order to determine selectivities for various arenes. The relative selectivities were calculated by the following method: equimolar amounts of C_6H_6 and the arenes were used for all catalytic runs and the product ratios were determined by integration of appropriate resonances. The product ratios were then divided by the number of aromatic hydrogens available for substitution. For instance, the product ratio from the $C_6H_5CF_3/C_6H_6$ experiment was 86:14 (the value for $C_6H_5CF_3$ includes both the *meta* and *para* substituted products). This product ratio is then divided by the available hydrogens (three for $C_6H_5CF_3$ and six for C_6H_6) to give a ratio of 28.7:3. Normalizing the result yields the final relative selectivity of 12.3/1. A summary of the results is given in Figure 61. The values for $C_6H_5CF_3$ and *p*-xylene are consistent with the earlier observations regarding the general rates of borylation; electron withdrawing groups promote substitution and steric interactions hinder the rate of substitution. At first glance, the values for $C_6H_5CH_3$ and $C_6H_5NMe_2$ appears contrary to the rate observations; however, the molar concentration of the solvent mixture probably was not equal considering the differences in boiling point (C_6H_6, bp 80 °C; $C_6H_5CH_3$, bp 111 °C; $C_6H_5CF_3$, bp 102 °C; $C_6H_5NMe_2$, bp 193 °C) and the temperature at which the catalytic reactions take place. A significant vapor pressure due to C_6H_6 may have been present in the NMR tube, thus skewing all the values for the substituted arenes. A competition experiment was also performed to examine the selectivity of the catalysis for C–H bonds versus C–D bonds. A one to one molar mixture of C_6H_6 and C_6D_6 was used under otherwise typical reaction conditions and a ratio of $k_H/k_D = 2.15$ for the catalytic reaction was calculated based on integration of the aromatic resonances with respect to the pinacolate methyl resonance. This observation is consistent with the slow step of the reaction involving the activation of an arene C–H bond.
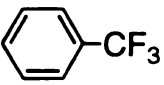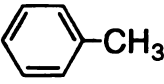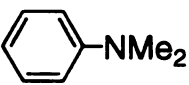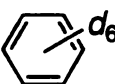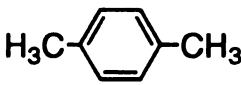
solvent mixture C_6H_6 : arene	relative selectivity C_6H_6 : arene
⟨benzene⟩-CF$_3$	1 : 12.3
⟨benzene⟩-CH$_3$	1 : 2.41
⟨benzene⟩-NMe$_2$	1 : 1.46
⟨benzene⟩-d_6	2.15 : 1
H$_3$C-⟨benzene⟩-CH$_3$	19 : 1

Figure 61. Solvent mixtures and relative ratios for competitive borylation of arenes. All solvent mixtures are one-to-one C_6H_6:arene.

At this time, the mechanism of this process is unknown; however, some speculations can be made. Clearly, the thermal stability of **31** in benzene solutions is significant. Arene borylation cannot occur by either simple C–H oxidative addition/C–B reductive elimination (Eq 38) or Ir–B/C–H metathesis pathways (Eq 39). Also, the concentration of **28** does not significantly increase throughout the course of the reaction, as would be expected if these pathways were in operation. The observation that catalysis by **31** occurs faster than the conversion of **48** to **31** and the fact that **48** is not observed in solution implies that [Cp*Ir(PMe₃)], a postulated intermediate in related reactions, is not being generated.

97

$$\text{(38)}$$

$$\text{(39)}$$
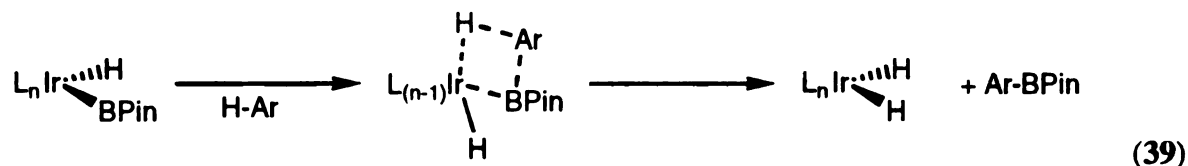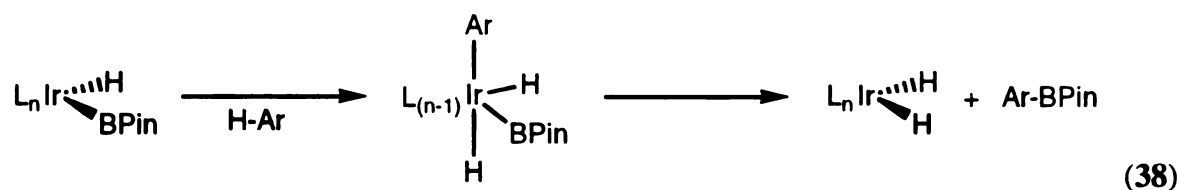
The formation of a cationic boryl species *via* hydride abstraction by HBPin (Figure 62) is unlikely. The opposite trend in the rate of reaction of arenes is observed with a related cationic complex. CD_2Cl_2 solutions of $Cp^*Ir(PMe_3)(Me)OTf$ react sluggishly with $C_6H_5CF_3$ in comparison to benzene and toluene.[160]
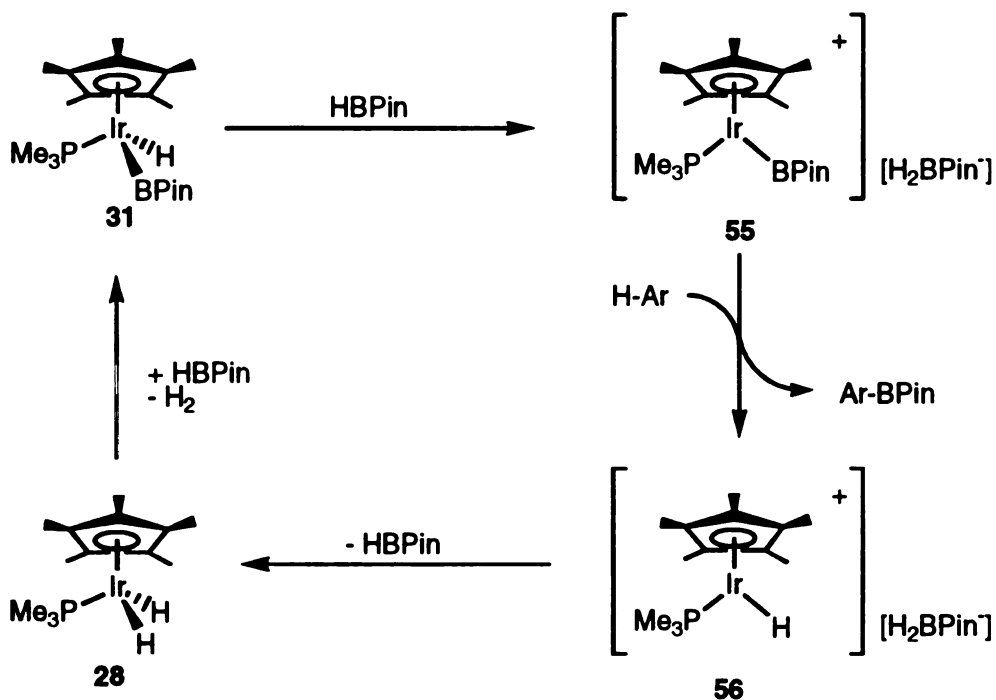
Figure 62. Proposed catalytic cycle involving a cationic iridium boryl species.

Looking beyond these possibilities, the mechanism must include the following empirical facts; 1) HBPin must be present in order for C–H functionalization to occur, 2) steric interactions appear to affect the substitution patterns, and 3) the k_H/k_D value indicates that C–H bond breaking process is likely a part of the rate limiting step of the reaction.

To date, few examples of hydrocarbon functionalization have been reported; therefore, the results presented in this chapter represent a significant step toward realizing this ultimate goal. Although the catalytic boration proceeds at high temperature and high catalyst loading, aromatic hydrogens are selectively substituted in the presence of alkyl groups. Further work is needed in this system to elucidate the mechanism by which borylation occurs. Also, new systems that have recently been reported to activate C–H bonds, such as (PCP)MH$_2$ (M = Ir, Rh) and tris(pyrazolylborate)platinumalkyl complexes may prove fruitful in these endeavors as well.[161-163]

CHAPTER 5

EXPERIMENTAL

General Considerations

All manipulations were performed using glove box, Schlenk or vacuum-line techniques. Benzene, diethyl ether, heptane, pentane, tetrahydrofuran and toluene were pre-dried over sodium and distilled from sodium/benzophenone ketyl. Methylenechloride was pre-dried over $CaCl_2$ and distilled from CaH_2. DME (dimethoxyethylene) was dried with CaH_2 and distilled from $LiAlH_4$. Cyclohexane was purified and dried according to the method reported by Perrin and Armarego. $CDCl_3$ was dried with and stored over 3Å sieves. CD_2Cl_2 was dried with 4Å sieves. C_6D_6 and toluene-d_8 were dried and distilled from 3Å sieves and stored over a sodium mirror. $CDCl_2F$ was prepared according to literature method. NEt_3 was refluxed over CaH_2 and freshly distilled prior to use. Argon and nitrogen were purified by passage through a column of MnO on silica or vermiculite. $(PPh_3)_2Pt(\eta^2-C_2H_4)$,[87] $(PPh_3)_2Pt(CH_2)_4$,[113] $Pt(nbe)_3$,[164] $Pt(COD)_2$,[164] $Cp*Ir(PMe_3)H_2$,[65] $Cp*Ir(PMe_3)(Ph)H$,[66] $Cp*Ir(PMe_3)(cy-C_6H_{11})H$,[66] HC_5Me_5,[165] $Me_3SnB(NMe_2)_2$,[166] 1,2-bis[p-(trifluoromethyl)phenyl]acetylene,[167] 1-chloro-5-hexene,[168] acetic acid 5-hexenyl ester,[168] $[HB(C_6F_5)_2]_2$,[153] and PMe_3[169] were prepared according to literature methods. $B_2(OR_2)_2$ derivatives were prepared according to the literaature method except that trace HCl impurities were removed by washing the solid with triethylamine prior to pentane extraction and crystallization of the product.[170] HBCat and HBPin were prepared by reacting $BH_3·THF$ (Aldrich) with catechol (Aldrich) and pinacol (Aldrich) respectively. The THF was then distilled from the solution at atmospheric pressure and the remaining solution vacuum distilled to give the boranes as clear viscous liquids. DBCat and DBPin were prepared by bubbling B_2D_6, generated from $NaBD_4$ and $BF_3·Et_2O$, through a THF solution of the appropriate diol. Ar–BPin[125] and CyBPin[171] were prepared according to

100

literature methods. Cp*Ir(PMe₃)D₂ was prepared by stirring an ether solution of Cp*Ir(PMe₃)H₂ with degassed D_2O, followed by drying with $MgSO_4$ and crystallization from pentane. 1-Hexyne, 4-octyne, phenylacetylene, 1-phenyl-1-propyne, methyl propargyl ether, dimethyl acetylene dicarboxylate, 1-hexene, 1,5-hexadiene, norbornene, norbornadiene, vinyl anisole, and p-(trifluoromethyl)styrene were all purchased from commercial sources and distilled prior to use. Ethylene was purchased from Matheson and used as received.

^1H NMR spectra were recorded on Varian Gemini–300, VXR–300, inova–300 or VXR–500 spectrometers and referenced to residual proton solvent signals. ^2H, ^{11}B, ^{13}C, ^{19}F and ^{31}P spectra were recorded on Varian VXR–300 or inova–300 spectrometers operating at 46.04, 96.19, 75.43, 282.22, 121.44, and 111.86 MHz, respectively. Deuterium chemical shifts are referenced to residual deuterium solvent signals of an external standard of the same solvent that the sample is dissolved in. Boron chemical shifts are referenced to a neat $BF_3 \cdot Et_2O$ external standard. Carbon chemical shifts are referenced to solvent signals. Fluorine chemical shifts are referenced to a neat $CFCl_3$ external standard. Phosphorous chemical shifts are referenced to an 85% phosphoric acid external standard. Tin chemical shifts are referenced to a neat $SnMe_4$ external standard. Coupling constants involving tin are taken as the average of the ^{117}Sn and ^{119}Sn satellites except for those values given in the ^{119}Sn NMR data. Photolytic experiments were performed in a 450 W Rayonet photolysis unit equipped with 300 nm lamps. The area in which NMR tubes were exposed to photolysis was cooled by an internal fan, keeping the temperature at approximately 30 °C. Elemental analyses were performed on a Perkin Elmer Series II CHNS/O Analyzer 2400 or by Desert Analytics (Tuscon, AZ). Mass spectroscopic data were obtained on a portable Trio-1 VG Masslab Ltd. Mass spectrometer. GC analysis of catalytic mixtures were performed on a Hewlett Packard 58980A Gas Chromatograph. Mass spectral data were obtained at the Michigan State University Mass Spectrometry Facility which is supported, in part, by a grant (DRR-

Syntheses

cis-(PPh₃)₂Pt(BCat)₂ (2). $(PPh_3)_2Pt(\eta^2-C_2H_4)56$ (100 mg, 0.134 mmol) and B_2Cat_2 (35 mg, 0.15 mmol) were placed in a flask and dissolved in 5 mL of toluene. A white precipitate formed immediately. The solution was stirred for 2 h at room temperature, and the supernatant was removed via cannula. Additional product was obtained by removing the solvent under reduced pressure and washing the residue with toluene (2 mL). The overall yield was 96 mg (75%). ^1H NMR (C_6D_6): 6.54 (m, 4 H, $BO_2C_6H_4$), 6.77 (m, 4 H, $BO_2C_6H_4$), 6.80 (m, 18 H, $P(C_6H_5)_3$), 7.55 (m, 12 H, $P(C_6H_5)_3$). ^{11}B NMR ($CDCl_3$ was used for the sake of making a solution concentrated enough, quartz NMR tube): rt, δ 48.5 $(v_{1/2} = 1845$ Hz). ^{31}P NMR ($CDCl_3$ was used in order to take low temperature spectra): rt, δ 28.9 $(^1J_{Pt-P} = 1629$ Hz, $v_{1/2} = 60$ Hz); –50 °C, δ 28.9 $(^1J_{Pt-P} = 1646$ Hz, $v_{1/2} = 31$ Hz). Anal. Calcd for $C_{48.5}H_{55}B_2O_4P_2ClPt$: C, 57.29; H, 5.45. Found: C, 55.28; H, 5.27. Mp: 193–195 °C (dec).

cis-(PPh₃)₂Pt(BPin)₂ (3). $(PPh_3)_2Pt(\eta^2-C_2H_4)$ (100 mg, 0.134 mmol) and B_2Pin_2 (35 mg, 0.15 mmol) were placed in a flask and dissolved in 5 mL of toluene. The golden yellow solution was stirred for 2 h at room temperature, and subsequent solvent evaporation yielded a light orange-yellow powder. The residue was recystallized from CH_2Cl_2/ethanol, washed with hexanes, and dried in *vacuo* to give white crystals (91 mg, 70%). ^1H NMR (C_6D_6): 1.02 (s, 24 H, $BO_2C_6H_{12}$), 6.88 (m, 18 H, $P(C_6H_5)_3$), 7.58 (m, 12 H, $P(C_6H_5)_3$). ^{11}B NMR $(C_6D_6$, quartz NMR tube): 46.3 $(v_{1/2} = 1830$ Hz). ^{31}P NMR (C_6D_6): 29.77 $(^1J_{Pt-P} = 1506$ Hz). Mp: 183–187 °C (dec). Anal. Calcd for $C_{48.5}H_{55}B_2O_4P_2ClPt$: C, 57.29; H, 5.45. Found: C, 55.28; H, 5.27. Analyses for crystalline samples of $X \cdot (CH_2Cl_2)_{1/2}$ were consistently low in carbon. Although this compound has

been structurally characterized, the combustion analysis was not reported. Our melting points for crystalline materials were consistently 40 °C higher than the reported value.

cis-(PPh₃)₂Pt(SnMe₃)[B(NMe₂)₂] (4). $(PPh_3)_2Pt(\eta^2\text{-}C_2H_4)$ (300 mg, 0.402 mmol) was placed in a flask and dissolved in 5 mL toluene. $Me_3Sn\text{-}B(NMe_2)_2$ (105 mg, 0.402 mmol) was then added via syringe. The solution was heated at 45°C for 3 hrs after which the solvent was removed in *vacuo*. The residue was dissolved in methylene chloride, layered with ethanol and placed in a –5°C freezer. Yellow crystals (260 mg, 66%) were collected after 12 hrs. An additional crop of crystals (28 mg, 7%) was obtained after reducing the mother liquor and replacing it in the –5°C freezer. ^{1}H NMR (CDCl₃); δ – 0.46 (s, 9 H, Sn(CH_3)₃, $^2J_{H-Sn}$ = 38 Hz, $^3J_{H-Pt}$ = 8 Hz); δ 2.53 (s, 12 H, B(N(CH_3)₂)₂); δ 7.01–7.31 (m, 30 H, P(C₆H_5)₃). ^{11}B NMR (CDCl₃, quartz NMR tube); δ 45.9 (broad). ^{31}P NMR (CDCl₃, –45°C); δ 30.6 (d, $^1J_{P-Pt}$ = 2736 Hz, $^2J_{P-P}$ = 14.6, $^2J_{P-Sn(trans)}$ = 1487 Hz), δ 31.3 (broad, $^1J_{P-Pt}$ = 1404 Hz). ^{119}Sn (CDCl₃); δ –24.62 (dd, $^1J_{Sn-Pt}$ = 12,594 Hz, $^2J_{Sn-P(cis)}$ = 156 Hz, $^2J_{Sn-P(trans)}$ = 1519 Hz,). mp; 201–202°C (dec.). anal. Calc. C (52.57%), H (5.23%), N (2.85%). Found C (52.29%), H (5.15%), N (2.77%).

cis-(PPh₃)₂Pt(SnMe₃)₂ (6). This preparation is analogous to that reported in the literature. $(PPh_3)_2Pt(\eta^2\text{-}C_2H_4)$ (100 mg, 0.134 mmol) was placed in a flask and dissolved in 7 mL of toluene. A bright yellow solution formed on addition of Me₆Sn₂ (28 µL, 0.134 mmol), and within 15 min a bright yellow precipitate formed. After the solution was stirred for 2 h, the solvent was removed under reduced pressure to afford a bright yellow powder. ^{1}H NMR (C₆D₆): 0.40 (s, 18 H, Sn(CH_3)₃, $^4J_{Pt-H}$ = 8 Hz, $^3J_{Sn-H}$ = 20 Hz), 6.86 (m, 18 H, P(C₆H_5)₃), 7.46 (m, 12 H, P(C₆H_5)₃). ^{31}P NMR (C₆D₆): 35.1 ($^1J_{Pt-P}$ = 2621 Hz, $^2J_{Sn-P}$ = 614, 642 Hz).

Cp*Ir(PMe₃)(BCat)₂ (29). Cp*Ir(PMe₃)H₂ (150 mg, 0.37 mmol) and CatB–BCat (167 mg, 0.70 mmol) were loaded into a Schlenk tube and dissolved in 3 mL toluene. The solution was stirred at reflux for 24 hr. The solution was cooled to room temperature and layered with 10 mL pentane. White crystals (145 mg, 60%) deposited after several days

at –80 °C. ^{1}H NMR (C$_6$D$_6$); δ 1.48 (d, 9 H, P(CH$_3$)$_3$, $^2J_{H-P}$ = 11 Hz), 1.97 (d, 15 H, C$_5$(CH$_3$)$_5$, $^4J_{H-P}$ = 2 Hz), 6.75 (m, 2 H, BO$_2$C$_6$H$_4$), 7.05 (m, 2 H, BO$_2$C$_6$H$_4$). ^{11}B NMR (C$_6$D$_6$); δ 36. ^{31}P{^{1}H} NMR (C$_6$D$_6$); δ –39.5. Calc. C(46.82), H(5.03). Found C(48.53), H(5.24). M.p. 170–172 °C.

Cp*Ir(PMe$_3$)(BPin)H (31). A solution of Cp*Ir(PMe$_3$)H$_2$ (305 mg, 0.75 mmol) and HBPin (contaminated with 5% thf, 288 mg, 2.3 mmol), dissolved in 4 mL toluene, was heated at 125 °C for 4 days. The solution was then transferred to a Schlenk flask via cannula and the volatile materials removed under vacuum (three hours). Cp*Ir(PMe$_3$)(BPin)H (316 mg, 79%) was collected as an orange oil. ^{1}H NMR (C$_6$D$_6$); δ – 17.64 (d, 1 H, Ir–H, $^2J_{H-P}$ = 29 Hz), 1.17 (12 H, BO$_2$C$_6$H$_{12}$), 1.50 (d, 9 H, P(CH$_3$)$_3$, $^2J_{H-P}$ = 10 Hz), 2.10 (d, 15 H, C$_5$(CH$_3$)$_5$, $^4J_{H-P}$ = 2 Hz). ^{11}B NMR (C$_6$D$_6$); δ 33. ^{31}P{^{1}H} NMR (C$_6$D$_6$); δ –42.8. Calc. C(42.79), H(7.02). Found C(42.79), H(7.31).

Cp*Ir(PMe$_3$)H[HBH(C$_6$F$_5$)$_2$] (45). Cp*Ir(PMe$_3$)H$_2$ (200 mg, 0.493 mmol), dissolved in 2 mL toluene, was transferred via cannula to a suspension of [HB(C$_6$F$_5$)$_2$]$_2$ (170 mg, 0.246 mmol) in 3 mL toluene. The resulting solution was stirred at room temperature for 30 min. The volume of the solution was reduced to 3 mL and layered with 10 mL pentane. Yellow crystals (312 mg, 84%) deposit upon cooling at –78 °C for 24 hr. ^{1}H NMR (toluene–d_8, –70 °C); δ –15.91 (d, 2 H, Ir–H$_{term}$ and Ir–H–B, $^2J_{H-P}$ = 27 Hz), 0.88 (d, 9 H, P(CH$_3$)$_3$, $^2J_{H-P}$ = 11 Hz), 1.35 (15 H, C$_5$(CH$_3$)), 4.35 (br, 1 H, HB(C$_6$F$_5$)$_2$). ^{11}B NMR (C$_6$D$_6$); δ –43. ^{19}F NMR (C$_6$D$_6$); δ –131.2 (2 F), –160.1 (1 F), – 165.3 (2 F). ^{31}P{^{1}H} NMR (C$_6$D$_6$); δ –40.3. IR(Nujol mull, cm^{-1}) 2093, 1842, 1640. Calc. C(39.96), H(3.62). Found C(39.65), H(3.45). M.p. 139–144 °C.

Cp*Ir(PMe$_3$)(B(C$_6$F$_5$)$_2$)H (46). Cp*Ir(PMe$_3$)H(HBH(C$_6$F$_5$)$_2$) (510 mg, 0.68 mmol) was dissolved in 7 mL toluene and stirred in a closed vessel at 110 °C for 4 hr. The solvent was removed in *vacuo* and the oily residue is extracted with 3 x 7 mL pentane. The pentane extracts were reduced in volume to 4 mL and cooled to –78 °C. Yellow crystals (187 mg, 37 %) deposit after 12 hr. ^{1}H NMR (C$_6$D$_6$); δ –16.64 (d, 1 H, Ir–H, $^2J_{H-}$

$_P$ = 30 Hz), δ 0.96 (d, 9 H, P(CH_3)$_3$, $^2J_{H-P}$ = 11 Hz), 1.55 (d, 15 H, C$_5$(CH_3)$_5$, $^4J_{H-P}$ = 2

Hz). ^{11}B NMR (C$_6$D$_6$); δ 80. ^{19}F NMR (C$_6$D$_6$); δ –134.1 (2 F), –157.8 (1 F), –164.2 (2 F).

^{31}P{^{1}H} NMR (C$_6$D$_6$); δ –44.7. Calc. C(40.07), H(3.36). Found C(40.26), H(3.37). M.p.

179–182 °C.

Formation of Cp*Ir(PMe$_3$)(BCat)H (30). A solution of Cp*Ir(PMe$_3$)H$_2$ (10.0 mg,

0.0245 mmol), dissolved in 400 μL C$_6$D$_6$, was placed in a sealable NMR tube. HBCat

(2.6 μL, 0.025 mmol) was added to the tube via a microliter syringe and enough C$_6$D$_6$

was added to bring the volume of the solution to 600 μL. The solution was heated at 90

°C for 24 hr. Only one Ir containing product, consistent with formulation as

Cp*Ir(PMe$_3$)(BCat)H, was observed. ^{1}H NMR (C$_6$D$_6$); δ –17.12 (d, 2 H, Ir–H, $^2J_{H-P}$ = 29

Hz), 1.39 (d, 9 H, PMe$_3$, $^2J_{H-P}$ = 10 Hz), 2.08 (d, 15 H, C$_5$Me$_5$, $^4J_{H-P}$ = 2 Hz), 6.84 (m, 2

H, BO$_2$C$_6$H$_4$), 7.18 (m, 2 H, BO$_2$C$_6$H$_4$). ^{11}B NMR (C$_6$D$_6$); δ 36. ^{31}P{^{1}H} NMR (C$_6$D$_6$); δ

–42.9.

Formation of [(Cp*Ir(PMe$_3$)H)$_2$(μ-H)$^+$]. The non-pentane soluble portion of the

residue from the thermolysis of Cp*Ir(PMe$_3$)H[HBH(C$_6$F$_5$)$_2$] contains primarily a product

that was spectroscopically identical to the known cation [(Cp*Ir(PMe$_3$)H)$_2$(μ-H)$^+$] with

the accompanying anion HB(C$_6$F$_5$)$_3^-$. Attempts at crystallizing this compound have thus

far been unsuccessful. ^{1}H NMR (CD$_2$Cl$_2$, –80 °C); δ –23.01 (tt, 1 H, Ir–H$_{bridg}$, $^2J_{H-H}$ = 5

Hz, $^2J_{H-P}$ = 21 Hz), –19.18 (dd, 2 H, Ir–H$_{2(term)}$, $^2J_{H-H}$ = 5 Hz, $^2J_{H-P}$ = 34 Hz), 1.48 (d, 18

H, P(CH_3)$_3$, $^2J_{H-P}$ = 10 Hz), 1.93 (30 H, C$_5$(CH_3)$_5$), 3.4 (br, 1 H, HB(C$_6$F$_5$)$_3^-$). ^{1}H NMR

(CD$_2$Cl$_2$, 20 °C); δ –20.47 (br, 3 H, (H)Ir–H–Ir(H)), 1.60 (d, 9 H, PMe$_3$, $^2J_{H-P}$ = 10 Hz),

2.02 (d, 15 H, C$_5$Me$_5$, $^4J_{P-H}$ = 2 Hz), 3.6 (q, 1 H, H–B, $^1J_{B-H}$ = 90 Hz). ^{11}B NMR (CD$_2$Cl$_2$,

20 °C); δ –23.9 ($^1J_{H-B}$ = 90 Hz). ^{19}F NMR (CD$_2$Cl$_2$, 20 °C); δ –134.1 (2 F), –165.0 (1 F),

–167.9 (2 F). ^{31}P{^{1}H} NMR (CD$_2$Cl$_2$, 20 °C); δ –47.0.

Formation of [Cp*Ir(PMe$_3$)H$_3^+$]. Compound **45**, when dissolved in CDCl$_2$F or

CD$_2$Cl$_2$ resulted in the slow formation of 1 and [Cp*Ir(PMe$_3$)H$_3$][H$_2$B(C$_6$F$_5$)$_2$]. ^{1}H NMR

(CD$_2$Cl$_2$, –80 °C); δ –14.13 (dd, 2 H, Ir–H_{term}, $^2J_{H-H}$ = 48 Hz, $^2J_{H-P}$ = 13 Hz), δ –12.71

(td, 1 H, Ir–H–Ir, $^2J_{H-H}$ = 48 Hz, $^2J_{H-P}$ = 22 Hz), 1.71 (d, 9 H, P(CH_3)$_3$, $^2J_{H-P}$ = 10 Hz), 2.17 (15 H, C$_5$(CH_3)$_5$), 3.6 (br, 2 H, H_2B(C$_6$F$_5$)$_2^-$). ^{1}H NMR (CD$_2$Cl$_2$, 20 °C); δ –20.47 (br, 3 H, (H)Ir–H–Ir(H)), 1.60 (d, 9 H, PMe$_3$, $^2J_{H-P}$ = 10 Hz), 2.02 (d, 15 H, C$_5$Me$_5$, $^4J_{P-H}$ = 2 Hz), 3.6 (q, 1 H, H–B, $^1J_{B-H}$ = 90 Hz). ^{11}B NMR (CD$_2$Cl$_2$, 20 °C); δ –31.8 ($^1J_{H-B}$ = 85 Hz). ^{19}F NMR (CD$_2$Cl$_2$, 20 °C); δ –134.1 (2 F), –165.0 (1 F), –167.9 (2 F). ^{31}P{^{1}H} NMR (CD$_2$Cl$_2$, –80 °C); δ –37.9.

NMR Tube Reactions

cis-(PPh$_3$)$_2$Pt(η^2-4-octyne) with B$_2$Cat$_2$. *cis*-(PPh$_3$)$_2$Pt(η^2–4-octyne) (7.2 mg, 0.0087 mmol) and B$_2$Cat$_2$ (4.1 mg, 0.017 mmol) were mixed in C$_6$D$_6$ and transferred to a sealable NMR tube. After sealing, the tube was thawed, and traces of a white precipitate indicated *cis*-(PPh$_3$)$_2$Pt(BCat)$_2$ deposition. ^{1}H NMR indicated that *cis*-(PPh$_3$)$_2$Pt(BCat)$_2$, 4-octyne, and B$_2$Cat$_2$ were the sole soluble species. The tube was heated for 4 h at 80 °C to yield *cis*-(PPh$_3$)$_2$Pt(BCat)$_2$ (by ^{1}H and ^{31}P NMR) as the free alkyne was converted to the *cis*-4,5-diboryl-4-octene. ^{1}H NMR (C$_6$D$_6$): 0.90 (tr, 6 H, –CH$_2$CH$_2$CH_3), 1.53 (sextet, 4H, –CH$_2$CH_2CH$_3$), 2.49 (tr, 4 H, –CH_2CH$_2$CH$_3$), 6.73 (m, 4 H, BO$_2$C$_6$$H_4$), 6.91 (m, 4 H, BO$_2C_6$$H_4$). ^{11}B NMR (C$_6D_6$): 32.7.

Reaction of (PPh$_3$)$_2$Pt(BCat)$_2$ with Me$_6$Sn$_2$. *cis*-(PPh$_3$)$_2$Pt(BCat)$_2$ (100 mg, 0.104 mmol) and Me$_6$Sn$_2$ (21.6 μL, 0.208 mmol) were placed in a Schlenk tube and dissolved in 5 mL of toluene in a glovebox. The solution was stirred at 55 °C for 3 h. The solvent was removed *in vacuo* and the residue washed with 10 and 5 mL of pentane to yield 51 mg (49% yield) of a light tan solid. ^{1}H, ^{31}P, and ^{11}B NMR spectroscopy indicated formation of *cis*-(PPh$_3$)$_2$Pt(BCat)(SnMe$_3$). ^{1}H NMR (CDCl$_3$): –0.45 (m, 9 H, Sn(CH_3)$_3$ ($^5J_{P-H}$ = 0.9 Hz, $^4J_{Pt-H}$ = 12 Hz, $^3J_{Sn-H}$ = 42 Hz), 6.72 (m, 2 H, BO$_2$C$_6$$H_4$), 6.81 (m, 2 H, BO$_2C_6$$H_4$), 6.92–7.37 (m, 30 H, P(C$_6$$H_5$)$_3$). ^{31}P NMR (CDCl$_3$, –50 °C): 26.63 (d, trans

SnMe$_3$, $^2J_{P-P}$ = 23 Hz, $^1J_{Pt-P}$ = 2371 Hz, $^2J_{Sn-P}$ = 1268 Hz), 32.84 (br d, trans BCat, $^2J_{P-P}$ = 20 Hz, $^1J_{Pt-P}$ = 1761 Hz, $^2J_{Sn-P}$ = 815 Hz).

Reaction of cis-(PPh$_3$)$_2$Pt(BPin)$_2$ with Me$_6$Sn$_2$. (PPh$_3$)$_2$Pt(BPin)$_2$ (10 mg, 0.010 mmol) was dissolved in 600 μL of C$_6$D$_6$. Addition of Me$_6$Sn$_2$ (2.0 μL, 0.010 mmol) via syringe immediately generated a bright yellow solution. ^{1}H, ^{31}P, and ^{11}B NMR spectroscopy all indicated complete conversion to trans-(PPh$_3$)$_2$Pt(SnMe$_3$)$_2$ and B$_2$Pin$_2$.

Reaction of cis-(PPh$_3$)$_2$Pt(BPin)$_2$ with B$_2$Cat$_2$. (PPh$_3$)$_2$Pt(BPin)$_2$ (12.0 mg, 0.013 mmol) and B$_2$Cat$_2$ (3.0 mg, 0.013 mmol) were placed in a sealable NMR tube, and 600 μL of C$_6$D$_6$ was added via vacuum transfer. Upon warming of the sample to room temperature, traces of a white precipitate indicated (PPh$_3$)$_2$Pt(BCat)$_2$ deposition. ^{1}H, ^{31}P, and ^{11}B NMR spectroscopy all indicated conversion to (PPh$_3$)$_2$Pt(BCat)$_2$ and B$_2$Pin$_2$, as cis-(PPh$_3$)$_2$Pt(BPin)$_2$ was not detected.

Equilibrium of cis-(PPh$_3$)$_2$Pt(BCat)$_2$ with CO. (PPh$_3$)$_2$Pt(BCat)$_2$ (10.0 mg, 0.010 mmol) was dissolved in 600 μL of CD$_2$Cl$_2$ in a J. Young NMR tube. After the solution was frozen, the argon atmosphere was evacuated and replaced with CO. Upon warming of the sample to room temperature conversion to (PPh$_3$)$_2$Pt(CO)$_2$ had occurred as evidenced by ^{1}H and ^{31}P NMR spectra, and reductive elimination of B$_2$Cat$_2$ was confirmed by ^{11}B NMR. Chemical reversibility was confirmed by the regeneration of (PPh$_3$)$_2$Pt(BCat)$_2$ upon evacuation of the CO atmosphere.

Equilibrium of cis-(PPh$_3$)$_2$Pt(BPin)$_2$ with CO. (PPh$_3$)$_2$Pt(BPin)$_2$ (10.0 mg, 0.010 mmol) was dissolved in 600 μL of C$_7$D$_8$ in a J. Young NMR tube. After the solution was frozen, the argon atmosphere was evacuated and replaced with CO. Upon warming of the sample to room temperature, ^{1}H and ^{31}P NMR indicated complete conversion to (PPh$_3$)$_2$Pt(CO)$_2$. ^{11}B also confirmed reductive elimination of B$_2$Pin$_2$. After evacuation of the CO atmosphere, a trace of (PPh$_3$)$_2$Pt(BPin)$_2$ was regenerated.

Equilibrium of cis-(PPh$_3$)$_2$Pt(BPin)$_2$ with 2-butyne. (PPh$_3$)$_2$Pt(BPin)$_2$ (7.5 mg, 0.0077 mmol) was dissolved in 600 μL of C$_6$D$_6$ in a J. Young NMR tube. The

atmosphere above the frozen solution was evacuated and replaced with approximately 10 molar equiv of 2-butyne. Upon warming of the sample to room temperature, ^{1}H and ^{31}P NMR indicated nearly complete conversion to cis-$(PPh_3)_2Pt(\eta^2$-$CH_3CCCH_3)$, and reductive elimination of B_2Pin_2 was confirmed by ^{11}B NMR. Reversibility was demonstrated by regeneration of cis-$(PPh_3)_2Pt(BPin)_2$ upon evacuation of the 2-butyne atmosphere. Evacuation to dryness and dissolution of the residue in C_6D_6 showed cis-$(PPh_3)_2Pt(BPin)_2$ to be the major product (^{31}P NMR); however, ^{1}H NMR indicated that some diboration of 2-butyne had occurred.

Equilibrium of cis-$(PPh_3)_2Pt(BPin)_2$ with 4-octyne. $(PPh_3)_2Pt(BPin)_2$ (5.1 mg, 0.0052 mmol) was placed in a sealable NMR tube, 4.6 μL of 4-octyne was added via syringe, and C_7D_8 was added to 600 mL. After sealing, ^{31}P NMR spectra were recorded at 193, 213, 233, 253, and 273 K. The concentrations of cis-$(PPh_3)_2Pt(BPin)_2$, $(PPh_3)_2Pt(\eta^2$-4-octyne), B_2Pin_2, and 4-octyne were determined by the relative intensities of the Pt-containing species.

Reaction of cis-$(PPh_3)_2Pt(BCat)_2$ with PPh₃. cis-$(PPh_3)_2Pt(BCat)_2$ (10 mg, 0.010 mmol) and PPh₃ (30 mg, 0.11 mmol) were placed in an NMR tube and dissolved in 600 μL of CD_2Cl_2 to form a clear, colorless solution. ^{1}H, ^{31}P, and ^{11}B NMR (–80 and 20 °C) showed **2** to be the exclusive Pt-containing species.

Reaction of cis-$(PPh_3)_2Pt(BPin)_2$ with PPh₃. cis-$(PPh_3)_2Pt(BPin)_2$ (10 mg, 0.010 mmol) and PPh₃ (30 mg, 0.11 mmol) were dissolved in 600 μL of CD_2Cl_2 in an NMR tube. NMR spectra (^{1}H and ^{31}P at –80 °C) of the yellow solution indicated reductive elimination of B_2Pin_2 and formation of $(PPh_3)_3Pt$ and $(PPh_3)_4Pt$.

Crossover Experiment. cis-$(PPh_3)_2Pt(BCat)_2$ (4 mg, 0.0042 mmol), B_2Cat_2 (1 mg, 0.0042 mmol), and 4-octyne (4.6 L, 0.032 mmol) were placed in a sealable NMR tube and 595 μL of C_6D_6 was added while in a glovebox. The tube was flame-sealed, and the mixture was heated at 80 °C in a constant-temperature oil bath until **1** was consumed. The sealed tube was opened in the glovebox. The solution was transferred to a new

sealable tube, and 3-hexyne (2 μL, 0.02 mmol) was added. After flame-sealing, the solution was heated at 80 °C for 5 h. ^{1}H NMR spectra showed no evidence for diboration of hexyne.

Cp*Ir(PMe₃)D₂ + [HB(C₆F₅)₂]₂. Cp*Ir(PMe₃)D₂ (10.0 mg, 0.0245 mmol) and [HB(C₆F₅)₂]₂ (8.5 mg, 0.012 mmol) were dissolved in 600 μL toluene and transferred to a suba-capped NMR tube at room temperature. ^{2}H NMR at −70 °C indicated complete deuterium scrambling between the hydride and borane sites.

Cp*Ir(PMe₃)D₂ + HBCat. Cp*Ir(PMe₃)D₂ (10.0 mg, 0.025 mmol) and HBCat (2.6 μL, 0.025 mmol) were dissolved in 600 μL toluene in a sealable NMR tube. The tube was flame-sealed under an atmosphere of argon. ^{2}H NMR indicated complete deuterium scrambling between the hydride and borane sites after XX hr at 75 °C.

Cp*Ir(PMe₃)D₂ + HBPin. Cp*Ir(PMe₃)D₂ (10.0 mg, 0.025 mmol) and HBPin (3.6 μL, 0.025 mmol) were dissolved in 600 μL toluene in a sealable NMR tube. The tube was flame-sealed under an atmosphere of argon. ^{2}H NMR indicated complete deuterium scrambling between the hydride and borane sites after XX hr at 75 °C.

Cp*Ir(PMe₃)(cy-C₆H₁₁)H + 6, 12, or 24 equiv. HBPin. Cp*Ir(PMe₃)(cy-C₆H₁₁)H (10 mg, 0.021mmol) was dissolved in 300 μL C6D6 and transferred to a sealable NMR tube. HBPin was added to the sealable NMR tube via microsyringe and C₆D₆ was added to make the total volume of the solution 600 μL. The tube was frozen in liquid nitrogen and flame-sealed under an atmosphere of argon. After thawing, the reaction was heated at 95 °C or 135 °C and examined by ^{1}H, ^{11}B, and ^{31}P NMR. Compounds **31** and **48-d₆** were the primary Ir containing products and cy-C₆H₁₂ and cy-C₆H₁₁–BPin were the organic products. Product distribution was dependent on the reaction conditions (see Chapter 4 for details).

Cp*Ir(PMe₃)(Cy)H with [HB(C₆F₅)₂]₂. Cp*Ir(PMe₃)(Cy)H (10.6 mg, 0.021 mmol) and [HB(C₆F₅)₂]₂ (7.6 mg, 0.011 mmol) were placed in a suba–capped NMR tube and dissolved in 600 μL C₆D₆. The reaction was complete at room temperature in the amount

of time needed to walk to the NMR spectrometer and take a spectrum (15 minutes). ^{1}H, ^{11}B, ^{19}F and ^{31}P NMR indicate quantitative formation of Cp*Ir(PMe$_3$)H$_2$ and CyB(C$_6$F$_5$)$_2$.

Cp*Ir(PMe₃)(Ph)H with HCat. Cp*Ir(PMe$_3$)(Ph)H (8.9 mg, 0.019 mmol) was placed in a sealable NMR tube. The sides of the tube were washed down with 200 μL C$_6$D$_6$ and then HBCat (11.8 μL, 0.11 mmol) was added via microsyringe. Enough C$_6$D$_6$ was added to bring the total volume of the solution to 540 μL. The tube was then frozen in N$_{2(l)}$ and quickly sealed. Upon thawing of the solution, the reaction was heated at 150 °C in an oil bath and monitored by ^{1}H, ^{11}B and ^{31}P NMR.

Cp*Ir(PMe₃)(Ph)H with HBPin. Cp*Ir(PMe$_3$)(Ph)H (9.0 mg, 0.019 mmol) was placed in a sealable NMR tube. The sides of the tube were washed down with 200 μL C$_6$D$_6$ and then HBPin (32 μL, 0.22 mmol) was added via microsyringe. Enough C$_6$D$_6$ was added to bring the total volume of the solution to 540 μL. The tube was then frozen in N$_{2(l)}$ and quickly sealed. Upon thawing of the solution, the reaction was heated at 150 °C in an oil bath and monitored by ^{1}H, ^{11}B and ^{31}P NMR.

Cp*Ir(PMe₃)H(HBH(C₆F₅)₂) + PMe₃. Cp*Ir(PMe$_3$)H(HBH(C$_6$F$_5$)$_2$) (10.0 mg, 0.013 mmol) was dissolved in 600 μL toluene-d_8 in a J. Young NMR tube. The tube was frozen and the head space above the sample evacuated. Two molar equivalents of PMe$_3$ were then added by vacuum transfer. The tube was thawed and immediately placed in a spectrometer pre-set to –70 °C. ^{1}H and ^{31}P NMR indicated complete conversion to Cp*Ir(PMe$_3$)H$_2$ and a Lewis acid-base adduct between HB(C$_6$F$_5$)$_2$ and PMe$_3$ (see below).

[HB(C₆F₅)₂]₂ + PMe₃. [HB(C$_6$F$_5$)$_2$]$_2$ (5.0 mg, 0.0072 mmol) was dissolved in 600 μL toluene-d_8 in a J. Young NMR tube. The tube was frozen and the headspace above the sample evacuated. Two molar equivalents of PMe$_3$ were then added by volumetric gas transfer. ^{1}H NMR (C$_6$D$_6$); δ 0.76 (d, 9 H, CH_3, $^2J_{\text{H–P}}$ = 1.5 Hz), 3.25 (br quart, 1 H, BH, $^1J_{\text{H–B}}$ = 76 Hz). ^{11}B NMR (C$_6$D$_6$); δ –25.7 (tr, average $^1J_{\text{B–H/B–P}}$ = 88 Hz). ^{19}F NMR (C$_6$D$_6$); δ –131.0 (2 F), –157.8 (1 F), –163.6 (2 F). ^{31}P NMR (C$_6$D$_6$); δ –9.1 (br quart, $^1J_{\text{P–B}}$ = 90 Hz).

HBCat + NEt₃. HBCat (4.4 μL, 0.042 mmol) and NEt₃ (5.8 μL, 0.042 mmol) were dissolved in 600 μL C_6D_6 in a suba-capped NMR tube. ^1H and ^{11}B NMR indicated a Lewis acid-base interaction. ^1H NMR (C_6D_6); δ 0.69 (tr, 9 H, NCH₂CCH_3, $^4J_{H-H}$ = 7 Hz), 2.27 (quart, 6 H, NCH_2CH₃, $^4J_{H-H}$ = 7 Hz), 6.82 (m, 2 H, BO₂C₆H_4), 7.04 (m, 2 H, BO₂C₆H_4). ^{11}B NMR (C_6D_6) ; δ 11 ($^1J_{H-B}$ = 299Hz).

HBPin + NEt₃. HBPin (6.1 μL, 0.042 mmol) and NEt₃ (5.8 μL, 0.042 mmol) were dissolved in 600 μL C_6D_6 in a suba-capped NMR tube. ^1H and ^{11}B NMR indicated no Lewis acid-base interaction. ^1H NMR (C_6D_6); δ –17.64 (tr, 9 H, NCH₂CH_3, $^2J_{H-H}$ = 29 Hz), 1.17 (quart, 6 H, NCH_2CH₃), 1.50 (m, 2 H, BO₂C₆H_4), 2.10 (m, 2 H, BO₂C₆H_4). ^{11}B NMR (C_6D_6) ; δ –17.64.

[HB(C₆F₅)₂]₂ + NEt₃. [HB(C₆F₅)₂]₂ (10 mg, 0.014 mmol) and NEt₃ (4.0 μL, 0.029 mmol) were dissolved in 600 μL C_6D_6 in a suba-capped NMR tube. ^1H NMR (C_6D_6); δ 0.39 (tr, 9 H, NCH₂CH_3, $^2J_{H-H}$ = 7 Hz), 2.54 (quart, 6 H, NCH_2CH₃, $^2J_{H-H}$ = 7 Hz), 1.50 (m, 2 H, BO₂C₆H_4), 2.10 (m, 2 H, BO₂C₆H_4). ^{11}B NMR (C_6D_6) ; δ –9 ($^1J_{H-B}$ = 98 Hz). ^{19}F NMR (C_6D_6); δ –128.2 (2 F), –157.2 (1 F), –163.5 (2 F).

Kinetic Experiments

All kinetic experiments were run in sealed NMR tubes with a total solution volume of 600 μL. PPh₃ was added to the tubes in the form of 0.2 M solutions of PPh₃ in C_6D_6 or C_7D_8. The reactions were heated in constant temperature oil baths (Cole-Parmer Polystat Constant Temperature Circulator or Tekmar RCT) or in the Varian 300 MHz spectrometer when the reaction temperature and completion times were convenient.

A typical experimental run for the stoichiometric diboration of alkynes by cis-(PPh₃)₂Pt(BCat)₂ is described as follows: cis-(PPh₃)₂Pt(BCat)₂ (5.0 mg, 0.0052 mmol) and 4-octyne (4.6 μL, 0.032 mmol) were placed in an NMR tube. In a drybox, 595 μL of C_6D_6 was added via syringe. The solution was frozen in liquid nitrogen, and the tube was

flame-sealed. The tube was heated briefly to dissolve the Pt complex. The tube was then placed in a constant-temperature oil bath. At specific intervals the tube was removed from the oil bath and the reaction was quenched by rapid cooling in an ice bath. ^{1}H NMR spectra were then recorded at room temperature. The progress of the reaction was monitored to 3 half-lives by measuring the disappearance of the catecholate resonance at 6.54.

A typical experimental run under catalytic conditions is described as follows: cis-(PPh$_3$)$_2$Pt(BCat)$_2$ (4 mg, 0.0042 mmol), CatB-BCat (6 mg, 0.025 mmol), 4-octyne (3.7 μL, 0.025 mmol), and C$_6$D$_6$ (595 μL) were added to an NMR tube. The tube was then brought out of the glovebox and flame-sealed. The mixture was heated to 50 °C in the Varian 300 MHz NMR spectrometer, and the reaction was monitored to 3 half-lives completion. A program supplied within the spectrometer's software was used to take scans of the mixture at specified intervals, and the time-dependent alkyne concentration was calculated by integrating the resonance of the methylene group adjacent to the alkyne triple bond.

A typical experimental run for the reaction of HBCat or HBPin with Cp*Ir(PMe$_3$)H$_2$ is described as follows: In a drybox, Cp*Ir(PMe$_3$)H$_2$ (10.0 mg, 0.025 mmol) was dissolved in 300 mL C$_6$D$_6$ and transferred to a sealable NMR tube. HBCat (15.7 μL, 0.15 mmol) was added to the tube via microsyringe and C$_6$D$_6$ was added to the tube to make the solution volume 600 μL. The solution was frozen in liquid nitrogen, and the tube was flame-sealed with an atmosphere of argon gas. The tube was stored in the −15 C freezer for an hour and then heated in a constant temperature oil bath. At specific intervals the tube was removed from the oil bath and the reaction quenched by rapid cooling in an ice bath. ^{1}H NMR spectra were then recorded at room temperature. The progress of the reaction was monitored through 3 half-lives by measuring the disappearance of the Cp* and PMe$_3$ resonances of 28.

Catalytic Diboration of Alkynes

Diboration of 1,2-Bis(p-anisolyl)acetylene. 1,2-bis(p-anisolyl)acetylene58 (50 mg, 0.21 mmol), B_2Cat_2 (50 mg, 0.21 mmol), and 2.5 mol % **1** were dissolved in 4 mL of toluene. The solution was heated at reflux for 4 h, and then the solvent was removed in *vacuo*. A 20 mL volume of Et_2O was added, and the mixture was filtered. Evaporation of the filtrate yielded 74 mg (74%) of the diborylated product. ^1H NMR ($CDCl_3$): 3.76 (s, 3 H, OCH_3, 6.76 (m, 2 H, $BO_2C_6H_4$), 7.05 (m, 4 H, $C_6H_4OCH_3$), 7.11 (m, 2 H, $BO_2C_6H_4$). ^{11}B NMR ($CDCl_3$): 32.3. EI/MS: m/z = 476 (M^+), I = 100 (100); m/z = 477 ($[M + 1]^+$), I = 30 (30); m/z = 475 ($[M - 1]^+$), I = 48 (45). Mp; 146–151 °C.

Diboration of 1,2-Bis[p-(trifluoromethyl)phenyl]acetylene. 1,2-Bis[p-(trifluoromethyl)phenyl]acetylene (57 mg, 0.18 mmol), B_2Cat_2 (43 mg, 0.18 mmol), and 2.5% **1** were dissolved in 4 mL of toluene. The solution was heated at reflux for 2 h, and then the solvent was removed in *vacuo*. A 5 mL volume of Et_2O was added, and the mixture was filtered. Evaporation of the filtrate yielded 85 mg (85%) of the diborylated product. ^1H NMR ($CDCl_3$): δ 7.09 (m, 4 H, $C_6H_4CF_3$), 7.27 (m, 2 H, $BO_2C_6H_4$), 7.49 (d, 2 H, $BO_2C_6H_4$). ^{11}B NMR ($CDCl_3$): δ 31.5. EI/MS: m/z = 552 (M^+), I = 100 (100); m/z = 553 ($[M + 1]^+$), I = 31 (30); m/z = 551 ($[M - 1]^+$), I = 51 (45). Mp; 140–145 °C.

Protonolysis of Diborylated Phenylacetylenes.[172] A 51 mg amount of the alkene derived from diboration of 1,2-bis(p-anisolyl)acetylene (0.11 mmol) was dissolved in 0.5 mL of diglyme. Several drops of glacial acetic acid were added, and the solution was heated at 45 °C for 15 h. The solvent was removed in *vacuo*. Formation of the *cis*-stilbene was confirmed by comparing the ^1H NMR shift of the olefinic protons (6.43 ppm) to the literature value (6.44 ppm).

A 50 mg amount of the alkene derived from diboration of 1,2-bis[p-(trifluoromethyl)phenyl]acetylene (0.091 mmol) was dissolved in 0.5 mL of diglyme. Several drops of glacial acetic acid were added, and the solution was heated at reflux for

12 h. The solvent was removed in *vacuo*. Formation of the *cis*-stilbene was confirmed by comparing the ^{1}H NMR shift of the olefinic protons (6.70 ppm) to the literature value (6.72 ppm).

Catalytic Stannaboration of Alkynes

A series of sealable NMR tubes experiments were performed in order to examine the catalytic activity of **1**. In each tube was placed **1** (2 mg, 0.002 mmol), Me$_3$Sn–B(NMe$_2$)$_2$ (10 mg, 0.042 mmol), and an alkyne (0.042 mmol). 600 mL of benzene-d_6 was added and the tubes were flame-sealed under vacuum. The reactions were followed by ^{1}H and ^{11}B NMR. 1-Hexyne and 4-octyne reacted smoothly at 75°C to yield single products in approximately 8 hrs. Diphenylacetylene, phenylacetylene, and 1-phenyl-1-propyne reacted slowly at 75°C. Upon raising the temperature to 90°C the reactions proceeded to near completion but were accompanied by catalyst decomposition. Diphenylacetylene yielded a single product as opposed to phenylacetylene and 1-phenyl-1-propyne, which both formed more than one isomer. None of 1,2-bis[p-(trifluoromethyl)phenyl]acetylene, methyl propargyl ether, nor dimethyl acetylene dicarboxylate showed clean reactivity at lower temperatures and catalyst decomposition occurred at higher temperatures.

Stannaboration of 1-hexyne. 1-hexyne (118 mg, 1.45 mmol), Me$_3$Sn-B(NMe$_2$)$_2$ (382 mg, 1.45 mmol) and 5 mole % catalyst **1** (71 mg, 0.073 mmol) were placed in a flask and dissolved in 4 mL toluene. The solution was heated at 80°C for 36 hr at which time the reaction was judged complete by GC analysis. The solvent was removed in *vacuo* leaving an oily brown residue. The residue was taken up in hexane and washed through neutral Alumina. The hexane was removed leaving a golden oil (353 mg, 71%). In order to remove a small amount of PPh$_3$ that was present due to decomposition of catalyst, the pure oil can be isolated by kugelrohr distillation(60°C, 0.1 mmHg). ^{1}H NMR (C$_6$D$_6$); δ 0.23 (s, 9 H, Sn(CH$_3$)$_3$, ^{2}J$_{H-Sn}$ = 52 Hz), δ 0.92 (t, 3 H, CH$_3$), δ 1.37 (m, 2

H, CH_2) δ 1.46 (m, 2 H, CH_2) δ 2.46 (t, 2 H, C=CCH_2), δ 2.61 (s, 12 H, B(N(CH_3)$_2$)$_2$), δ

6.51 (s, 1 H, HC=C, $^3J_{H-Sn}$ = 193 Hz). ^{13}C NMR (C$_6$D$_6$); δ -8.7 (SnMe$_3$, $^1J_{C-Sn}$ = 312

Hz), δ 14.2 (CH$_3$), δ 22.8 (CH$_2$), δ 40.9 (B(NMe$_2$)$_2$), δ 32.7 (CH$_2$), δ 44.7 (C=C(Sn)CH$_2$,

$^2J_{C-Sn}$ = 67 Hz), δ 145.3 (broad, BC=CSn), δ 156.7 (BC=CSn, $^1J_{C-Sn}$ = 489 Hz). ^{11}B NMR

(C$_6$D$_6$); δ 30.7. ^{119}Sn (C$_6$D$_6$); δ –50.3.

Stannaboration of 4-octyne. 4-octyne (148 mg, 1.34 mmol), Me$_3$Sn–B(NMe$_2$)$_2$ (352

mg, 1.34 mmol and 5 mole % catalyst **1** (66 mg, 0.067 mmol) were placed in a flask and

dissolved in 4 mL toluene. The solution was heated at 80°C for 36 hr at which time the

reaction was judged complete by GC analysis. The solvent was removed in *vacuo* leaving

an oily brown residue. The residue was taken up in hexane and washed through neutral

Alumina. The hexane was removed leaving a dark golden oil (340 mg, 68%). In order to

remove a small amount of PPh$_3$ that was present due to decomposition of catalyst, the

pure oil can be isolated by kugelrohr distillation(70°C, 0.1 mmHg). ^{1}H NMR (C$_6$D$_6$); δ

0.23 (s, 9 H, Sn(CH_3)$_3$, $^2J_{H-Sn}$ = 50 Hz), δ 0.98 (t, 6 H, CH_3), δ 1.43 (m, 4 H, CH_2) δ 2.31

(m, 2 H, CH_2(B)C=C), δ 2.47 (t, 2 H, C=C(Sn)CH_2), δ 2.57 (s, 12 H, B(CH_3)$_2$). ^{13}C NMR

(C$_6$D$_6$); δ –8.3 (SnMe$_3$, $^1J_{C-Sn}$ = 306 Hz), δ 14.4 (CH$_3$), δ 15.4 (CH$_3$), δ 23.2 (CH$_2$), δ 23.8

(CH$_2$), δ 35.5 (CH$_2$(B)C=C, $^4J_{C-Sn}$ = 80 Hz), δ 36.5 (C=C(Sn)CH$_2$, $^2J_{C-Sn}$ = 67 Hz), δ 40.8

(B(NMe$_2$)$_2$), δ 147.1 (BC=CSn, $^1J_{C-Sn}$ = 542 Hz), δ 156.2 (broad, BC=CSn,). ^{11}B NMR

(C$_6$D$_6$); δ 30.7. ^{119}Sn (C$_6$D$_6$); δ –52.8. EI/MS; m/z = 359.2 ([M-Me]$^+$), I=100(100); m/z =

360.3 ([M-Me]+1$^+$), I=20.9(19.2); m/z = 361.2 ([M-Me]+2$^+$), I=16.3(14.8); m/z = 358.3

([M-Me]-1$^+$), I=75.53(57.9); m/z = 357.3 ([M-Me]-2$^+$), I=92.5(78.9); m/z = 356.3 ([M-

Me]-3$^+$), I=66.7(44.2); m/z = 355.2 ([M-Me]-4$^+$), I=57.0(46.1).

Stannaboration of diphenylacetylene. Diphenylacetylene (167 mg, 0.938 mmol),

Me$_3$Sn–B(NMe$_2$)$_2$ (246 mg, 0.938 mmol) and 6 mole % catalyst **1** (54 mg, 0.056 mmol)

were placed in a flask and dissolved in 4 mL toluene. The solution was heated at 75°C

for 60 hr at which time the reaction was judged only 30% complete by GC analysis. The

temperature of the bath was raised to 85°C for another 60 hr. ^{1}H NMR analysis of the

mixture indicated the absence of free stannyl-borane and approximately 20% unreacted diphenylacetylene. An additional 50 mg Me$_3$Sn–B(NMe$_2$)$_2$ was added to the flask and heated for an additional 48 hrs. The solvent was removed in *vacuo* leaving an oily brown residue. The residue was taken up in hexane and washed through neutral Alumina, Activity I. The hexane was removed leaving a dark golden oil (353 mg, 60%). The oil was dissolved in a small amount of heptane and placed in a –80°C freezer to precipitate PPh$_3$ that was present due to decomposition of the catalyst. ^{1}H NMR (C$_6$D$_6$); δ 0.19 (s, 9 H, Sn(CH_3)$_3$, $^2J_{H-Sn}$ = 53 Hz), δ 2.66 (s, 12 H, B(N(CH_3)$_2$)$_2$), δ 6.82–7.18 (m, 10 H, C$_6H_5$(B)C=C(Sn)C$_6H_5$. ^{13}C NMR (C$_6$D$_6$); δ –8.1 (SnMe$_3$, $^1J_{C-Sn}$ = 312 Hz), δ 40.8 (B(NMe$_2$)$_2$), δ 143.6 (C(B)C=CSn), δ 147.3 (BC=C(Sn)C), δ 151.5 (BC=CSn, $^1J_{C-Sn}$ = 489 Hz), δ 157.5 (broad, BC=CSn). ^{11}B NMR (C$_6$D$_6$); δ 31.2. ^{119}Sn (C$_6$D$_6$); δ –43.1. EI/MS; m/z = 427.1 ([M-Me]$^+$), I=100(100); m/z = 428.1 ([M-Me]+1$^+$), I=23.9(24.9); m/z = 429.1 ([M-Me]+2$^+$), I=16.0(15.7); m/z = 426.1 ([M-Me]-1$^+$), I=60.8(60.8); m/z = 425.1 ([M-Me]-2$^+$), I=83.0(78.8); m/z = 424.1 ([M-Me]-3$^+$), I=48.0(45.5); m/z = 423.1 ([M-Me]-4$^+$), I=46.2(45.0).

Catalytic Diboration of Olefins

A typical catalytic reaction involving a gaseous olefin was prepared in the following manner: CatB–BCat (224 mg, 0.94 mmol) and 3 mol% Pt(COD)$_2$ were loaded into a FisherPorter flask and dissolved in 3 mL toluene. The mixture was taken out, immediately frozen and placed under vacuum, whereupon ethylene (1 atm) was introduced. The mixture was warmed to room temperature and allowed to stir for several hours. The solvent was removed in *vacuo* and the crude product collected.

A typical catalytic reaction involving a solid or liquid olefin was prepared in the following manner: CatB–BCat (262 mg, 1.10 mmol) and 3 mol% Pt(COD)$_2$ were loaded into a Schlenk flask. 4-Vinylanisole (148 mg, 1.10 mmol), dissolved in 3 mL toluene,

was then added to the solids in the flask. After stirring for 30 minutes at room temperature. The solvent was removed in *vacuo* and the crude product collected.

Yields reported are based on the crude material collected from bottom of the flask except where further purification is indicated. The solid products were collected by scraping down the sides and bottom of the flask and transferring to a tared vial. The oil products were collected by pipetting the contents from the bottom of the flask to a tared vial.

1,2-bis(catecholboryl)hexane (500 mg, 1.55 mmol) was converted to the corresponding diol in 46% yield by a basic oxidative workup and was identical to ^{1}H and ^{13}C NMR of purchased 1,2-hexanediol.

Diboration of Ethylene. The crude product was isolated as a light tan solid in 84% yield and can be sublimed as a white solid in 75% yield. ^{1}H NMR (CDCl$_3$); δ 1.61 (s, 4 H, H_2C–CH_2), 7.05 (m, 4 H, BO$_2$C$_6$$H_4$), 7.18 (m, 4 H, BO$_2C_6$$H_4$). ^{13}C{^{1}H} NMR (CDCl$_3$); δ 4.0 (br, 2 C, C–B), 112.3 (2 C, BO$_2$C$_6$H$_4$), 112.5 (2 C, BO$_2$C$_6$H$_4$), 122.5 (4 C, BO$_2$C$_6$H$_4$), 148.3 (4 C, BO$_2$C$_6$H$_4$). ^{11}B{^{1}H} NMR (CDCl$_3$); δ 35. EI/MS; m/z = 266.1 (M$^+$), I = 100(100); m/z = 267.3 ([M+1]$^+$), I = 11(16); m/z = 264.9 ([M-1]$^+$), I = 74 (47). Analysis calculated for C$_{14}$H$_{12}$B$_2$O$_4$: C, 63.25; H, 4.55. Found: C, 63.36; H, 4.63.

Diboration of 1-Hexene. The crude product was isolated as a brown oil in 83% yield. The product decomposes upon Kugelrohr distillation. ^{1}H NMR (CDCl$_3$); δ 0.90 (t, 3 H, CH_3, 7.1 Hz), 1.38 (m, 4 H, CH_2CH_2), 1.50–1.70 (m, 3 H, (BCat)CH(H)CH(BCat)CH_2), 1.80 (m, 1 H, (BCat)CH(H)CH(BCat)), 1.93 (m, 1 H, (BCat)CH$_2$CH(BCat)), 7.05 (m, 4 H, BO$_2$C$_6$$H_4$), 7.18 (m, 4 H, BO$_2C_6$$H_4$). ^{13}C{^{1}H} NMR (CDCl$_3$); δ 12.1 (br, 1 C, C–B), 14.0 (CH$_3$), 18.1 (br, 1 C, C–B), 22.8 (CH$_2$), 31.0 (CH$_2$), 33.2 (CH$_2$), 112.3 (4 C, BO$_2$C$_6$H$_4$) , 122.4 (4 C, BO$_2$C$_6$H$_4$) , 148.2 (4 C, BO$_2$C$_6$H$_4$). ^{11}B{^{1}H} NMR (CDCl$_3$); δ 35. EI/MS; m/z = 322.2 (M$^+$), I = 100(100); m/z = 323.2 ([M+1]$^+$), I = 21(20); m/z = 321.2 ([M-1]$^+$), I = 47(44).

117

Diboration of vinylanisole. The crude product was isolated as a light brown solid in 94% yield. The product does not sublime, melt or decompose at temperatures up to 180°C. ^{1}H NMR (CDCl$_3$); δ 1.89 (dd, J = 16.8, 7.1 Hz, 1 H, CH_2CH), 2.13 (dd, J = 16.8, 9.7 Hz, 1 H, CH_2CH), 3.29 (t, 1 H, CH$_2$CH, $^3J_{H-H}$ = 9 Hz), 3.76 (s, 3 H, OCH_3), 6.85(m, 2 H, C$_6$$H_4$), 7.03 (m, 4 H, BO$_2C_6$$H_4$), 7.16 (m, 4 H, BO$_2C_6$$H_4$), 7.29 (m, 2 H, C$_6$$H_4$). ^{13}C{^{1}H} NMR (CDCl$_3$); δ 14.2 (br, 1 C, C–B), 24.9 (br, 1 C, C–B), 55.2 (OCH$_3$), 112.3 (2 C, BO$_2$C$_6$H$_4$), 112.5 (2 C, BO$_2$C$_6$H$_4$), 114.2 (2 C, C$_6$H$_4$OMe), 122.5 (2 C, BO$_2$C$_6$H$_4$), 122.6 (2 C, BO$_2$C$_6$H$_4$), 128.9 (2 C, C$_6$H$_4$OMe), 134.8 (1 C, C$_6$H$_4$OMe), 148.2 (4 C, BO$_2$C$_6$H$_4$), 157.8 (1 C, C$_6$H$_4$OMe). ^{11}B{^{1}H} NMR (CDCl$_3$); δ 35. EI/MS; m/z = 372.2 (M$^+$), I = 100(100); m/z = 373.3 ([M+1]$^+$), I = 21(23); m/z = 371.2 ([M-1]$^+$), I = 46(48).

Diboration of 4-(trifluoromethyl)styrene. The crude product was isolated as a light brown solid in 95% yield and can be sublimed as a white solid in 60% yield. ^{1}H NMR (CDCl$_3$); δ 1.95 (dd, J = 16.7, 7.0 Hz, 1 H, CH_2CH), 2.21 (dd, J = 16.7, 9.3 Hz, 1 H, CH_2CH), 3.45 (dd, J = 9.3, 7.1 Hz, 1 H, CH$_2$CH), 7.07 (m, 4 H, BO$_2$C$_6$$H_4$), 7.21 (m, 4 H, BO$_2C_6$$H_4$), 7.55 (m, 4 H, C$_6$$H_4CF_3$). ^{13}C{^{1}H} NMR (CDCl$_3$); δ 13.6 (br, 1 C, C–B), 26.0 (br, 1 C, C–B), 112.4 (2 C, BO$_2$C$_6$H$_4$), 112.6 (2 C, BO$_2$C$_6$H$_4$), 122.7 (2 C, BO$_2$C$_6$H$_4$), 122.8 (2 C, BO$_2$C$_6$H$_4$), 125.7 (2 C, C$_6$H$_4$CF$_3$), 128.3 (2 C, C$_6$H$_4$CF$_3$), 147.1 (1 C, C$_6$H$_4$CF$_3$), 148.1 (4 C, BO$_2$C$_6$H$_4$), (resonances due to CF$_3$ and ipso C attached to CF$_3$ were not observable). ^{11}B{^{1}H} NMR (CDCl$_3$); δ 34. EI/MS; m/z = 410.2 (M$^+$), I = 100(100); m/z = 411.2 ([M+1]$^+$), I = 22(22); m/z = 409.1 ([M-1]$^+$), I = 51(51). Mp: 95–96°C.

Diboration of 6-Chloro-1-hexene. The crude product was isolated as a brown oil in 85% yield. The product decomposes upon Kugelrohr distillation. ^{1}H NMR (CDCl$_3$); δ 1.48–1.70 (m, 5 H, CH_2CH_3), 1.82(m, 3 H, CH_2CH), 1.93 (m, 1H, CH$_2$CH), 3.54 (t, J = 6.9 Hz, 2 H, CH$_2$Cl), 7.05 (m, 4 H, BO$_2$C$_6$$H_4$), 7.18 (m, 4 H, BO$_2C_6$$H_4$). ^{13}C{^{1}H} NMR (CDCl$_3$); δ 12.1 (br, 1 C, C–B), 18.0 (br, 1 C, C–B), 26.1 (CH$_2$), 32.56 (CH$_2$), 32.65 (CH$_2$), 44.9 (CH$_2$), 112.3 (2 C, BO$_2$C$_6$H$_4$), 112.4 (2 C, BO$_2$C$_6$H$_4$), 122.47 (2 C,

$BO_2C_6H_4$), 122.53 (2 C, $BO_2C_6H_4$), 148.2 (4 C, $BO_2C_6H_4$). $^{11}B\{^1H\}$ NMR (CDCl$_3$); δ 35. EI/MS; m/z = 356.1 (M$^+$), I = 100(100); m/z = 357.2 ([M+1]$^+$), I = 32(34); m/z = 358.2 ([M+2]$^+$), I = 33(34); m/z = 355.0 ([M-1]$^+$), I = 55(46).

Diboration of acetic acid 5-hexenyl ester. The crude product was isolated as a brown oil in 88% yield. The product decomposes upon Kugelrohr distillation. ^1H NMR (CDCl$_3$); δ 1.39–1.78 (m, 6 H), 1.84 (m, 1 H), 1.95 (m, 1 H), 2.02 (s, 3 H, CH$_3$), 2.03 (m, 1 H, CH$_2$CH), 4.08 (t, J = 6.8 Hz, 2H, CH_2OCOCH$_3$) 7.06 (m, 4 H, $BO_2C_6H_4$), 7.19 (m, 4 H, $BO_2C_6H_4$). $^{13}C\{^1H\}$ NMR (CDCl$_3$); δ 12.0 (br, 1 C, C–B), 18.0 (br, 1 C, C–B), 20.94 (), 25.1 (CH$_3$), 28.6 (CH$_2$), 32.9 (CH$_2$), 64.3 (CH$_2$OCH$_3$), 112.3 (2 C, $BO_2C_6H_4$), 112.4 (2 C, $BO_2C_6H_4$), 122.45 (2 C, $BO_2C_6H_4$), 148.1 (4 C, $BO_2C_6H_4$), 171.2 (C=O). $^{11}B\{^1H\}$ NMR (CDCl$_3$); δ 35. EI/MS; m/z = 380.2 (M$^+$), I = 100(100); m/z = 381.3 ([M+1]$^+$), I = 48(22); m/z = 379.3 ([M-1]$^+$), I = 50(46).

Diboration of Norbornene. The crude product was isolated as a light tan solid in 93% yield and can be sublimed as a white solid in 85% yield. ^1H NMR (CDCl$_3$); δ 1.44 (m, 3 H), 1.73 (m, 3 H), 1.83 (s, 4 H), 2.65 (s, 2 H), 6.93 (s, 8 H, $BO_2C_6H_4$). $^{13}C\{^1H\}$ NMR (CDCl$_3$); δ 28.4 (br, 2 C, C–B), 31.9 (2 C), 38.5 (1 C, bridgehead CH$_2$), 39.0 (2 C, bridgehead CH), 112.0 (4 C, $BO_2C_6H_4$), 122.2 (4 C, $BO_2C_6H_4$), 148.1 (4 C, $BO_2C_6H_4$). $^{11}B\{^1H\}$ NMR (CDCl$_3$); δ 35. EI/MS; m/z = 332.2 (M$^+$), I = 100(100); m/z = 333.2 ([M+1]$^+$), I = 17(21); m/z = 331.0 ([M-1]$^+$), I = 62(46). Mp 89–90°C.

Tetraboration of Norbornadiene. The crude product was isolated as a tan solid in 89% yield. Attempts to sublime result in melting and decomposition at temperatures nearing 180°C. ^1H NMR (CDCl$_3$); δ 1.99 (s, 2 H), 2.15 (2, 4 H), 3.12 (s, 2 H), 6.96 (s, 8 H, $BO_2C_6H_4$). $^{13}C\{^1H\}$ NMR (CDCl$_3$); δ 30.8 (br, 4 C, C–B), 39.0 (1 C, bridgehead CH$_2$), 41.7 (2 C, bridgehead CH), 112.1 (8 C, $BO_2C_6H_4$), 122.4 (8 C, $BO_2C_6H_4$), 148.1 (8 C, $BO_2C_6H_4$). $^{11}B\{^1H\}$ NMR (CDCl$_3$); δ 35. EI/MS; m/z = 568.2 (M$^+$), I = 100(100); m/z = 569.2 ([M+1]$^+$), I = 29(32); m/z = 567.2 ([M-1]$^+$), I = 92(82); m/z = 566.1 ([M-2]$^+$), I = 29(33).

Diboration of 1,5-Hexadiene. The crude product was isolated as a brown oil in 82% yield. The product decomposes upon Kugelrohr distillation. ^{1}H NMR (CDCl$_3$); δ 1.49–2.07 (m, 5 H, (BCat)CH$_2$(BCat)CHCH$_2$R), 2.23 (m, 2 H, RC*H*$_2$CHCH$_2$), 4.94 (m, 1 H, CHCH(*H*)), 5.02 (m, 1 H CHC*H*(H))), 5.82 (m, 1 H, C*H*CH$_2$), 7.04 (m, 4 H, BO$_2$C$_6$H$_4$), 7.15 (m, 4 H, BO$_2$C$_6$H$_4$). ^{13}C{^{1}H} NMR (CDCl$_3$); 12.0 (br, 1 C, C–B), 18.1 (br, 1 C, C–B), 32.5 (CH$_2$), 32.8 (CH$_2$), 112.3 (4 C, BO$_2$C$_6$H$_4$), 115.0 (CH$_2$CHR), 122.4 (4 C, BO$_2$C$_6$H$_4$), 138.3 (CH$_2$CHR), 148.2 (4 C, BO$_2$C$_6$H$_4$). ^{11}B{^{1}H} NMR (CDCl$_3$); δ 35. EI/MS; m/z = 320.1 (M$^+$), I = 100(100); m/z = 321.2 ([M+1]$^+$), I = 18(20); m/z = 319.0 ([M-1]$^+$), I = 55(46).

Tetraboration of 1,5-Hexadiene. The crude product was isolated as a brown solid in 87% yield. Attempts to sublime result in melting and decomposition at temperatures nearing 180°C. ^{1}H NMR (CDCl$_3$); δ 1.54–1.77 (m, 4 H, RCH$_2$CH$_2$R), 1.83 (m, 2 H), 1.98 (br m, 4 H), 7.03 (m, 4 H, (BO$_2$C$_6$*H*$_4$)), 7.12 (m, 4 H, (BO$_2$C$_6$*H*$_4$)). ^{13}C{^{1}H} NMR (CDCl$_3$); δ 12.0 (br, 2 C, C–B), 18.1 (br, 2 C, C–B), 32.2 and 32.3 (2 C, equal intensity, probably due to R,S-enantiomers, CH$_2$CH$_2$), 112.3 (4 C, BO$_2$C$_6$H$_4$), 112.4 (4 C, BO$_2$C$_6$H$_4$), 122.4 (8 C, BO$_2$C$_6$H$_4$), 148.2 (8 C, BO$_2$C$_6$H$_4$). ^{11}B{^{1}H} NMR (CDCl$_3$); δ 35. EI/MS; m/z = 558.3 (M$^+$), I = 100(100); m/z = 559.3 ([M+1]$^+$), I = 28(31); m/z = 557.2 ([M-1]$^+$), I = 86(83).

Catalytic Boration of Arenes

A typical experimental run for the catalytic borylation of arenes with HBPin by Cp*Ir(PMe$_3$)(BPin)H is described as follows: In a drybox, Cp*Ir(PMe$_3$)(BPin)H (9.8 mg, 0.018 mmol) was weighed into a test tube and dissolved in 300 mL C$_6$D$_6$. HBPin (13.4 μL, 0.092 mmol) was added to the solution via microsyringe and C$_6$D$_6$ was added to make the solution volume 540 μL. The solution was thoroughly mixed and transferred to a sealable NMR tube. The tube was frozen in liquid nitrogen and flame-sealed with an

atmosphere of argon gas. Upon thawing the tube was heated at 150 °C in an oil bath. The reaction was monitored by ^{1}H, ^{11}B and ^{31}P NMR. The resonance due to C_6D_5–BPin was clearly increasing in intensity. The reaction was judged complete (60 hrs) by monitoring the disappearance of the resonance due to pinacolborane in the ^{1}H and ^{11}B NMR.

Isolation of Ph–BPin From a Catalytic Experiment. A solution of **31** (80 mg, 0.15 mmol) and HBPin (100 mg, 0.75 mmol), dissolved in 4.3 mL toluene, was heated at 150 °C 5 days in a thick–walled air–free flask. The solution was then transferred to a round bottom flask and the benzene removed on the rotary evaporator. The residue was chromatographed on silica with CH_2Cl_2 to yield Ph–BPin (85 mg, 53% based on HBPin).

Crystal Structure Determinations and Refinement

Crystals of **2** for X-ray analysis were grown from a saturated toluene solution at –15 °C. Crystals of **4** for X-ray analysis were grown by diffusion of EtOH into CH_2Cl_2 solutions of the complex at 5 °C. The crystals were covered in a heavy hydrocarbon oil. A suitable crystal was chosen and mounted on a glass fiber. **2** crystallized with a molecule of toluene. **4** crystallized with a molecule of CH_2Cl_2. The data sets were collected at 183 K on a Siemens P3/V diffractometer using Mo Kα X-radiation($\lambda = 0.71069$ Å). Intensity data were collected in the range 4.0 Ω 2θ Ω 55.0° using ω/2θ scans. The final unit cell parameters were obtained by least-squares refinement of 25 reflections that had been accurately centered on the diffractometer. Three standard reflections were recorded after every 150 scans, and no significant change in intensity was observed. The structures were solved using SHELXL-93 and was refined by full-matrix least-squares on all F^2 data. All non-hydrogen atoms were solved with anisotropic thermal parameters. Hydrogen atoms were included in calculated positions and allowed to ride on the parent carbon atoms with isotropic thermal parameters. Crystallograpic computations were performed on a Silicon Graphics Indigo computer.

Crystals of **29** for X-ray analysis were grown from a saturated toluene solution at –80 °C. Crystals of **45** for X-ray analysis were grown by layering a toluene solution of **45** with heptane and cooling at –30 °C. Crystals of **46** for X-ray analysis were grown from a saturated pentane solution at –80 °C. The crystals were covered in a heavy hydrocarbon oil and a suitable crystal for each was mounted on a glass fiber. The data sets were collected at 183 K on a Siemens CCD diffractometer using Mo Kα X-radiation(λ = 0.71073 Å). Data were collected as 90 second frames in a hemisphere of space. The final unit cell parameters were obtained by least-squares refinement of accurately centered reflections obtained from 60 frames of collected data. Smart was used to obtain a unit cell and Saint was used to integrate the collected frames. SADABS was tehn used to apply absorption corrections to the data. The structures were solved using SHELXL–86. Atomic coordinates and thermal parameters were refined using the full-matrix least-squares program, SHELXL–97, and calculations were based on F2 data. All non-hydrogen atoms were refined anisotropically. All crystallograpic computations were performed on Silicon Graphics Indigo computers. All hydrogen atoms not bound to metal centers were placed in calculated positions and allowed to "ride" their parent carbon atoms without further restraint. The hydride hydrogens in compounds **45** and **46** were refined isotropically and found in chemically reasonable positions in Fourier difference maps. In compounds **45** and **46**, the pentamethylcyclopentadienyl ligands were disordered (rotated along the Ir-Cp*$_{centroid}$ axis) and an appropriate model was used in the refinement.

Tables of pertinent data collection parameters for all compounds crystallographically characterized are given in Appendix A.

Appendix A. Summary of crystal data and structure refinement

	2	4
Empirical formula	$C_{48}H_{38}B_2O_4P_2Pt$	$C_{44}H_{53}BCl_2N_2P_2PtSn$
Formula weight	1049.57	1067.31
Temperature	293(2)	183(2)
Wavelength	0.71069	0.71069
Crystal system	Triclinic	Triclinic
Space group	$P/1$(no. 2)	P–1
a (Å)	11.304(3)	11.278(2)
b (Å)	21.248(4)	12.117(2)
c (Å)	11.206(3)	17.219(3)
α, deg	103.33(2)	73.300(14)
β, deg	116.14(2)	79.050(12)
γ, deg	74.64(2)	88.749(14)
V Å^3	2309.7(10)	2211.5(6)
Z	2	2
D_{calc}, Mg m^{-3}	1.509	1.603
Absorption coefficient	3.154	3.949
F(000)	1052	1056
Crystal size (mm)	0.10 x 0.10 x 0.40	0.98 x 0.49 x 0.22
2θ range collected, deg	1.00 to 22.59	2.02 to 27.59
Index ranges	$0 \leq h \leq 10$	$-4 \leq h \leq 14$
	$-22 \leq k \leq 22$	$-15 \leq k \leq 15$
	$-12 \leq l \leq 10$	$-21 \leq l \leq 22$
Reflections collected	5231	10763
Unique reflections	5231	10223
R_{int}	R(int) = 0.00851	R(int) = 0.0211
Refinement method	Full-matrix least-squares on F^2	Full–matrix least-squares on F^2
Data / restraints / par	5174 / 407 / 614	10206 / 18 / 508
GOF on F^2	1.045	1.088
Final R indices [I>2σ(I)]	$R1 = 0.0692$, $wR2 = 0.1751$	$R1 = 0.0647$, $wR2 = 0.1632$
R indices (all data)	$R1 = 0.1148$, $wR2 = 0.3791$	$R1 = 0.0745$, $wR2 = 0.1931$
Largest diff. peak and hole (e Å^3)	2.119 and –3.991	9.938 and –5.855

Appendix A (cont). Summary of crystal data and structure refinement

	29	45
Empirical formula	$C_{25}H_{32}B_2IrO_4P$	$C_{25}H_{27}BF_{10}IrP$
Formula weight	641.30	751.45
Temperature	173(2) K	173(2) K
Wavelength	0.71069 Å	0.71073 Å
Crystal system	monoclinic	monoclinic
Space group	P2(1)/n	P2(1)/n
a (Å)	11.359(3)	12.807(3)
b (Å)	14.658(4)	14.017(3)
c (Å)	15.306(3)	15.155(3)
α, deg	90	90
β, deg	91.77(2)	95.48(3)
γ, deg	90	90
V Å^3	2547.2(11)	2708.1(9)
Z	4	4
D_{calc}, Mg m^{-3}	1.672	1.843
Absorption coefficient	5.333 mm^{-1}	5.072 mm^{-1}
F(000)	1264	1456
Crystal size (mm)	0.25 x 0.36 x 0.48	0.36 x 0.45 x 0.54
2θ range collected, deg	2.20 to 24.99	1.98 to 28.26
Index ranges	0<=h<=13	-16<=h<=16
	0<=k<=17	-17<=k<=18
	-18<=l<=18	-19<=l<=19
Reflections collected	4725	31128
Unique reflections	4481	6469
R_{int}	0.0679	0.0230
Refinement method	Full-matrix least-squares on F^2	Full-matrix least-squares on F^2
Data / restraints / par	4451 / 0 / 298	6469 / 25 / 470
GOF on F^2	1.000	1.051
Final R indices [I>2σ(I)]	R1 = 0.0471 wR2 = 0.1194	R1= 0.0166 wR2 = 0.0378
R indices (all data)	R1 = 0.0934 wR2 = 0.1930	R1 = 0.0218 wR2 = 0.0390
Largest diff. peak and hole (e Å^3)	2.706 and -3.753	0.387 / -0.879

Appendix A (cont). Summary of crystal data and structure refinement

	46
Empirical formula	$C_{25}H_{25}BF_{10}IrP$
Formula weight	749.43
Temperature	173(2) K
Wavelength	0.71073 Å
Crystal system	monoclinic
Space group	P2(1)/n
a (Å)	12.678(3)
b (Å)	13.933(3)
c (Å)	15.192(3)
α, deg	90
β, deg	92.79(3)
γ, deg	90
V Å^3	2680.4(9)
Z	4
D_{calc}, Mg m^{-3}	1.857
Absorption coefficient	5.124 mm^{-1}
F(000)	1448
Crystal size (mm)	0.13 x 0.31 x 0.34
2θ range collected, deg	1.98 to 28.22
Index ranges	-16<=h<=16
	-18<=k<=18
	-19<=l<=19
Reflections collected	20638
Unique reflections	6160
R_{int}	0.0213
Refinement method	Full-matrix least-squares on F^2
Data / restraints / par	6160 / 25 / 438
GOF on F^2	1.048
Final R indices [I>2σ(I)]	R1 = 0.0201 wR2 = 0.0464
R indices (all data)	R1 = 0.0273 wR2 = 0.0483
Largest diff. peak and hole (e Å^3)	1.261 / -0.932

Appendix B. Derivation of Rate Expressions For Chapter 3

In Figure 24, the time dependent concentrations for **2, 17, 18** and **5** are governed by the Eqs B1–4:

$$\frac{-d[2]}{dt} = k_4[2] - k_{-4}[17][PPh_3] \tag{B1}$$

$$\frac{d[17]}{dt} = k_4[2] + k_5[18] - (k_{-4}[PPh_3] + k_5[RC\equiv CR])[17] \tag{B2}$$

$$\frac{d[18]}{dt} = k_5[RC\equiv CR][17] - (k_{-5} + k_6)[18] \tag{B3}$$

$$\frac{d[5]}{dt} = k_6[18] \tag{B4}$$

Application of the steady state approximation to [**18**] yields Eq B5, and combination of the steady state expression for [**17**] and Eq B5 gives B6. The first order rate law in Eq B7 follows from substitution of the expression for [**17**] (Eq B6) in Eq B1:

$$\frac{d[18]}{dt} \approx 0 \implies [18] = \left(\frac{k_5[RC\equiv CR]}{k_{-5} + k_6}\right)[17] \tag{B5}$$

$$\frac{d[17]}{dt} \approx 0 \implies [17] = \left(\frac{k_5 + k_6}{k_{-4}(k_{-5} + k_6) + k_5 k_6[RC\equiv CR]}\right)[2] \tag{B6}$$

$$\therefore \quad \frac{-d[2]}{dt} = \left(\frac{k_4 \, k_5 \, k_6}{k_{-4}\,(k_{-5} + k_6)\,[PPh_3] + k_5 \, k_6 \, [RC \equiv CR]} \right) [2] \tag{B7}$$

In applying the equilibrium approximation to Figure 25, the assumption in Eq B8 is made:

$$\frac{-d[2 + 17 + 18]}{dt} \approx \frac{d[5]}{dt} = k_6\,[18] \tag{B8}$$

From the equilibrium constants, K_1 and K_2, [2] and [17] can be expressed in terms of [18] (Eqs B9 and B10):

$$K_2 = \frac{[18]}{[17]\,[RC\equiv CR]} \quad \Longrightarrow \quad [17] = \frac{[18]}{K_2\,[RC\equiv CR]} \tag{B9}$$

$$K_1 = \frac{[17][PPh_3]}{[2]} \quad \Longrightarrow \quad [2] = \frac{[17][PPh_3]}{K_1} \quad \Longrightarrow \quad [2] = \frac{[18][PPh_3]}{K_1\,K_2\,[RC\equiv CR]} \tag{B10}$$

Eqs B9 and B10 provide an expression of [18] in terms of [2 + 17 + 18] (Eq B12), and substitution for [18] in Eq B8 gives the final form of the rate law in Eq B13:

$$[2 + 17 + 18] = \left(1 + \frac{1}{K_2\,[RC\equiv CR]} + \frac{[PPh_3]}{K_1\,K_2\,[RC\equiv CR]} \right) [18] \tag{B11}$$

127

$$\therefore \quad [18] = \left(\frac{K_1 K_2 [RC\equiv CR]}{K_1 + [PPh_3] + K_1 K_2 [RC\equiv CR]} \right) [2 + 17 + 18] \tag{B12}$$

$$\frac{-d[2 + 17 + 18]}{dt} = \left(\frac{k_6 K_1 K_2 [RC\equiv CR]}{K_1 + [PPh_3] + K_1 K_2 [RC\equiv CR]} \right) [2 + 17 + 18] \tag{B13}$$

Under catalytic conditions the diboryl complex, **2**, is regenerated. The rate laws that govern the time dependent concentrations of the species in Figure 28 are given below:

$$\frac{-d[2]}{dt} = k_4 [2] - k_{-4} [17] [PPh_3] - k_6 [18] \tag{B14}$$

$$\frac{d[4]}{dt} = k_4 [2] + k_5 [18] (k_{-4} [PPh_3] + k_5 [RC\equiv CR]) [17] \tag{B15}$$

$$\frac{d[18]}{dt} = k_5 [RC\equiv CR] [17] - (k_5 + k_6) [18] \tag{B16}$$

$$\frac{d[RC\equiv CR]}{dt} = -k_6 [18] + k_5 [18] - k_5 [RC\equiv CR] [17] \tag{B17}$$

Applying the steady state approximation to [**17**] and [**18**] in Eqs B15 and B16 yield the expressions in Eqs B18 and B19:

$$[17] = \frac{k_4 [2] + k_5 [18]}{k_{-4} [PPh_3] + k_5 [RC\equiv CR]} \tag{B18}$$

128

$$[17] = \left(\frac{k_{-5} + k_6}{k_5 \, [RC \equiv CR]} \right) [18] \quad \text{(B19)}$$

Application of the steady-state approximation to [2] in Eq B14, with substitution of the value for [17] in Eq B18, yields Eq B20. Similarly, substitution of the expression for [17] in Eq B19 in Eq B17 gives Eq B21:

$$[18] = \left(\frac{k_4 \, k_5 \, [RC \equiv CR]}{k_{-4} \, (k_{-5} + k_6) \, [PPh_3] + k_5 \, k_6 \, [RC \equiv CR]} \right) [2] \quad \text{(B20)}$$

$$\frac{d[RC \equiv CR]}{dt} = - k_6 \, [17] \quad \text{(B21)}$$

Combining Eqs B20 and B21 gives the rate law in Eq B22:

$$\frac{-d[RC \equiv CR]}{dt} = \left(\frac{k_4 \, k_5 \, k_6 \, [RC \equiv CR]}{k_{-4} \, (k_{-5} + k_6) \, [PPh_3] + k_5 \, k_6 \, [RC \equiv CR]} \right) [2] \quad \text{(B22)}$$

Applying the equilibrium approximation to the cataytic reaction in Figure 29 gives Eq B23:

$$\frac{-d[RC \equiv CR + 18]}{dt} \approx \frac{-d[5]}{dt} = k_6 \, [18] \quad \text{(B23)}$$

From the equilibrium constants in Eqs B24 and B25, [18] can be expressed in terms of

$[18 + RC\equiv CR]$ (Eq B27):

$$K_2 = \frac{[18]}{[RC\equiv CR][17]} \implies [RC\equiv CR] = \frac{[18]}{K_2[17]} \tag{B24}$$

$$K_1 = \frac{[17][PPh_3]}{[2]} \implies [17] = \frac{K_1[2]}{[PPh_3]} \implies [RC\equiv CR] = \frac{[PPh_3][18]}{K_1K_2[2]} \tag{B25}$$

$$[RC\equiv CR + 18] = \left(1 + \frac{[PPh_3]}{K_1K_2[2]}\right)[18] \tag{B26}$$

$$\therefore \quad [18] = \left(\frac{K_1K_2[2]}{[PPh_3] + K_1K_2[2]}\right)[RC\equiv CR + 18] \tag{B27}$$

Substituting this expression for [18] in Eq B23 gives the rate law in Eq B28:

$$\frac{-d[RC\equiv CR + 18]}{dt} = \left(\frac{k_6 K_1 K_2[2]}{[PPh_3] + K_1 K_2[2]}\right)[RC\equiv CR + 18] \tag{B28}$$

130

APPENDIX C. Kinetic Details

Platinum Kinetics

Data for stoichiometric [PPh₃] dependence at 90 °C.

The rates were determined by measuring the disappearance of catecholate peaks of **2**. The experiments were performed in a constant temperature oil bath.

[**2**] = 8.7 mM; [4-octyne] = 52 mM

[PPh₃]	k_{obs}
0 mM	0.050 sec⁻¹
2.2	0.041
8.7	0.018
17	0.011
22	0.0095
35	0.0058

Data for variable temperature stoichiometric with 1 eq. PPh₃.

The rates were determined by measuring the disappearance of catecholate peaks of **2**. The experiments were performed in a constant temperature oil bath.

[**2**] = 8.7 mM; [4-octyne] = 52 mM; [PPh₃] =8.7 mM

temp	k_{obs}
343 K	0.0019 sec⁻¹
353	0.0065
363	0.018
373	0.046
383	0.12

Data for stoichiometric [4-octyne] dependence with 8 eq. PPh₃.at 105 °C.

The rates were determined by measuring the disappearance of catecholate peaks of **2**. The experiments were performed in a constant temperature oil bath.

[**2**] = 8.7 mM; [PPh₃] = 70 mM

[4-octyne]	k_{obs}
26 mM	0.0099 sec^{-1}
52	0.019
104	0.037
209	0.082
261	0.098

Data for stoichiometric various alkynes at 70 °C.

The rate for 4-octyne was determined by measuring the disappearance of catecholate peaks of **2**. The 4-octyne experiment was performed in the spectrometer. The rates or the substituted diphenyl acetylenes were determined by measuring the relative ^{31}P intensities of **2** and (PPh₃)₂Pt(η^2-acetylene) at –40 °C. The acetylene experiments were performed in a constant temperature oil bath.

[**2**] = 8.7 mM; [alkyne] = 52 mM

alkyne	k_{obs}
4-octyne	0.014 sec^{-1}
Diphenylacetylene	0.0064
Bis(p-anisyl)acetylene	0.0047
Bis[p-(trifluoromethyl)phenyl]acetylene	fast

Data for stoichiometric [4-octyne] dependence with 0 PPh₃ at 70 °C

The rates were determined by measuring the disappearance of catecholate peaks of 2. The experiment was performed in the spectrometer.

[2] = 8.7 mM

[4-octyne]	k_{obs}
26 mM	0.013 sec^{-1}
52	0.014

Data for catalytic dependence of [4-octyne] and [B₂Cat₂] with 8 eq. PPh₃ at 105 °C.

The rates were determined by measuring the integrals of methylene protons alpha to unsaturated bond in 4-octyne and diborylated 4-octyne. Experiments were heated in a constant temperature oil bath.

[2] = 7.0 mM; [PPh₃] = 56 mM

[B₂Cat₂]	[4-octyne]	k_{obs}
42 mM	42 mM	0.0030 sec^{-1}
42	84	0.0031
84	42	0.0030

Data for catalytic [PPh₃] dependence at 100 °C

The rates were determined by measuring the integrals of methylene protons alpha to unsaturated bond in 4-octyne and diborylated 4-octyne. Experiments were heated in a constant temperature oil bath.

$[2] = 7.0$ mM; $[B_2Cat_2] = 42$ mM; [4-octyne] = 42 mM

[PPh₃]	k_{obs}
7.0	0.017 sec^{-1}
3.5	0.029
1.7	0.052
0.9	0.074

Iridium Kinetics

Data for the addition of HBCat to 28.

The rates were determined by measuring the integrals of the Cp* resonance of compounds **28**, **29**, and **30**. Experiments were performed in C_6D_6 and heated in a constant temperature oil bath.

[28]	[HBCat]	Temp	k_{obs}
42 mM	250 mM	40.0 °C	2.9×10^{-4} sec^{-1} *
42	500	40.0	4.0×10^{-4}
84	500	40.0	8.0×10^{-4}
42	250	21.5	4.2×10^{-5}
42	250	30.0	1.5×10^{-4}
42	250	50.0	5.8×10^{-4}
42	250	60.0	1.3×10^{-3}
42	250	70.0	2.5×10^{-3}
42 (**28**-d_2)	250 (DBCat)	40.0	1.8×10^{-4}

References

(1) Brown, H. C.; Subba Rao, B. C. *J. Am. Chem. Soc.* **1956**, *78*, 5694.

(2) Männig, D.; Nöth, H. *Angew. Chem., Int. Ed.* **1985**, *24*, 878-879.

(3) Burgess, K.; Ohlmeyer, M. J. *Chem. Rev.* **1991**, *91*, 1179-1191.

(4) Miyaura, N.; Suzuki, A. *Chem. Rev.* **1995**, *91*, 2457-2483.

(5) Hartwig, J. F.; Waltz, K. M.; Muhoro, C. N.; He, X.; Eisenstein, O.; Bosque, R.; Maseras, F. *Advances in Boron Chemistry*; Siebert, W., Ed.; The Royal Society of Chemistry, 1997, pp 373-396.

(6) Wadepohl, H. *Angew. Chem., Int. Ed.* **1997**, *36*, 2441-2444.

(7) Irvine, G. J.; Lesley, M. J. G.; Marder, T. B.; Norman, N. C.; Rice, C. R.; Robins, E. G.; Roper, W. R.; Whittell, G. R.; Wright, L. J. *Chem. Rev.* **1998**, *98*, 2685-2722.

(8) Braunschweig, H. *Angew. Chem., Int. Ed.* **1998**, *37*, 1786-1801.

(9) Smith, M. R., III *Prog. Inorg. Chem.* **1999**, *48*, 505-567.

(10) Braunschweig, H.; Wagner, T. *Angew. Chem., Int. Ed.* **1995**, *34*, 825-826.

(11) Braunschweig, H.; Kollan, C.; Englert, U. *Angew. Chem., Int. Ed.* **1998**, *37*, 3179-3180.

(12) Wrackmeyer, B. *Angew. Chem., Int. Ed.* **1999**, *38*, 771-772.

(13) Peters, J. C.; Odom, A. L.; Cummins, C. C. *J. Chem. Soc., Chem. Commun.* **1997**, 1995-1996.

(14) Lantero, D. R.; Motry, D. H.; Ward, D. L.; Smith, M. R., III *J. Am. Chem. Soc.* **1994**, *116*, 10811-10812.

(15) He, X.; Hartwig, J. F. *Organometallics* **1996**, *15*, 400-407.

(16) Westcott, S. A.; Marder, T. B.; Baker, R. T.; Calabrese, J. C. *Can. J. Chem.* **1993**, *93*, 930-936.

(17) Nguyen, P.; Lesley, G.; Taylor, N. J.; Marder, T. B.; Pickett, N. L.; Clegg, W.; Elsegood, M. R. J.; Norman, N. C. *Inorg. Chem.* **1994**, *33*, 4623-4624.

(18) Baker, R. T.; Calabrese, J. C.; Westcott, S. A.; Nguyen, P.; Marder, T. B. *J. Am. Chem. Soc.* **1993**, *115*, 4367-4368.

(19) Nguyen, P.; Blom, H. P.; Westcott, S. A.; Taylor, N. J.; Marder, T. B. *J. Am. Chem. Soc.* **1993**, *115*, 9329-9330.

(20) Kono, H.; Ito, K.; Nagai, Y. *Chem. Lett.* **1975**, 1095-1096.

(21) Dai, C; Stringer, G.; Corrigan, J. F.; Taylor, N. J.; Marder, T. B.; Norman, N. C. *J. Organomet. Chem.* **1996**, *513*, 273-275.

(22) Lantero, D. R.; Ward, D. L.; Smith, M. R., III *J. Am. Chem. Soc.* **1997**, *119*, 9699-9708.

(23) Hartwig, J. F.; De Gala, S. R. *J. Am. Chem. Soc.* **1994**, *116*, 3661-3662.

(24) Hartwig, J. F.; Bhandari, S.; Rablen, P. R. *J. Am. Chem. Soc.* **1994**, *116*, 1839-1844.

(25) Seyferth, D.; Raab, G.; Grim, S. O. *J. Org. Chem.* **1961**, *26*, 3034-3035.

(26) Parshall, G. W. *J. Am. Chem. Soc.* **1964**, *86*, 361-364.

(27) Nöth, H.; Schmid, G. *Angew. Chem. Int. Ed.* **1963**, *2*, 623.

(28) Nöth, H.; Schmid, G. *J. Organomet. Chem.* **1966**, *5*, 109-119.

(29) Nöth, H.; Schmid, G. *J. Organomet. Chem.* **1967**, *7*, 129-134.

(30) Shriver, D. F. *J. Am. Chem. Soc.* **1963**, *85*, 3509-3510.

(31) Braunschweig, H.; Wagner, T. *Chem. Ber.* **1994**, *127*, 1613-1614.

(32) Braunschweig, H.; Wagner, T. *Z. Naturforsch.* **1996**, *51B*, 1618-1618.

(33) Muhoro, C. N.; Hartwig, J. F. *Angew. Chem. Int. Ed.* **1997**, *36*, 1510-1512.

(34) Bell, R. A.; Cohen, S. A.; Doherty, N. M.; Threlkel, R. S.; Bercaw, J. F. *Organometallics* **1986**, *5*, 972-975.

(35) Zhang, J.; Lou, B.; Guo, G.; Dai, L. *J. Org. Chem.* **1991**, *56*, 1670-1672.

(36) Westcott, S. A.; Blom, H. P.; Marder, T. B.; Baker, R. T. *J. Am. Chem. Soc.* **1992**, *114*, 8863-8869.

(37) Brands, K. M. J.; Kende, A. S. *Tetrahedron Lett.* **1992**, *33*, 5887-5890.

(38) Evans, D. A.; Fu, G. C.; Hoveyda, A. H. *J. Am. Chem. Soc.* **1988**, *110*, 6917-6918.

(39) Evans, D. A.; Fu, G. C.; Hoveyda, A. H. *J. Am. Chem. Soc.* **1992**, *114*, 6671-6679.

(40) Burgess, K.; Ohlmeyer, M. J. *Tetrahedron Lett.* **1989**, *30*, 5857-5860.

(41) Evans, D. A.; Fu, G. C. *J. Am. Chem. Soc.* **1991**, *113*, 4042-4043.

(42) Considerable debate regarding the insertion step centers around whether the olefin inserts into the Rh-H bond or the Rh-B bond prior to reductive elimination. See refs. 43 and 44 for ab Inito treatment and discussion.

(43) Musaev, D. G.; Mebel, A. M.; Morokuma, K. *J. Am. Chem. Soc.* **1994**, *116*, 10693-10702.

(44) Dorigo, A. E.; Schleyer, P. von R. *Angew. Chem. Int. Ed.* **1995**, *34*, 115-118.

(45) Harrison, K. N.; Marks, T. J. *J. Am. Chem. Soc.* **1992**, *114*, 9220-9221.

(46) Burgess, K.; Jaspars, M. *Tetrahedron Lett.* **1993**, *34*, 6813-6816.

(47) Westcott, S. A.; Blom, H. P.; Marder, T. B.; Baker, R. T.; Calabrese, J. C. *Inorg. Chem.* **1993**, *32*, 2175-2182.

(48) Parks, D. J.; Piers, W. E.; Yap, G. P. A. *Organometallics* **1998**, *17*, 5492-5503.

(49) Motry, D. H.; Brazil, A. G.; Smith, M. R., III *J. Am. Chem. Soc.* **1997**, *119*, 2743-2744.

(50) Hartwig, J. F.; Muhoro, C. N.; He, X.; Eisenstein, O.; Bosque, R.; Maseras, F. *J. Am. Chem. Soc.* **1996**, *118*, 10936-10937.

(51) von H. Spence, R. E. ; Parks, D. J.; Piers, W. E.; MacDonald, M.-A.; Zaworotko, M. J.; Rettig, S. J. *Angew. Chem. Int. Ed.* **1995**, *34*, 1230-1233.

(52) Nozaki, K.; Wakamatsu, K.; Nonaka, T.; Tuckmantel, W.; Oshima, K.; Utimoto, K. *Tetrahedron Lett.* **1986**, *27*, 2007-2010.

(53) Sharma, S.; Oehlschlager, A. C. *Tetrahedron Lett.* **1988**, *29*, 261-264.

(54) A recent review has recently been published concerning transition metal-catalyzed E-B additions to unsaturated organic substrates. See ref. 55.

(55) Han, L.-B.; Tanaka, M. *J. Chem. Soc., Chem. Commun.* **1999**, 395-402.

(56) Ceron, P.; Finch, A.; Frey, J.; Kerrigan, J.; Parsons, T.; Urry, G.; Schlesinger, H. I. *J. Am. Chem. Soc.* **1959**, *81*, 6368-6371.

(57) Massey, A. G. *Adv. Inorg. Chem. Radiochem.* **1983**, *26*, 1-53.

(58) Brotherton, R. J.; McCloskey, A. L.; Boone, J. L.; Manasevit, H. M. *J. Am. Chem. Soc.* **1960**, *82*, 6245-6248.

(59) Brotherton, R. J.; McCloskey, A. L.; Petterson, L. L.; Steinberg, H. *J. Am. Chem. Soc.* **1960**, *82*, 6242-62445.

(60) Moezzi, A.; Olmstead, M. M.; Power, P. P. *J. Am. Chem. Soc.* **1992**, *114*, 2715-2717.

(61) Ishiyama, T.; Matsuda, N.; Miyaura, N.; Suzuki, A. *J. Am. Chem. Soc.* **1993**, *115*, 11018-11019.

(62) Arndtsen, B. A.; Bergman, R. G.; Mobley, T. A.; Peterson, T. H. *Acc. Chem. Res.* **1995**, *28*, 154-162.

(63) Arndtsen, B. A.; Bergman, R. G. *Science* **1995**, *270*, 1970-1973.

(64) Janowicz, A. H.; Bergman, R. G. *J. Am. Chem. Soc.* **1982**, *104*, 352-354.

(65) Janowicz, A. H.; Bergman, R. G. *J. Am. Chem. Soc.* **1983**, *105*, 3929-3939.

(66) Buchanon, J. M.; Stryker, J. M.; Bergman, R. G. *J. Am. Chem. Soc.* **1986**, *108*, 1537-1550.

(67) Hoyano, J. K.; Graham, W. A. G. *J. Am. Chem. Soc.* **1982**, *104*, 3723-3725.

(68) Hoyano, J. K.; McMaster, A. D.; Graham, W. A. G. *J. Am. Chem. Soc.* **1983**, *105*, 7190-7191.

(69) Jones, W. D.; Feher, F. J. *J. Am. Chem. Soc.* **1984**, *106*, 1650-1663.

(70) Jones, W. D.; Kosar, W. P. *J. Am. Chem. Soc.* **1986**, *108*, 5640-5641.

(71) Schaller, C. P.; Cummins, C. C.; Wolczanski, P. T. *J. Am. Chem. Soc.* **1996**, *118*, 591-611.

(72) Bennett, J. L.; Wolczanski, P. T. *J. Am. Chem. Soc.* **1997**, *119*, 10696-10719.

(73) Cummins, C. C.; Schaller, C. P.; Van Duyne, G. D.; Wolczanski, P. T.; Chan, A. W. E.; Hoffmann, R. *J. Am. Chem. Soc.* **1991**, *113*, 2985-2994.

(74) Holtcamp, M. W.; Labinger, J. A.; Bercaw, J. E. *J. Am. Chem. Soc.* **1997**, *119*, 848-849.

(75) Stahl, S. S.; Labinger, J. A.; Bercaw, J. E. *J. Am. Chem. Soc.* **1996**, *118*, 5961-5976.

(76) Hackett, M.; Ibers, J. A.; Whitesides, G. M. *J. Am. Chem. Soc.* **1988**, *110*, 1436-1448.

(77) Hackett, M.; Whitesides, G. M. *J. Am. Chem. Soc.* **1988**, *110*, 1449-1462.

(78) Thompson, M. E.; Baxter, S. M.; Bulls, A. R.; Burger, B. J.; Nolan, M. C.; Santarsiero, B. D.; Schaefer, W. P.; Bercaw, J. F. *J. Am. Chem. Soc.* **1987**, *109*, 203-219.

(79) Fendrick, C. M.; Marks, T. J. *J. Am. Chem. Soc.* **1986**, *108*, 425-437.

(80) Smegal, J. A.; Hill, C. L. *J. Am. Chem. Soc.* **1983**, *105*, 3515-3521.

(81) Groves, J. T.; Nemo, T. E. *J. Am. Chem. Soc.* **1983**, *105*, 6243-6248.

(82) Wayland, B. B.; Ba, S.; Sherry, A. E. *J. Am. Chem. Soc.* **1991**, *113*, 5305-5311.

(83) Gol'dshleger, N. F.; Es'kova, V. V.; Shilov, A. E.; Shteinman, A. A. *Zh. Fiz. Khim. (Engl. Transl.)* **1972**, *46*, 785-786.

(84) Periana, R. A.; Taube, D. J.; Evitt, E. R.; Loffler, D. G.; Wentrcek, P. R.; Voss, G.; Masuda, T. *Science* **1993**, *259*, 340-343.

(85) For leading references see ref. 86.

(86) Stahl, S. S.; Labinger, J. A.; Bercaw, J. E. *Angew. Chem., Int. Ed.* **1998**, *37*, 2180-2192.

(87) Camalli, M.; Caruso, F.; Chaloupka, S.; Leber, E. M.; Rimml, H.; Venanzi, L. M. *Inorg. Chim. Acta.* **1990**, *73*, 2263-2274.

137

(88) Clegg, W.; Lawler, F. J.; Lesley, G.; Marder, T. B.; Norman, N. C.; Orpen, A. G.; Quayle, M. J.; Rice, C. R.; Scott, A. J.; Souza, F. E. S. *J. Organomet. Chem.* **1998**, *550*, 183-192.

(89) Lawlor, F. J.; Norman, N. C.; Pickett, N. L.; Robins, E. G.; Nguyen, P.; Lesley, G.; Marder, T. B.; Ashmore, J. A.; Green, J. C. *Inorg. Chem.* **1998**, *37*, 5282-5288.

(90) Ishiyama, T.; Matsuda, N.; Murata, M.; Ozawa, F.; Suzuki, A.; Miyaura, N. *Organometallics* **1996**, *15*, 713-720.

(91) Lesley, G.; Nguyen, P.; Taylor, N. J.; Marder, T. B.; Scott, A. J.; Clegg, W.; Norman, N C. *Organometallics* **1996**, *15*, 5137-5154.

(92) Clegg, W.; Johann, T. R. F.; Marder, T. B.; Norman, N. C.; Orpen, G. A.; Peakman, T. M.; Quayle, M. J.; Rice, C. R.; Scott, A. J. *J. Chem. Soc., Dalton Trans.* **1998**, 1431-1438.

(93) Kerr, A.; Marder, T. B.; Norman, N. C.; Orpen, A. G.; Quayle, M. J.; Rice, C. R.; Timms, P. L.; Whittell, G. R. **1998**, 319-320.

(94) Curtis, D.; Lesley, M. J. G.; Norman, N. C.; Orpen, A. G.; Starbuck, J. *J. Chem. Soc., Dalton Trans.* **1999**, 1687-1694.

(95) Debaerdemaeker, T.; Berhalter, K.; Weiseman, C.; Brune, H. A. *Acta. Crystallogr., Sect. C.* **1987**, *43*, 1253-1255.

(96) Clegg, W.; Elsegood, M. R. J.; Lawlor, F. J.; Norman, N. C.; Pickett, N. L.; Robins, E. G.; Scott, A. J.; Nguyen, P.; Taylor, N. J.; Marder, T. B. *Inorg. Chem.* **1998**, *37*, 5289-5293.

(97) Trotter, J. *Acta. Crystall.* **1961**, *14*, 1135-1138.

(98) A similar conclusion was reached by considering the covalent radii of Pt(II) in platinum compounds and B in Cat_2B_2. See ref. 7.

(99) To our knowledge there are only two other metal complexes that simultaneously contain stannyl and boryl ligands. See refs. 15 and 100.

(100) Onozawa, S.; Hatanaka, Y.; Sakakura, T.; Shimada, S.; Tanaka, M. *Organometallics* **1996**, *15*, 5450-5452.

(101) Schmid, G.; Boese, R.; Blaser, D. Z *Naturforsch.* **1982**, *37B*, 1230-1233.

(102) Conditions for the preparation of and ^1H, ^{11}B, ^{13}C, and ^{119}Sn and mass spectroscopic data for the stannylborated products of 1-hexyne, 4-octyne and diphenyl acetylene are listed in the Experimental section.

(103) Reamey, R. H.; Whitesides, G. M. *J. Am. Chem. Soc.* **1984**, *106*, 81-85.

(104) Rickard, C. E. F.; Roper, W. R.; Williamson, A.; Wright, L. J. *Angew. Chem. Int. Ed.* **1999**, *38*, 1110-1113.

(105) Another method involved comparing Pt-Cl bond lengths in the series of compounds trans-$(PPh_3)_2Pt(Cl)X$ (X = BCat, Me, H). See ref. 7.

(106) Evans, D. A.; Fu, G. C.; Anderson, B. A. *J. Am. Chem. Soc.* **1992**, *114*, 6679-6685.

(107) Burgess, K.; van der Donk, W. A.; Westcott, S. A.; Marder, T. B.; Baker, R. T.; Calabrese, J. C. *J. Am. Chem. Soc.* **1992**, *114*, 9350-9359.

(108) Muhoro, C. N.; He, X.; Hartwig, J. F. *J. Am. Chem. Soc.* **1999**, *121*, 5033-5046.

(109) Motry, D. H.; Smith, M. R., III *J. Am. Chem. Soc.* **1995**, *117*, 6615-6616.

(110) Ishiyama, T.; Yamamoto, M.; Miyaura, N. *J. Chem. Soc., Chem. Commun.* **1997**, 689-690.

(111) Concurrently, Marder et. al. arrived at similar conclusions regarding the mechanism of B-B addition to alkynes in this system. See Ref. 91

(112) Komiya, S.; Albright, T. A.; Hoffmann, R.; Kochi, J. K. *J. Am. Chem. Soc.* **1977**, *99*, 8440-8447.

(113) McDermott, J. X.; White, J. F.; Whitesides, G. M. *J. Am. Chem. Soc.* **1976**, *98*, 6521-6528.

(114) Gillie, G.; Stille, J. K. *J. Am. Chem. Soc.* **1980**, *102*, 4933-4941.

(115) Pyun, C. W. *J. Chem. Ed.* **1971**, *48*, 194-196.

(116) McCarthy, T. J.; Nuzzo, R. G.; Whitesides, G. M. *J. Am. Chem. Soc.* **1981**, *103*, 3396-3405.

(117) Wilkins, R. G. *Kinetics and Mechanism of Transition Metal Complexes*; VCH: Weiheim, 1991.

(118) Samsel, E. G.; Norton, J. R. *J. Am. Chem. Soc.* **1984**, *106*, 5505-5512.

(119) Burger, B. J.; Santarsiero, B. D.; Trimmer, M. S.; Bercaw, J. E. *J. Am. Chem. Soc.* **1988**, *110*, 3134-3146.

(120) Lowry, T. H.; Richardson, K. S. *Mechanism and Theory in Organic Chemistry*; 2nd ed. ed.; Harper and Row: New York, 1981.

(121) Birk, J. P.; Halpern, J.; Pickard, A. L. *Inorg. Chem.* **1968**, *7*, 2672-2673.

(122) The group of Miyaura simultaneously reported diboration of alkenes utilizing a Pt(dba)$_2$ (dba = dibenzylideneacetone). See ref. 110.)

(123) Rablen, P. R.; Hartwig, J. F.; Nolan, S. P. *J. Am. Chem. Soc.* **1994**, *116*, 4121-4122.

(124) Rablen, P. R.; Hartwig, J. F. *J. Am. Chem. Soc.* **1996**, *118*, 4648-4653.

(125) Ishiyama, T.; Murata, M.; Miyaura, N. *J. Org. Chem.* **1995**, *60*, 7508–7510.

(126) Murata, M.; Watanabe, S.; Masuda, Y. *J. Org. Chem.* **1997**, *62*, 6458–6459.

(127) Iverson, C. N.; Smith, M. R. III *J. Am. Chem. Soc.* **1995**, *117*, 4403-4404.

(128) Dai, C.; Stringer, G.; Marder, T. B.; Baker, R. T.; Scott, A. J.; Clegg, W.; Norman, N. C. *Can. J. Chem.* **1996**, *74*, 2026-2031.

(129) The standard method for the preparation of pinacolborane and its analogs uses ether type solvents, such as thf or dimethoxyethane (dme). Althogh the boiling point of most boranes, including HBPin, is much higher than the ethers, it is very difficult to totally separate thf or dme from the borane.

(130) Hartwig, J. F.; He, X. *Angew. Chem. Int. Ed.* **1996**, *35*, 315–317.

(131) Hartwig, J. F.; He, X. *Organometallics* **1996**, *15*, 5350–5358.

(132) Baker, R. T.; Nguyen, P.; Marder, T. B.; Westscott, S. A. *Angew. Chem. Int. Ed.* **1995**, *34*, 1336-1338.

(133) Burger, P.; Bergman, R. G. *J. Am. Chem. Soc.* **1993**, *115*, 10462-10463.

(134) Woerpel, K. A.; Bergman, R. G. *J. Am. Chem. Soc.* **1993**, *115*, 7888-7889.

(135) Golden, J. T.; Peterson, T. H.; Holland, P. L.; Bergman, R. G.; Andersen, R. A. *J. Am. Chem. Soc.* **1998**, *120*, 223-224.

(136) The average ½ life for the first two ½ lives was 45 minutes at 120 °C.

(137) Negishi, E.; Katz, J.-J.; Brown, H. C. *J. Am. Chem. Soc.* **1972**, *94*, 4025-4027.

(138) Gilbert, T. M.; Hollander, F. J.; Bergman, R. G. *J. Am. Chem. Soc.* **1985**, *107*, 3508-3516.

(139) Gilbert, T. M.; Bergman, R. G. *J. Am. Chem. Soc.* **1985**, *107*, 3502-3507.

(140) Stoutland, P. O.; Bergman, R. G. *J. Am. Chem. Soc.* **1985**, *108*, 4581-4582.

(141) Heinekey, D. M.; Millar, J. M.; Koetzle, T. F.; Payne, N. G.; Zilm, K. W. *J. Am. Chem. Soc.* **1990**, *112*, 909-919.

(142) Robertson, G. B.; Tucker, P. A. *Aust. J. Chem.* **1988**, *41*, 283-291.

(143) Ricci Jr., J. S.; Koetzle, T. F.; Fernandez, M.-J.; Maitlis, P. M.; Green, J. C. *J. Organomet. Chem.* **1986**, *299*, 383-389.

(144) Robertson, G. B.; Tucker, P. A. *Aust. J. Chem.* **1987**, *40*, 1043-1052.

(145) Bau, R.; Schwertfeger, C. J.; Garlaschelli, L.; Koetzle, T. F. *J. Chem. Soc., Dalton. Trans.* **1993**, 3359-3362.

(146) Baranger, A. M.; Hollander, F. J.; Bergman, R. G. *J. Am. Chem. Soc.* **1993**, *115*, 7890-7891.

(147) Baranger, A. M.; Bergman, R. G. *J. Am. Chem. Soc.* **1994**, *116*, 3822-3835.

(148) Glueck, D. S.; Newman Winslow, L. J.; Bergman, R. G. *Organometallics* **1991**, *10*, 1462-1479.

(149) Siegel, J. S.; Anet, F. A. L. *J. Org. Chem.* **1988**, *53*, 2629-2630.

(150) Kegley, S. E.; Pinhas, A. R. *Spectroscopy*; University Science Books: Mill Valley, CA, 1986, pp 20-23.

(151) Related boryls have recently been reported. See ref. 152.

(152) Peterson, T. H.; Golden, J. T.; Bergman, R. G. *Organometallics* **1999**, *18*, 2005-2020.

(153) Parks, D. J.; von h. Spence, R. E.; Piers, W. E. *Angew. Chem., Int. Ed.* **1995**, *34*, 809–811.

(154) Initial products are isotopically pure as judged by ^{1}H NMR ((PMe₃) resonances can be resolved for Ir-H/D isotopomers). Over the course of the reaction HBX₂ will scramble into the deuteride position to some extent.

(155) Trialkylaluminum compounds react with compound **28** to yield alkanes and Ir-Al bonds. See Ref. 135.

(156) An excellent review of metal-mediated nucleophilic aromatic substitutions has recently appeared. See ref. 157.

(157) Pike, R. D.; Sweigart, D. A. *Coord. Chem. Rev.* **1999**, *187*, 183-222.

(158) Diversi, P.; Iacoponi, S.; Ingrosso, G.; Laschi, F.; Lucherini, A.; Pinzino, C.; Uccello-Barretta, G.; Zanello, P. *Organometallics* **1995**, *14*, 3275-3287.

(159) Jones, W. D.; Feher, F. J. *J. Am. Chem. Soc.* **1982**, *104*, 4240-4242.

(160) Personal communication, Cho, J.-Y.

(161) Gupta, M.; Hagen, C.; Kaska, W. C.; Cramer, R. E.; Jensen, C. M. *J. Am. Chem. Soc.* **1997**, *119*, 840-841.

(162) Liu, F.; Pak, E. B.; Singh, B.; Jensen, C. M.; Goldman, A. S. *J. Am. Chem. Soc.* **1999**, *121*, 4086-4087.

(163) Wick, D. D.; Goldberg, K. I. *J. Am. Chem. Soc.* **1997**, *1997*, 10235-10236.

(164) Green, M.; Howard, J. A. K.; Spencer, J. L.; Stone, F. G. A. *J. Chem. Soc., Dalton Trans.* **1977**, 271-277.

(165) Fendrick, C. M.; Schertz, L. D.; Mintz, E. A.; Marks, T. J. *Inorg. Syn.* **1990**, *28*, 193-198.

(166) Nöth, H.; Schwerthöffer, R. *Chem. Ber.* **1981**, *114*, 3056-3062.

(167) Cummins, C. H. *Tetrahedron Lett.* **1994**, *35*, 857-860.

(168) Ashby, E. C.; Oswald, J. *J. Org. Chem.* **1988**, *53*, 6068-6076.

(169) Luetkens, M. L. Jr.; Sattellberger, A. P.; Murray, H. H.; Basil, J. D.; Fackler, J. P. *Inorg. Syn.* **1990**, *28*, 305-310.

(170) Nöth, H. *Z Naturforsch.* **1984**, *39b*, 1463-1466.

(171) Tokuda, M.; Chung, V. V.; Inagaki, K.; Itoh, M. *J. Chem. Soc., Chem. Commun.* **1977**, 690-691.

(172) Brown, H. C.; Gupta, S. K. *J. Am. Chem. Soc.* **1975**, *97*, 5249-5255.

(173) % conversion refers to the amount of Cp*Ir(PMe$_3$)(Cy)H that has been used up in the reaction (at least three 1/2 lives). "% **31**" and "% actual **48**" refer to the amounts of Cp*Ir(PMe$_3$)(BPin)H and Cp*Ir(PMe$_3$)(C$_6$D$_5$)D produced at the point of % converson listed. "% Theor. **48**" and "% Theor. CyH" refer to the amount of Cp*Ir(PMe$_3$)(C$_6$D$_5$)D and *cy*-C$_6$H$_{12}$ expected based on just the thermolysis of pure Cp*Ir(PMe$_3$)(*cy*-C$_6$H$_{11}$)H. Ref. 66 was used to calculate the appropriate k$_{obs}$ values needed (as discussed in the text). "% Cy-BPin" and "% actual CyH" refer to the percent yield of organic products at the point of % conversion listed.